The Geochemistry and Petrogenesis of the Saltpeterkop Carbonatite Complex near Sutherland, Northern Cape, South Africa

Manoka Marageni

Thesis presented for the degree of Master of Science in Geochemistry

Department of Geological Sciences

University of Cape Town

February 2018

Supervisors: Dr. Philip Janney & Dr. Lynnette Greyling

I know the meaning of plagiarism and declare that all of the work in the thesis, except for that which is properly acknowledged, is my own

Manoka Marageni

February 2018

ABSTRACT

The Saltpeterkop Carbonatite Complex is a Late Cretaceous (≈76 Ma) volcanic and shallow intrusive magmatic feature located approximately 20 km southeast of Sutherland in the Northern Cape. It is unusual among southern African carbonatite complexes in that it has not been deeply eroded, and retains a significant vestige of its original volcanic features. The main geologic expression of the Complex is a ≈1.5 km diameter tuff ring, located on top of prominently updomed and fractured Beaufort Group (Karoo) sediments, that appears to have formed as the result of a major diatreme-type eruption. The volcaniclastic breccias making up the tuff ring have been heavily altered and silicified by hydrothermal activity, and thick (mm to tens of cm) Fe oxide-rich crusts, which appear to represent the alteration products of Fe-rich carbonatites, are common in this area. Outside of the central ring structure are numerous shallow intrusions (dykes, sills and irregular shapes), satellite breccia pipes and pipe-shaped intrusions that host fresh to only moderately altered igneous rocks. The main igneous rock types include (in decreasing order of abundance): carbonatite, potassic trachyte, olivine melilitite and ultramafic lamprophyre. This thesis provides the first detailed petrographic and geochemical description of these rocks (e.g., major and trace elements) and attempts to explain several aspects of their petrogenesis. The olivine melilitites and ultramafic lamprophyres are the most primitive igneous rocks in the complex and have experienced only minor to moderate extents of differentiation, respectively. They apppear to have been derived by low-degrees of partial melting of a carbonated, likely phlogopite-bearing mantle source. The lamprophyres appear to have been derived by melting at shallower depths than the melilitites based on REE constraints. The carbonatites range from relatively primitive to highly differentiated and they form a nearly continuous compositional range with the ultramafic lamprophyres and melilitites. This seems to argue against a major role for liquid immiscibility in their origin. Their REE content (up to 2 wt.% total REE oxides) correlates with their extent of differentiation. The potassic trachytes are plausibly linked to melts of mafic lower continental crust that has been metasomatised by hydrous potassium-rich carbonatitic melts and which have experienced significant fractional crystallization and assimilation of upper crustal sedimentary rocks during emplacement.

ACKNOWLEDGEMENTS

I would like to thank the following persons and organisations:

-I would like to thank both of my supervisors, Dr Philip Janney & Dr. Lynnette Greyling, as this thesis would not have been possible without the time and effort that they both invested into this project. Philip is thanked in particular for his attention to detail throughout the project as well as for always making time in his busy schedule be it to discuss new data, answer my many questions or to go through the various manuscript/thesis drafts that landed on his desk with increasing frequency towards the end.

-My parents (Mr M.P. Marageni and Mrs M.M. Moshapo) and sister Mususumeli Marageni for supporting me throughout the project.

-Miss Midana Amanda Mmboyi for understanding and always being there for me.

-Dr. Luc Chevallier (Council for Geosciences, Bellville) for generously providing access to his extensive sample collection, for sharing his detailed field maps, and for valuable consultations on the geology of Saltpeterkop.

-Prof. Wilhelm J. Verwoerd (Stellenbosch University) for generously providing sample materials and for useful conversations on the petrology of Saltpeterkop carbonatites.

-Dr. Johann Diener (UCT) for kind assistance with the crustal melt modeling using the THERMOCALC program.

-Mr. Charl DuPlessis (Farm Matjiesfontein), Mr. and Mrs. Elias Basson (Farm Portugals Rivier), Mr. Delphius Symington (Farm Blauuw Blommetjies Keep) and Mr. Andre Jordaan (Manager, Rogge Cloof Private Sutherland Estate) for permission and/or assistance in accessing field sites at and in the vicinity of Saltpeterkop.

-Mr. Michael Kirchner, Mr. Chad Peel and Mr. Siyanda Mabaso for field assistance in obtaining some of the samples documented in this thesis.

-Mr. Jonathan van Rooyen (UCT) for assistance with sample preparation for XRF

-Ms. Christel Tinguely (UCT) for technical assistance with solution ICP-MS analysis.

-Mr. Nic Laidler (UCT) for assistance with X-ray diffraction measurements

-Mr. David Wilson and Ms. Rene van der Merwe (UCT) for preparation of numerous polished thin sections.

-Finally, funding from the Centre for Integrated Mineral and Energy Resource Analysis (CIMERA, an NRF-DST Centre of Excellence) is gratefully acknowledged, both for providing

my MSc bursary and supplying funds for research costs, without which this research would not have been possible.

Table of Contents

List of Figures

List of Tables

Appendix 1. Mineral Compositions

Appendix 2. Whole-rock Geochemical Data

Appendix 3. Mineral-melt partition coefficients

1. INTRODUCTION

Southern Africa contains an abundance of alkaline igneous rocks such as kimberlites, olivine melilitites and carbonatites as well as differentiated rocks such as trachytes, phonolites and syenites. Many of these are economically important due to the fact that they convey diamonds to the surface or contain valuable rare metals. The ultimate origins of alkaline magmatism remain poorly understood as it tends to occur in an intraplate tectonic environment and cannot therefore be related to plate boundary processes. Origins for this magmatism have been proposed to be related to tectonic/lithospheric processes (extension or shearing; e.g., Jelsma et al., 2009), small-scale convection in the shallow asthenosphere (e.g., King and Ritsema, 2000) and the expression of deep-seated mantle plumes (e.g., le Roex and Lanyon, 1998).

The Saltpeterkop carbonatite complex is a Late Cretaceous volcanic and intrusive complex, located roughly 20 km ESE of the town of Sutherland in the Northern Cape, and is composed of a variety of igneous rock types exposed mainly as dykes and sills, as well as volcaniclastic breccias and sediments. It has been proposed to form part of the Western Cape olivine melilitite province (Janney et al., 2002) and the nearest other locality in this province is the Sutherland Commonage olivine melililitite dyke/sill complex located within the town of Sutherland (Viljoen, 1988), and which is approximately of the same age. The Western Cape melilitite province extends roughly 300 km south from the Sutherland area and also includes a small number of olivine melilitite localities (generally small subvolcanic pipe-like intrusions) near the towns of Robertson and Heidelberg in the Western Cape province, as well as submarine alkali basalts and phonolites dredged from the continental shelf southeast of Cape Agulhas. As a whole, the province ranges in age from roughly 70 Ma around Sutherland to 58 Ma at its southern extremity on the Alphard Bank. Overall the Western Cape melilitite province is oriented nearly north-south, which is significantly different from the northeastward direction of African plate motion, but the age-distance relationship for the province is similar to what would be expected for the action of a stationary mantle hotspot under the moving African plate over this time interval.

Previously, geochemical data for the Saltpeterkop complex has only been reported for olivine melilitites from one locality (e.g., Duncan et al., 1978; Mclver and Ferguson 1979; Boctor and Yoder, 1986) and for certain elements reported from drill-cores in the summit region

of the complex (Verwoerd et al., 1995). There has not previously been a systematic attempt to document the whole-rock major and trace element compositions of igneous rocks from Saltpeterkop, and this thesis aims to provide such data. The aim of this study is therefore to provide a survey of the igneous rocks present, including their petrographic and geochemical variability, and attempt to relate their petrogeneses through the use of relatively simple modeling techniques. In turn, these data and interpretations can be used to form the basis for more specialised future investigations. Many of the igneous rocks present are enriched in the rare earth elements and special attention will be paid to understanding the processes of rare earth element enrichment in the mantle sources and parent magmas of the Saltpeterkop igneous rocks. It is important to note here that, unlike some previous authors (McIver and Ferguson, 1979), the Sutherland Commonage melilitite is treated as separate and distinct from the Saltpeterkop complex for the purposes of this thesis, mainly based on evidence for distinct ages for the two localities as described below.

1.1 The Saltpeterkop Carbonatite Complex – an overview

The Saltpeterkop carbonatite complex, (32°28'31.36"S, 20°50'24.96"E) is located 20 km east-south-east of the town of Sutherland in South Africa's Northern Cape Province (Figure 1.1). The Saltpeterkop complex is centred on an approximately 1 km diameter ring structure at a base altitude of approximately 1500 m and a peak elevation of 1766 m above sea level for the Saltpeterkop peak on the north side of the ring. The tuff ring is elevated roughly 250 m above the surrounding land surface (Figure 1.2), and slopes gently away on all sides (Verwoerd et al., 1995). The ring structure, as a whole, forms a distinctive feature, easily recognized from the air, that is shaped like a bull's eye (de Wet, 1975). The elevated ring has been interpreted as an eroded volcanic tuff-ring composed largely of volcaniclastic breccia (Verwoerd et al., 1990). Regionally nearly flat-lying Beaufort group sedimentary rocks are strongly updomed within 10 km of Saltpeterkop, with dips adjacent to the ring structure as great as 60° (Newton, 1987).

The Saltpeterkop complex is of particularly captivating interest for two reasons. First, it represents one of the only southern African carbonatites that has not been deeply eroded and therefore preserves significant sequences of volcaniclastic deposits, and second because it includes a variety of igneous rocks, such as carbonatite, potassic trachyte, olivine melilitite and ultramafic lamprophyre. These are present as breccias and as shallow (hypabyssal) intrusive

features including dykes, sills and irregular intrusions. The preservation of volcaniclastic deposits and shallow intrusives are in stark contrast to most carbonatite complexes which have been deeply eroded (e.g., Spitskop in South Africa and Dicker Willem and Marinkas Quellen in southern Namibia; Verwoerd, 1993), Second, Saltpeterkop contains a wide variety of igneous rock types, including primitive (olivine melilitite, ultramafic lamprophyre) and differentiated (potassic trachyte) silicate rocks as well as variably calcium-, magnesium- and iron-rich carbonatites. Saltpeterkop, therefore, presents an ideal opportunity to study the petrogenetic relationships between carbonatite and associated alkaline silicate rocks and provide clues to their origin.

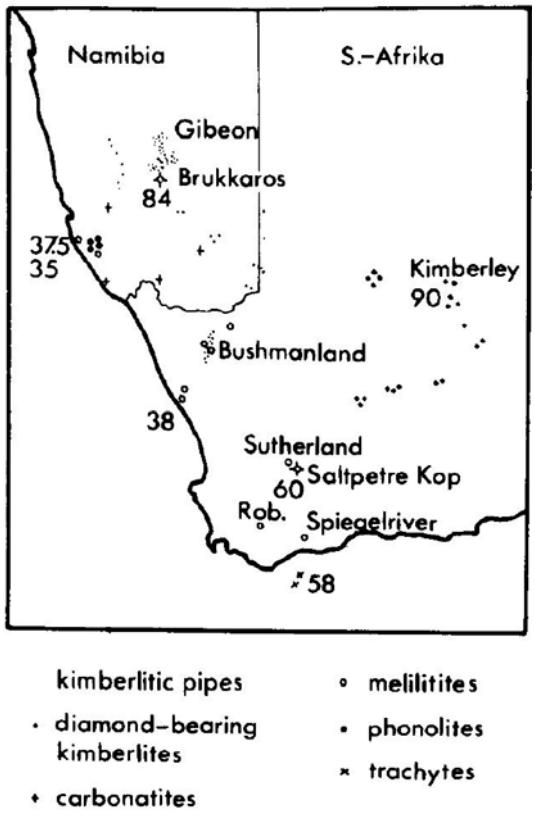

Figure 1.1. *Map of southern Africa showing distribution of kimberlite pipes, carbonatites and other types of alkaline igneous rocks (Brey, 1978).*

The Saltpeterkop complex has experienced extensive hydrothermal alteration with the volcaniclastic rocks of the tuff ring and its immediate surroundings being the most affected (Verwoerd, 1990). The extent of hydrothermal alteration decreases with increasing distance

from the centre of the complex, and so the vast majority of igneous rocks described in this thesis were sampled more than 1 km from the center of the ring structure.

Age constraints on the Saltpeterkop complex are relatively sparse, but the few radiometric constraints on its age are consistent: a 74.7 ± 3 Ma date obtained by Duncan et al. (1978) on a phlogopite megacryst from the Silver Dam breccia pipe obtained by the K-Ar technique, and a 76.5 ± 3.3 Ma date obtained by Malarkey et al. (2010) by the Rb-Sr isochron technique on a variety of minerals separated from an olivine melilite sample from the M5 pipe. Duncan et al. (1978) also obtained an age of 75 ± 3 Ma for a sample of the Sutherland Commonage melilitite by the whole-rock K-Ar technique. Phillips et al. (2000) cast doubt on the accuracy of this K-Ar age and stated that an unpublished 66 ± 1 Rb-Sr isochron age determined by K.S. Viljoen on phlogopite separates from the Sutherland Commonage melilitite was, in their view, a more likely age for all alkaline magmatism near Sutherland.

Figure 1.2. *Satellite photo of the Saltpeterkop carbonatite complex (Google Earth image).*

de Wet (1975) suggested the following sequence of events for emplacement of the Saltpeterkop carbonatite complex: (1) emplacement of a 3 to 4 km diameter pluton at ≈1 km depth, causing updoming and deformation of the overlying sedimentary rocks, (2) eruption of the main vent and formation of the tuff ring and the volcaniclastic sediments covering the interior of the ring structure, (3) onset of emplacement of carbonatitic dykes, sills and plugs, (4)

emplacement of trachyte intrusions concurrent with continued carbonatitic activity, and (5) prolonged hydrothermal activity and alteration concentrated at the central vent and tuff ring. The timing of olivine melilitite dyke, sill and satellite diatreme emplacement was not constrained by de Wet (1975), and he did not recognise ultramafic lamprophyre as a separate rock type present. Models for the origin and evolution of the Saltpeterkop complex from previous workers are described in the next chapter. McIver and Ferguson (1979) postulated that the rock types at Saltpeterkop originated by a variety of processes including fractional crystallization, liquid immiscibility, and crystal-liquid reaction phenomena.

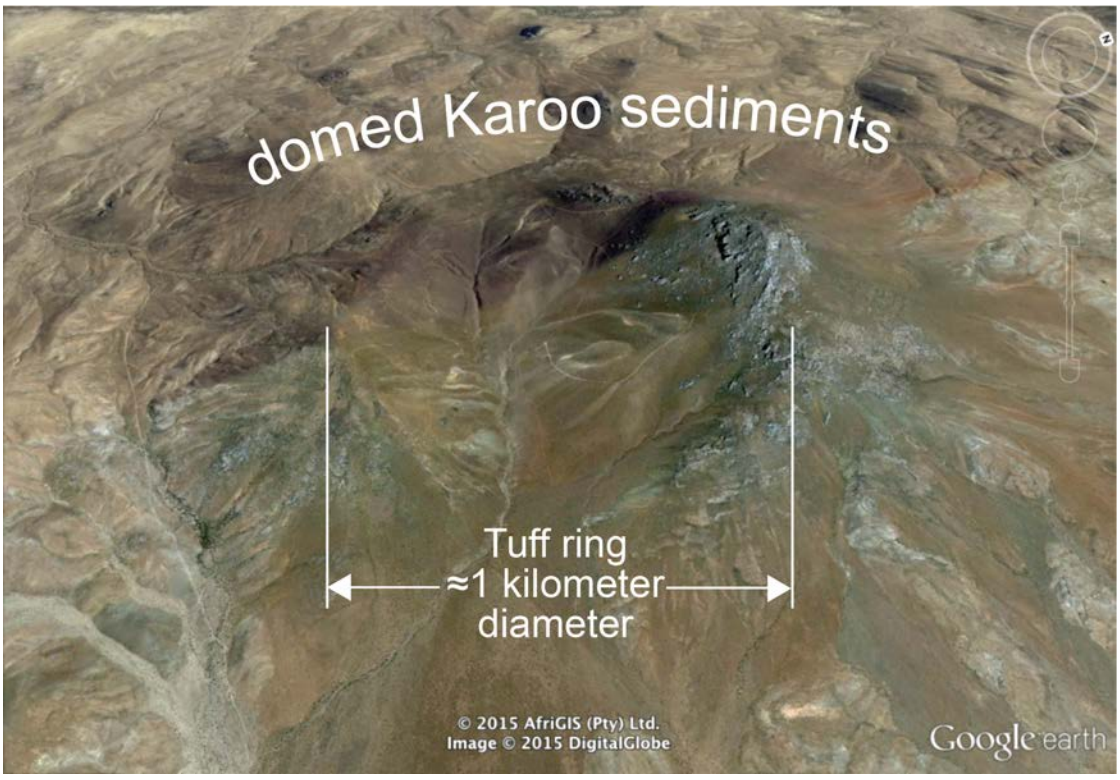

Figure 1.3. *Oblique view of Saltpeterkop as viewed from the southeast (Google Earth image).*

1.2 Economic deposits and the rare earth elements

Coring campaigns were carried out at Saltpeterkop in the 1980s and 1990s searching for possible epithermal gold mineralisation, but this was not found (Verwoerd et al., 1995). The only economic metals present in the rocks of the Saltpeterkop complex are the rare earth elements, which reach concentrations as high as 1.7 wt.% total rare earth oxides in some of the carbonatites. The rare earth elements (REEs) have attracted the interest of economic geologists

for many years due to their important role in magnets, batteries and many electronic devices. The term "REE" includes the lanthanides (the 14 naturally occurring elements from La to Lu), and also often the elements Y and Sc, which have similar ionic radii and +3 valence states. However, in this thesis, the term rare earth elements will only be used to refer to the naturally occurring lanthanide elements.

1.2.1 Mineralisation at Saltpeterkop

Verwoerd et al. (1995) postulated that mineralisation occurred in three stages at the Saltpeterkop carbonatite complex:

1) Magmatic stage, which is represented by formation of pyrochlore, sulphides and magnetite in carbonatite, where the elements of possible economic interest are Nb, Zr, Y and Ce.
2) Mesothermal stage, associated with the introduction of ferric hydrates along joints of country rock, as well as brecciation of carbonatite and replacement of primary carbonate minerals by ankerite and, in some cases, haematite.
3) Epithermal stage, which occurred in the weathered zone of carbonatite and hydrothermally altered breccia. The silicification of the tuff ring would have occurred in this stage and potentially economic minerals formed in this stage are goethite and jarosite.

Verwoerd et al. (1995) noted that the evidence for the first two stages has been largely overprinted by the extensive hydrothermal alteration of the third stage. It should be pointed out again that Verwoerd et al. (1995) did not generate or have access to data for rare earth elements (aside from the quasi-RE element Y), so this model does not specifically address REE mineralisation.

1.3 Causes and significance of REE enrichment in igneous rocks

1.3.1 Mantle metasomatism and partial melting

Metasomatism is process in which the chemical composition of a rock is altered due to the introduction of fluid or melt components, termed metasomatic agents (Yardley, 2011). The

metasomatic interaction may lead to mineral replacement but the original rock texture may remain (resulting in pseudomorphed textures). In the mantle, it can be difficult to distinguish between the metasomatism caused by melts and volatile-rich (e.g., carbonatitic or hydrous) fluids because of near-complete miscibility between these liquids.

Partial melting is a process fundamentally different from metasomatism and, in a way, may be viewed as an opposing process (i.e., extraction of a partial melt results in depletion in the more easily fusible minerals and incompatible elements, which are typically enriched by metasomatism). It is possible, however, for melts extracted from one area of the mantle to act as metasomatic agents and enrich another region, and such processes are often invoked to explain the generation of incompatible element-enriched and fertile sources in the lithosphere (e.g., Wilson et al., 1995)

Metasomatism normally occurs via two processes, infiltration and diffusion (Yardley, 2011). Infiltration metasomatism occurs by transfer of solute species in solution infiltrating through the host rock. Infiltration is compelled by pressure and concentration gradients between the infiltrating fluid and pores and fractures within the rock. Diffusional metasomatism is the process by which elements in a mobile metasomatic agent diffuse into the minerals of a stationary solid medium. Diffusional metasomatism is compelled by chemical activity gradients present at the mineral grain boundaries, where elements in areas with high chemical potential migrate to areas of lower chemical potential. The key difference between these processes is that infiltration occurs in response to external fluid pressure gradients that cause the fluids to move, whereas diffusion occurs in response to internal chemical potential gradients.

1.3.2 The significance of carbonatites as economic rare earth element deposits

Carbonatites are composed dominantly of carbonate minerals (principally calcite and dolomite) and contain a myriad of silicate, oxide and phosphate accessory minerals, many of which contain significant concentrations of the REE and other rare metals. Fresh magmatic carbonatite typically has REE contents of less than 0.5 wt.% rare earth oxides (REO; i.e., total rare earth elements in oxide form reported as weight percent; Hornig-Kjarsgaard, 1998), which can be increased up to ≈3 wt% via 'primary' mineralization by late-stage magmatic fluids (Wall, 2004; Wall and Zaitsev, 2004). The richest REE deposits hosted within carbonatites typically represent near-surface portions of the deposit that have experienced extensive interaction with

ground or meteoric water resulting in the selective dissolution of most carbonate minerals and enrichment in the REE due to their insolubility in aqueous fluids at low temperature and pressure. Such "supergene" enrichment processes can increase REE grades to more than 10 wt. % REO (Castor & Hedrick, 2006). Well-known and exploited carbonatite-hosted REE deposits include those of Mountain Pass in California, USA, Fen in Norway, Mount Weld in Western Australia and numerous localities in the Kola Peninsula, Russia (e.g., Wall et al., 2004; Castor, 2008; Hoatson et al., 2011).

Southern Africa is poised to become a major global REE supplier in the future due to the high concentration of carbonatites in this region (Fig. 1.4), as well as improvements over recent decades in transportation and other infrastructure. Large, high-grade carbonatite-hosted rare earth element deposits have been identified and are in development in virtually every southern African country (Fig. 1.4): Angola (e.g., Virulundo), Malawi (e.g., Kangankunde), Mozambique (e.g., Mt. Muambe), Namibia (e.g., Lofdal), South Africa (e.g., Zandkopsdrift), Zambia (e.g., Nkombwa Hill), Zimbabwe (e.g., Katete). New such deposits are being discovered in the region with regularity (Harmer & Nex, 2016).

With rare exception, carbonatites are believed to be derived from the Earth's mantle. The strong enrichment of carbonatites in the light REE and other elements that are incompatible in mantle minerals (e.g., Ba, Sr, Nb) strongly argues for the mantle sources of carbonatites having been modified by metasomatism. Portions of the mantle that have been fluxed with low-degree partial melts will be enriched in carbonate minerals and incompatible elements (e.g., Ionov et al., 1993), forming an ideal mantle source for carbonatite magmas. Due to the lower temperatures required to melt carbonate-bearing source lithologies, low-degree partial melts of such rocks will be enriched in carbonate and poorer in silicate components than higher-degree melts (e.g., Dalton and Presnall, 1998). Carbonatites may originate either as direct primary melts of carbonate-bearing mantle lithologies (e.g., carbonated peridotite; Eggler, 1978) or through differentiation of hybrid carbonate-silicate magmas. Formation of carbonatites by differentiation may occur through liquid immiscibility at crustal pressures and/or fractional crystallization and settling of silicate minerals and oxide minerals leaving behind a carbonate-rich residual melt (e.g., Lee and Wyllie, 1998).

Carbonatites are largely restricted to continental settings, although a few examples are

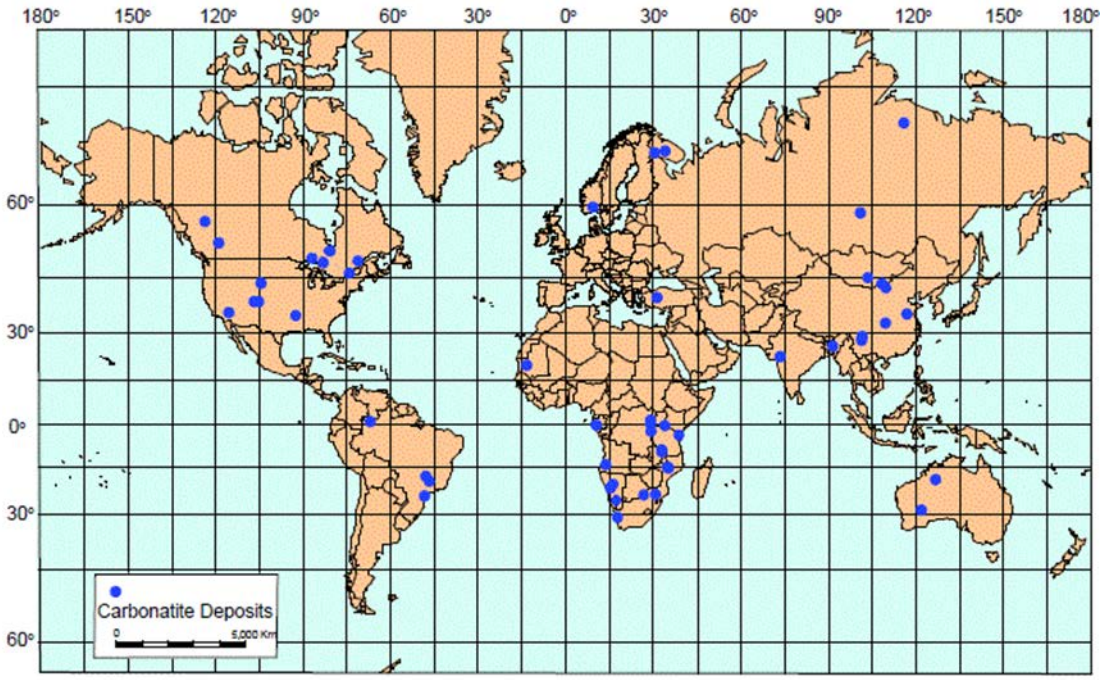

Figure 1.4. *Map of carbonatite-hosted REE deposits with proven economic potential. Note the concentration of these deposits in southern Africa. From Berger et al. (2009).*

found on ocean islands. Carbonatites have been found on every continent except Antarctica, but they are particularly abundant in southern Africa (Fig. 1) and most of these are Phanerozoic in age (Woolley, 2001). It is not obvious why this is the case, but it is likely related to the facts that (1) southern Africa has not been affected by a major orogeny for the past 400 Myr, meaning that there have not been opportunities to partially melt or otherwise disrupt metasomatised mantle sources in the lithosphere by tectonic collisions since the end of the Proterozoic, and (2) an unusually high concentration of hot spots have passed beneath southern Africa in the past 200 Myr (e.g., Tristan, Vema, Discovery, Shona, Marion, Comores; Hartnady & le Roex, 1985) and southern and eastern Africa are located above an upwelling region of the deep mantle with anomalously slow seismic velocities, alternately termed the 'African superplume' (e.g., Behn et al., 2004) or the 'African large low shear velocity province' (LLSVP; Garnero & McNamara, 2008).

In general, however, the only portions of southern African carbonatites that are deemed to represent economic REE deposits are the highly weathered and REE-enriched residual "cap zones" representing the upper 50-100 meters of carbonatite complexes, and which often only cover a portion of the carbonatite outcrop area (Harmer & Nex, 2016). These residual, lateritic

zones result from supergene processes of carbonate and phosphate dissolution by and re-precipitation from groundwater and meteoric water, and develop REE concentrations many times greater than that of the fresh or primary mineralized carbonatite.

1.4 Research Objectives

The principal objective of this study is to document the petrography and major and trace element compositions of samples of the diverse types of igneous rocks and related materials (e.g., breccias and crusts derived from igneous rocks) from the Saltpeterkop carbonatite complex and to determine the main processes responsible for their compositional variation, including their variable enrichments in rare earth elements. The aims for achieving this goal are listed below:

- Petrographic descriptions of thin sections of igneous rock samples from the Saltpeterkop carbonatite complex to provide insight into their mineralogy and textures, which aids in their classification and provides information on their crystallization history.
- Major and trace element data determined by X-ray fluorescence and solution inductively coupled plasma mass spectrometry (ICP-MS) for approximately 75 igneous samples from Saltpeterkop. The data are used for classification of the rocks, for petrogenetic interpretation and for characterisation of their sources.
- Use of these qualitative and quantitative data to evaluate, interpret and compare the diffrerent types of igneous rocks present in the Saltpeterkop carbonatite complex. Modelling of the evolution of these rocks is performed so as to relate their possible origins to each other and thereby provide a greater understanding of the origin of the Saltpeterkop complex.

2. GEOLOGICAL BACKGROUND

Saltpeterkop was first described by Rogers and Du Toit (1903) as a large volcanic neck surrounded by at least twenty smaller volcanic necks in the near vicinity.

2.1 Saltpeterkop Carbonatite Complex

The Saltpeterkop carbonatite complex is named after Saltpeterkop, itself a prominent conical peak composed of silicified volcaniclastic breccia rising to an elevation of 1766 m, that sits roughly 250 meters above a broad, dome-shaped hill. The complex is situated 20 km east-southeast of the town of Sutherland, and approximately 10 km south of the South African Astronomical Observatory. The Saltpeterkop peak is part of the summit tuff ring structure, which has an outer diameter of approximately 1.5 km (Verwoerd 1990). The breccias of the summit ring form an incomplete circular rim around a deposit of bedded tuffaceous material in the ring's interior, which is partly enclosed to the southwest by carbonatized breccia and small irregular bodies of carbonate-rich rocks which are described as sövite (de Wet, 1975). The tuff ring breccia has been intensely silicified during hydrothermal alteration and this silicification is responsible for its resistance to erosion (de Wet, 1975; Verwoerd, 1990).

The Saltpeterkop Complex is a hybrid volcanic and intrusive feature dominated by carbonatite and potassic trachyte (Verwoerd, 1990). Various authors have described Saltpeterkop as a volcanic neck (Rogers and Du Toit,1904), a breccia-filled pipe (de Wet, 1975), a diatreme (McIver and Ferguson,1979) and a volcano-plutonic alkaline ring complex positioned at the intersection of two regional fracture systems (Newton,1987). The complex is hosted by Karoo sedimentary rocks (Beaufort Group) which are intensely fractured and updomed. The sedimentary rocks are particularly strongly domed within 10 km of the centre of the ring structure, with dips as great as 60°, whereas, further away from the ring structure, the regional dip is northward at a shallow angle of 2-3°. It has been postulated that this updoming could have been caused by high gas pressures or the intrusion of a shallow magma body, resulting in deformaton, shattering and brecciation of the local sedimentary rocks (de Wet, 1975; Verwoerd, 1990). The Karoo sedimentary rocks are intruded by potassic trachyte (mainly as irregular bodies), as well as carbonatite (as dykes and sills), olivine melilitite (as dykes, sills and subvolcanic pipes) and rare ultramafic lamprophyre (as dykes and breccia pipes). The presence

of carbonatites at Saltpeterkop was first reported by Verwoerd (1967) and the presence of potassic trachyte was reported by de Wet (1975) who produced the first systematic description of the rock types at Saltpeterkop. McIver and Ferguson (1979) postulated that the melilititic, trachytic and carbonatitic eruptives at Saltpeterkop and the nearby Sutherland Commonage melilitite (a much smaller dyke/sill complex composed virtually entirely of olivine melilitite; Viljoen et al., 1988) originated by fractional crystallization, liquid immiscibility, and crystal liquid reaction phenomena operation in ascending CO_2-rich kimberlitic magmas, with the doming of the country rock ascribed to the pressure of exsolved volatiles.

It is important to note that more than 2/3 of all samples analysed in this thesis come from locations situated outside of the main ring structure (i.e., more than 1.3 km from the centre of complex, located approximately at 32°28'49"S, 20°50'30"E), due to the fact that nearly all samples within the ring structure itself have been strongly hydrothermal altered. The igneous rocks sampled are mainly intrusive (hypabyssal), and many are also strongly brecciated.

2.2 The Age of the Saltpeterkop Complex

The age of the Saltpeterkop Complex is approximately 75 Ma. This is based on a K-Ar age of 74.7 ± 3 Ma obtained on a phlogopite megacryst by Duncan et al. (1978) and a 76.5 ± 3.3 Ma age by the Rb-Sr isochron technique obtained on a variety of minerals separated from a sample of the M5 olivine melilitite pipe by Malarkey et al. (2010), within error of the older age.

The nearby Sutherland Commonage olivine melilitite locality was dated to be 74.8 ± 3 Ma by whole rock K-Ar (also by Duncan et al., 1978), but was subsequently dated to be 66 ± 1 Ma by the Rb-Sr isochron technique using phlogopite separates (K.S. Viljoen, unpublished, reported in Phillips et al., 2000). Phillips et al. (2000) have said, on the basis of comparison between K-Ar age data and that from more state-of-the-art techniques (e.g., $^{40}Ar/^{39}Ar$), that K-Ar ages are problematic and most are likely inaccurate. They stated that the 66 Ma age is a more robust age for all mafic alkaline magmatism near Sutherland.

2.3 Saltpeterkop regional fracture patterns

Regional fracture patterns around the Saltpeterkop Carbonatite Complex have been studied by Newton (1987) and Chevallier (1997). Saltpeterkop is situated at the intersection of two arcuate fracture swarms, a NE swarm and an EW swarm (Chevallier, 1997). Both swarms

cover an area approximately 200km long and 50km wide. Newton (1987) postulated that the intrusion of the Saltpeterkop diatreme location was determined by the pre-existing fractures but, in contrast, Chevallier (1997) proposed that the fractures around Saltpeterkop as well as fractures controlling the expression of kimberlites further to the northeast, were a result of circulation patterns of the asthenospheric mantle.

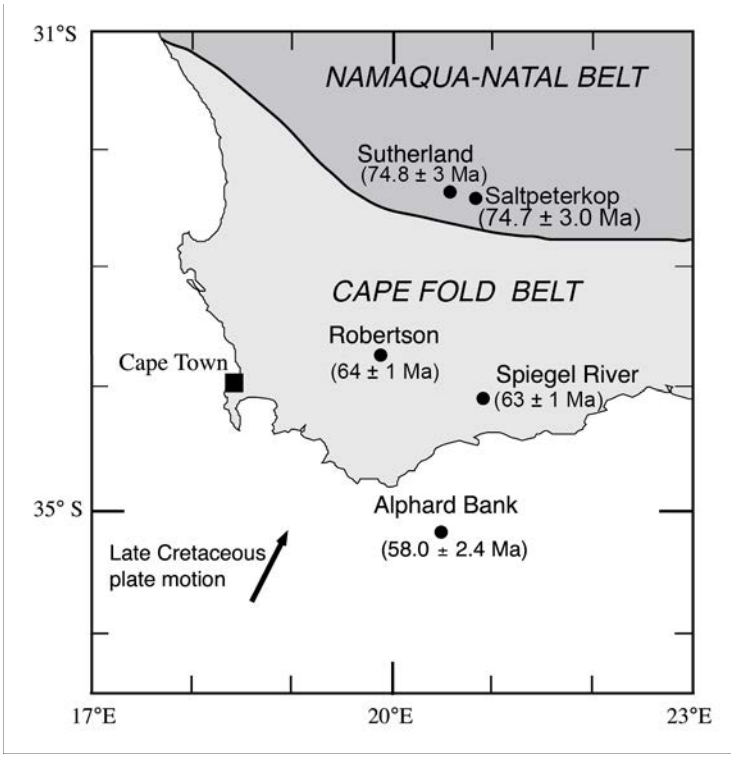

Figure 2.1. *Map of the Western Cape melilitite province adapted from Janney et al. (2002). Ages (by K-Ar) are from Dingle and Gentle (1972) and Duncan et al. (1978).*

2.4 Western Cape olivine melilitite province

Dingle and Gentle (1972) proposed that Saltpeterkop forms part of an age-progressive, roughly N-S oriented magmatic lineation extending from the Agulhas Bank to the southern Karoo. Janney et al. (2002) termed this lineation the "Western Cape olivine melilitite province" (Fig. 2.1), which includes early Palaeocene submarine alkali basalts and trachytes on the Alphard Bank as the youngest and most southerly member, as well as olivine melilitite diatremes of earliest Palaeocene age at Robertson and Spiegelrivier in the southern coastal region, and the Sutherland Commonage olivine melilitites and Saltpeterkop complex as its oldest and most northerly members. Duncan et al. (1978) proposed that this lineation is possibly related to the active Bouvet hotspot in the far south Atlantic. However, more recent plate motion models

(O'Connor et al., 2012) do not support this hypothesis, although it is true that the rate of plate motion calculated, if one assumes that the igneous rocks of the Western Cape melilitite province were generated by a stationary melt source, is similar to the projected speed of African plate motion over the period of 58 to 75 Ma (Janney et al., 2002).

2.5 The rocks of the of Saltpeterkop Complex

The Saltpeterkop Complex is a volcanic-intrusive igneous complex that consists mainly of volcaniclastic deposits as well as a variety of intrusive igneous rocks. The former includes the prominent central ≈1 km diameter tuff ring and crater-fill (mainly composed of volcaniclastic breccias and sediments; Fig. 2.2), as well as a small number of satellite pipes filled with volcaniclastic breccias (e.g., the Silver Dam breccia pipe) or, more rarely, hypabyssal olivine melilitite (e.g., the M5 and M6 olivine melilitite pipes; deWet, 1975). The vast majority of fresh igneous rocks of the complex are exposed as dykes (carbonatite, olivine melilitite and ultramafic lamprophyre), sills (carbonatite and olivine melilitite) and irregular intrusions (primarily potassic trachyte), although carbonatites, trachytes and ultramafic lamprophyres can also occur in pipe-like subvolcanic intrusions and brecciated forms without a clear intrusive context (Verwoerd et al., 1990). The intrusive rocks are hosted in Beaufort Group (Triassic) sedimentary rocks of the Karoo Supergroup (deWet, 1975), and Saltpeterkop is located near the southwestern margin of the Karoo sedimentary basin. In general, these intrusive igneous rocks are most prevalent on the outer slopes of the tuff ring and, more generally, within 2-3 kilometers of the centre of the ring structure. However, intrusive/subvolvanic igneous rocks apparently directly related to the Saltpeterkop complex exist as far as 17 km from the center of the complex.

The volcaniclastic breccias and sediments forming the ring structure and central depression apparently formed as the result of explosive volcanism, however the nature of the main magma type responsible for the explosive volcanism is not known due to the lack of

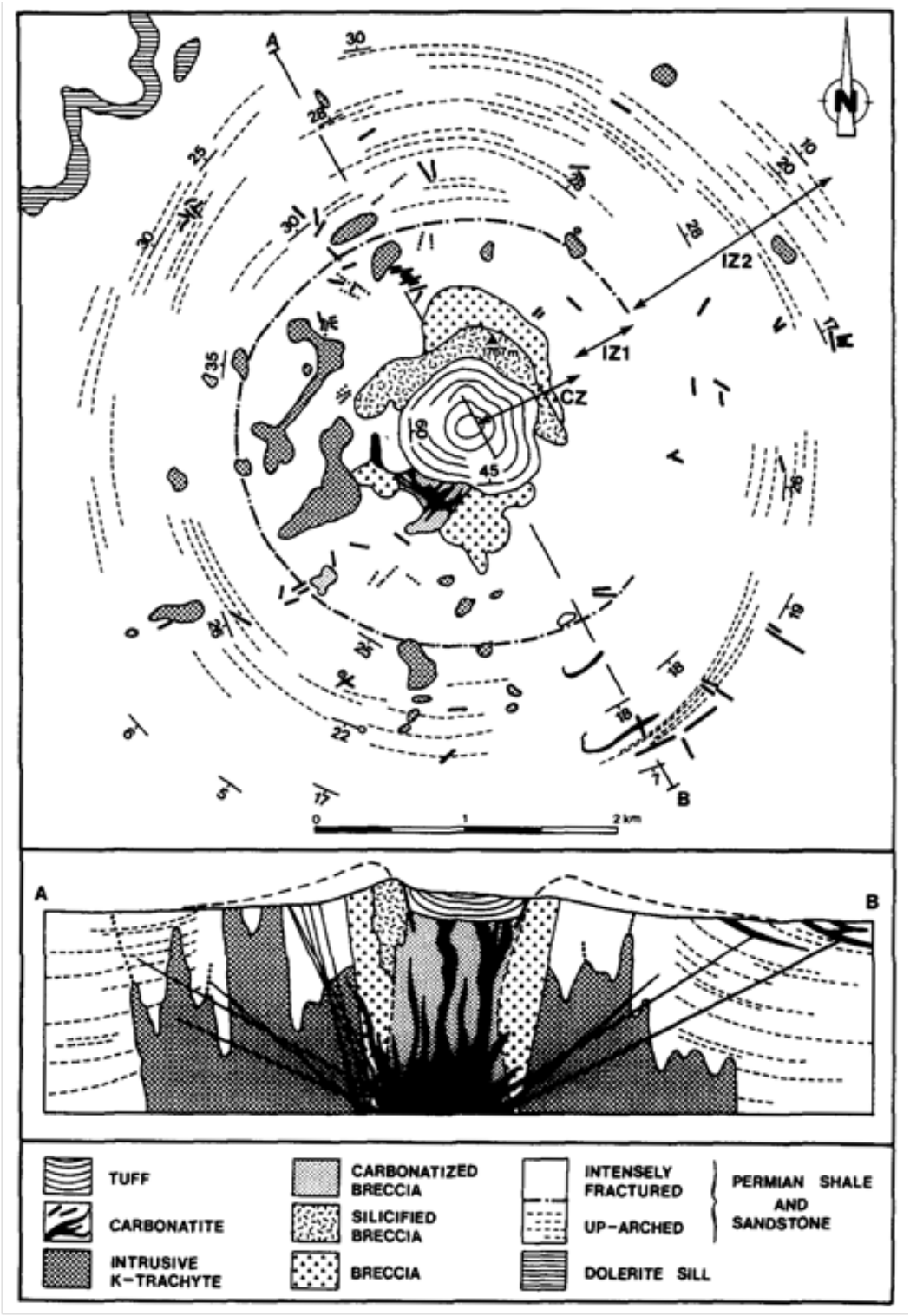

Figure 2.2. *Geological sketch map and cross section of the Saltpeterkop Complex from Verwoerd (1990). Dotted curves indicate deformation of regionally flat-lying Beaufort Group sedimentary rocks.*

recognisable extrusive rocks (e.g., lavas and magmatic pyroclastic rocks) and the fact that most volcaniclastic breccias have been extensively altered by hydrothermal activity (Verwoerd, 1990). The petrography and mineralogy of subvolcanic (hypabyssal) and intrusive alkaline and associated rocks at the Saltpeterkop Complex have been described to some extend by de Wet (1975), McIver & Ferguson (1979), Boctor & Yoder (1986), Verwoerd (1990) and Verwoerd et al. (1995), but none of these studies have provided detailed petrography, mineral chemistry or whole-rock major and trace element geochemistry of a representative selection of these igneous rocks, which is the main goal of this thesis.

2.5.1 Carbonatite

Saltpeterkop carbonatite occurs mainly as dykes and sills and, less commonly, as subvolcanic pipes and brecciated rocks of unclear, but likely volcaniclastic origin. de Wet (1975) described two textural types of carbonatites present: sövite, and alvikite.

According to de Wet (1975) Saltepeterkop sövites are essentially medium to coarse-grained (3-6 mm) rocks that consist of anhedral to subhedral calcite, goethite, pyrite and pyrochlore. The calcite crystals tend to have a sub-parallel orientation, and display twinning. de Wet (1975) also noticed that, in a few circumstances, the calcite crystals contained inclusions of dolomite. Saltpeterkop sövites also often contain fragments of the surrounding country rock. Saltpeterkop alvikites are fine-grained rocks that de Wet (1975) reported as consisting of hornblende, biotite and opaque oxide minerals set in a groundmass consisting mainly of elongated crystals of calcite with occasional K-feldspar.

2.5.2 Potassic trachyte

Potassic trachyte is described by de Wet (1975) as a porphyritic rock containing euhedral sanidine (up to 1 cm in size), euhedral nepheline (3 to 7 mm), rare biotite phenocrysts and, more rarely, apatite and fluorite microphenocrysts. The groundmass consists of devitrified glass, feldspar microlites and fine dusty oxide minerals. de Wet (1975) divided the potassic trachytes in two groups; contaminated and uncontaminated. The uncontaminated potassic trachytes have a red-brown colour when they are fresh and do not contain significant amounts of country rock, whilst the contaminated trachytes are lighter in colour, tend to be brecciated and contain a significant proportion of Beaufort sandstone country rock xenoliths within a trachyte matrix.

2.5.3 Olivine melilitites

Olivine melilitite occurs as dykes, sills and as pipe-shaped subvolcanic intrusions on all sides of the central ring complex (de Wet, 1975). The age relationships between the breccias, carbonatite dykes and olivine melilitites have not been established, but it will be assumed here as previous authors have done (e.g. Verwoerd, 1990), that all were emplaced contemporaneously, or nearly so. Olivine melilitite outcrops tend to have a 1-2 cm thick weathered rind on the surface but are fresh in the interior, with a dark gray colour. The melilitites typically have euhedral olivine phenocrysts ranging from 1 mm to 5 mm, as well as large amounts of melilite microphenocrysts and anhedral phlogopite set in aphanitic groundmass. de Wet (1975) mentioned that in some of the olivine melilites (e.g. M6) the olivine phenocrysts have rims of serpentine. The biotite phenocrysts, when present, can range up 2 cm in length, although they are far more commonly less than 1 mm in size (de Wet, 1975). The groundmass of the olivine melilitite typically consists of melilite, monticellite, phlogopite and nepheline, with spinel, perovskite apatite and wollastonite as accessory minerals (Malarkey et al., 2010). The melilite laths present are often oriented parallel to the olivine phenocrysts and may have spinel inclusions (de Wet, 1975; Malarkey et al., 2010). Perovskite appears as small (20μm-50μm) euhedral yellowish-brown crystals (de Wet, 1975). Apatite commonly occurs as needles (100 μm × 10 μm) in the groundmass (Malarkey et al., 2010).

2.5.4 Ultramafic lamprophyres

Ultramafic lamprophyres (in essence, rocks with more than 90 modal % mafic minerals + carbonate that do not fall within the conventional classifications for melilitites, carbonatites, kimberlites or lamproites) occur as rare dykes and pipes present in at least four main localities in the southern part of the Saltpeterkop complex and have not been described previously. Their petrography is described in Chapter 4.

2.5.5 Miscellaneous rock types

Fe and Mn oxide-rich crusts and mineralised breccias: Brown to black iron-rich oxide crusts are common as coatings on igneous and sedimentary rocks within 5 km of the central ring structure. There are many instances of breccias composed of Karoo sandstone clastic fragments (0.5 to 2.0 cm) that are cemented by iron oxide crusts. On the central tuff-ring itself, cobble-sized pieces (>10 mm) iron-rich oxide crust and, in places, massive iron-rich oxide deposits also

occur, most notably on the northwestern region portion of the tuff ring adjacent to the Saltpeterkop peak. It is possible that some of these crusts and coatings could represent altered late-stage ferrocarbonatite, but the thicker crusts and massive oxide deposits on the tuff ring are likely related to hydrothermal activity (Verwoerd et al., 1995).

Dolerites: Dolerite sills and dykes are fairly abundant in the area surrounding Saltpeterkop, although all of these appear to be related to the Jurassic Karoo large igneous province (e.g., Duncan and Marsh, 2006) rather than to Cretaceous alkaline magmatism. In some cases, dolerite occurs as xenoliths within Saltpeterkop intrusive rocks and volcaniclastic breccias. No dolerite data are presented in this thesis as they are unrelated to and pre-date the Saltpeterkop Complex magmatism.

3. SAMPLES AND METHODS

Samples in this study come from three sources: (1) field collection during visits in 2015, 2016 and 2017 and also from the research collections of (2) Prof. Wilhelm Verwoerd, Stellenbosch University and (3) Dr. Luc Chevallier of the Council for Geoscience (Bellville office). Additionally, data for three of the samples were originally reported in Janney et al. (2002; SPK-1, -2 and -3, all from the M5 olivine melilitite pipe). All sample preparation and analysis was performed in the Department of Geological Sciences at the University of Cape Town.

3.1 Sample locations and sample names.

Sampling was guided by maps in de Wet (1975), Verwoerd (1990) and unpublished field maps provided by Dr. Luc Chevallier. With regard to sample naming, all samples with a WV95 prefix come from the sample collection of Prof. W.J. Verwoerd. Those with a SP-# or SP# prefix (where the # is a two or three digit number, in some cases followed by a letter) are either from (a) the sample collection of Dr. L. Chevallier (SP-#, e.g., SP-25A, SP-400) or (b) samples collected in the field from locations confidently identified as the same outcrops as those from where the Chevallier samples came (SP#-n, e.g., SP31-1, SP38-1, SP43-2, SP206-3, etc.) with the final number simply used to differentiate separate samples from the same outcrop or feature. Other sample prefixes used in this study are SD- (designating volcaniclastic breccia samples from the **S**ilver **D**am breccia pipe on Farm Matjiesfontein), SKR- (designating samples obtained within or on the edges of the **S**altpeter**K**op **R**ing structure), and SK (e.g., SK1-1). A subset of the latter are samples from the M1, M2, M5 and M6 melilitite dyke, sill and pipe localities originally identified by de Wet (1975), which have sample numbers such as SKM1-1, SKM2-1, SKM5-1 and SKM6-1. Finally, several samples have SPKC- prefixes which are non-specific and apply variously to a variety of igneous rocks in the **S**alt**p**eter**k**op **C**omplex, mainly carbonatites and ultramafic lamprophyres.

3.2. Sample collection and rock type distribution

Samples were collected for this study during field trips in March 2015, March 2016 and June 2017. Due to the widely distributed nature of intrusive igneous activity associated with the

Table 3.1. List of sample information and locations from the Saltpeterkop Complex

Location	Type	Sample no.	Rock type	Latitude Deg	min	sec	Longitude Deg	min	sec	GPS location	Notes
Carbonatite localities											
WV95-20	dyke	WV95-20	carbonatite	32	29	33	20	49	24	N	in-situ
WV95-21	dyke	WV95-21	carbonatite	32	29	23	20	49	20	N	in-situ
WV95-22	breccia pipe/dyke	WV95-22	carbonatite	32	29	23	20	48	20	N	in situ
WV95-24	dyke	WV95-24	carbonatite	32	28	6.5	20	50	13	N	in situ
WV95-25	breccia pipe/dyke	WV95-25	carbonatitic breccia	"	"	"	"	"	"	N	in-situ
WV95-26	pipe or dyke	WV95-26	carbonatite	"	"	"	"	"	"	N	in-situ
WV95-28	unknown	WV95-28	carbonatite	32	29	55	20	51	19	N	
WV95-29	unknown	WV95-29	carbonatite	32	29	56	20	51	13	N	
SP16	breccia pipe/dyke	SP-16A	carbonatitic breccia	32	29	35	20	49	45	N	in-situ
SP16	"	SP-16C	carbonatitic breccia	"	"	"	"	"	"	N	in-situ
SP19	sill	SP-19A	carbonatite	32	26	5	20	48	55	N	in-situ
SP26	dyke	SP-26A	carbonatite	32	29	55	20	48	20	N	in-situ
SP26	dyke	SP-26B	carbonatite	32	29	55	20	48	20	N	in-situ
SP27A	breccia pipe/dyke	SP-27A	carbonatite	32	30	45	20	52	27	N	in-situ
SP27B	breccia pipe/dyke	SP-27B	carbonatite	32	30	50	20	52	40	N	in-situ
SP27C	sill	SP-27C	carbonatite	32	30	50	20	52	35	N	in-situ
SP27D	breccia pipe/dyke	SP-27D	carbonatite	"	"	"	"	"	"	N	in-situ
SP331A	dyke	SP-331A	carbonatite	32	28	15	20	50	0	N	in-situ
SP400	unknown	SP-400	carbonatite	32	29	35	20	50	1	N	
SP402	dyke	SP-402	carbonatite	32	29	28	20	51	20	N	in-situ
SP403	dyke	SP-403	carbonatite	"	"	"	"	"	"	N	in-situ
SP404	dyke	SP-404	carbonatite	"	"	"	"	"	"	N	in-situ
SPKC-4	dyke (?)	SPKC-4	altered carbonatite	32	28	48	20	50	11	Y	loose fragment
SPKC-6	dyke	SPKC-6	carbonatite	32	30	43	20	52	29	Y	in-situ
SPKC-8	breccia pipe/dyke	SPKC-8	carbonatitic breccia	32	29	40	20	50	28	Y	in-situ
SPKC-9	dyke	SPKC-9	carbonatite	32	29	41	20	50	36	Y	in-situ
SPKC-13	dyke	SPKC-13	carbonatite	32	29	52	20	52	1.3	Y	in-situ
SK1-B1	breccia pipe/dyke	SK1-B1	carbonatitic breccia	32	27	30	20	49	18	Y	loose fragment
Potassic trachyte localities											
WV95-23	irregular int.	WV95-23	Potassic trachyte	32	28	6	20	50	12	N	in-situ
WV95-23	irregular int.	WV95-23A	Potassic trachyte	"	"	"	"	"	"	N	in-situ
WV95-23	irregular int.	WV95-23B	Potassic trachyte	"	"	"	"	"	"	N	in-situ
WV95-23	irregular int.	WV95-23C	Potassic trachyte	"	"	"	"	"	"	N	in-situ
WV95-27	breccia dyke	WV95-27	Potassic trachyte	"	"	"	"	"	"	N	in-situ
SP307	unknown	SP307-3	Potassic trachyte	32	28	55	20	55	56	Y	float
SP307	unknown	SP307-4	Potassic trachyte	"	"	"	"	"	"	Y	float
SP401	irregular int.	SP-401	Potassic trachyte	32	29	39	20	50	20	Y	in-situ
SPK-CRB	breccia	SPK-CRB	Potassic trachyte	32	28	35	20	50	16	Y	large number of sandstone xenoli
SK1-B2	breccia	SK1-B2	Potassic trachyte	32	27	30	20	49	18	Y	in-situ
SK2-1	breccia	SK2-1	Potassic trachyte	32	28	23	20	49	32	Y	float
SKR-1	irregular int.	SKR-1	Potassic trachyte	32	28	44	20	50	12	Y	in-situ
SKR-5	breccia	SKR-5	trachytic breccia	32	29	0.5	20	50	29	Y	in-situ
M5	xenolith	SKM5-2	fine trachytic breccia	32	26	9	20	51	0	Y	near margin of ol. melilitite plug

The terms "breccia pipe" and "breccia dyke" refer primarily to carbonatitic or trachytic pipe or dyke features that contain a large amount of fragmental material (which may be of magmatic or country rock origin). "Breccia" simply refers to brecciated outcrops that do not have a clear intrusive origin (e.g., volcaniclastic breccias). Features labelled "pipe/dyke" refer to small, poorly exposed outcrops where it was not possible to determine the precise nature of the intrusion. "Irregular int." is a term used to describe intrusive trachyte bodies that do not appear to represent pipes, dykes or sills. Rock samples described as "breccias" may contain some xenolithic material. Locations for samples without GPS coordinates were determined from

Table 3.1. continued.

Location	Type	Sample no.	Rock type	Latitude Deg	min	sec	Longitude Deg	min	sec	GPS location	Notes
Olivine melilitite localities											
M1	sill	SKM1-1	olivine melilitite	32	28	30	20	49	26	Y	in-situ
M2	dyke	SKM2-1	olivine melilitite	32	28	32	20	49	29	Y	in-situ
M5	pipe	SKM5-1	olivine melilitite	32	26	9	20	51	0	Y	in-situ
M5	"	SPK-1	olivine melilitite	"	"	"	"	"	"	Y	in-situ
M5	"	SPK-2	olivine melilitite	"	"	"	"	"	"	Y	in-situ
M5	"	SPK-3	olivine melilitite	"	"	"	"	"	"	Y	in-situ
M6	pipe	SKM6-1	olivine melilitite	32	25	50	20	50	43	Y	in-situ
SP31	pipe	SP-31	olivine melilitite	32	28	16	20	46	51	N	in-situ, thin section only
SP31	pipe	SP31-3	olivine melilitite	32	28	16	20	46	51	Y	in-situ
SP31	"	SP31-4	olivine melilitite	"	"	"	"	"	"	Y	in-situ
SP43	dyke	SP-43	olivine melilitite	32	28	49	20	55	46	N	in-situ
SP43	"	SP43-1	olivine melilitite	"	"	"	"	"	"	Y	in-situ
SP43	"	SP43-2	olivine melilitite	"	"	"	"	"	"	Y	in-situ
SP43	"	SP43-3	olivine melilitite	"	"	"	"	"	"	Y	in-situ
SP206	dyke or pipe	SP206-1	olivine melilitite	32	34	38	20	42	19	Y	float
SP206	"	SP206-2	olivine melilitite	"	"	"	"	"	"	Y	in-situ (?)
SP206	"	SP206-3	olivine melilitite	"	"	"	"	"	"	Y	in-situ (?)
Ultramafic lamprophyre localitites											
WV95-19	breccia pipe/dyke	WV95-19	UM lamprophyre breccia	32	30	47	20	49	15	N	in-situ
SP38	breccia pipe	SP-38	UM lamprophyre breccia	32	29	16	20	45	26	N	in-situ
SP38	"	SP38-1	UM lamprophyre breccia	"	"	"	"	"	"	Y	in-situ
SP38	"	SP38-2	UM lamprophyre breccia	"	"	"	"	"	"	Y	in-situ
SP38	"	SP38-3	UM lamprophyre breccia	"	"	"	"	"	"	Y	in-situ
SP367	dyke	SP367-1	ultramafic lamprophyre	32	29	53	20	52	1	Y	in-situ
SPKC-12	breccia dyke	SPKC-12	UM lamprophyre breccia	32	29	55	20	51	59	Y	in-situ
SPKC-14	dyke	SPKC-14	ultramafic lamprophyre	32	29	40	20	50	52	Y	in-situ
Silver Dam	breccia pipe	SD-1G	UM lamprophyre breccia	32	29	14	20	48	19	Y	prepared from several loose fragr
Silver Dam	"	SD-1M	UM lamprophyre breccia	"	"	"	"	"	"	Y	prepared from several loose fragr
SKGB-1	breccia pipe/dyke	SKGB-1	altered UML breccia	32	28	31	20	49	27	Y	in-situ
Fe- & Mn-rich oxide crusts & oxide-rich breccia localities											
SK2-2	gossan/crust	SK2-2	Fe- & Mn-rich oxide crust	32	28	23	20	49	32	Y	float
SKR-2	gossan/crust	SKR-2	Fe- & Mn-rich oxide crust	32	28	44	20	50	14	Y	float
SKR-3	gossan/crust	SKR-3	Fe- & Mn-rich oxide crust	32	28	33	20	50	19	Y	float
SK2-3	min. breccia	SK2-3	Fe- & Mn-oxide rich breccia	32	28	23	20	49	32	Y	in-situ
SKR-4	min. breccia	SKR-4	Fe- & Mn-oxide rich breccia	32	28	33	20	50	19	Y	in-situ
Crustal xenolith localities											
Silver Dam	breccia pipe	SD-SHALE	shale	32	29	14	20	48	19	Y	upper crustal xenolith
Silver Dam	breccia pipe	SDCX-3	clinopyroxenite	"	"	"	"	"	"	Y	mid-/lower crustal xenolith
Silver Dam	breccia pipe	SDCX-4	amphibolite	"	"	"	"	"	"	Y	mid-/lower crustal xenolith
SP100	breccia pipe	SP-100	biotite schist xenolith	32	29	49	20	51	12	N	mid-/lower crustal xenolith

field sampling maps provided by W.J. Verwoerd and L. Chevallier. In "notes" section, samples described as "in-situ" were sampled in place, those described as fragmental were clearly from the outcrop but were not in place, those described as "float" had moved a significant distance and their precise origin location is unknown.

Complex, and the intense hydrothermal alteration that characterises the vicinity of the central tuff ring structure, the vast majority of samples (nearly 75%) come from locations more than 1.3 km from the centre of the Complex. It is important to note that, for the purposes of this study, the relatively small Sutherland Commonage olivine melilitite intrusive complex (Viljoen, 1988) is regarded as being separate from the Saltpeterkop Complex.

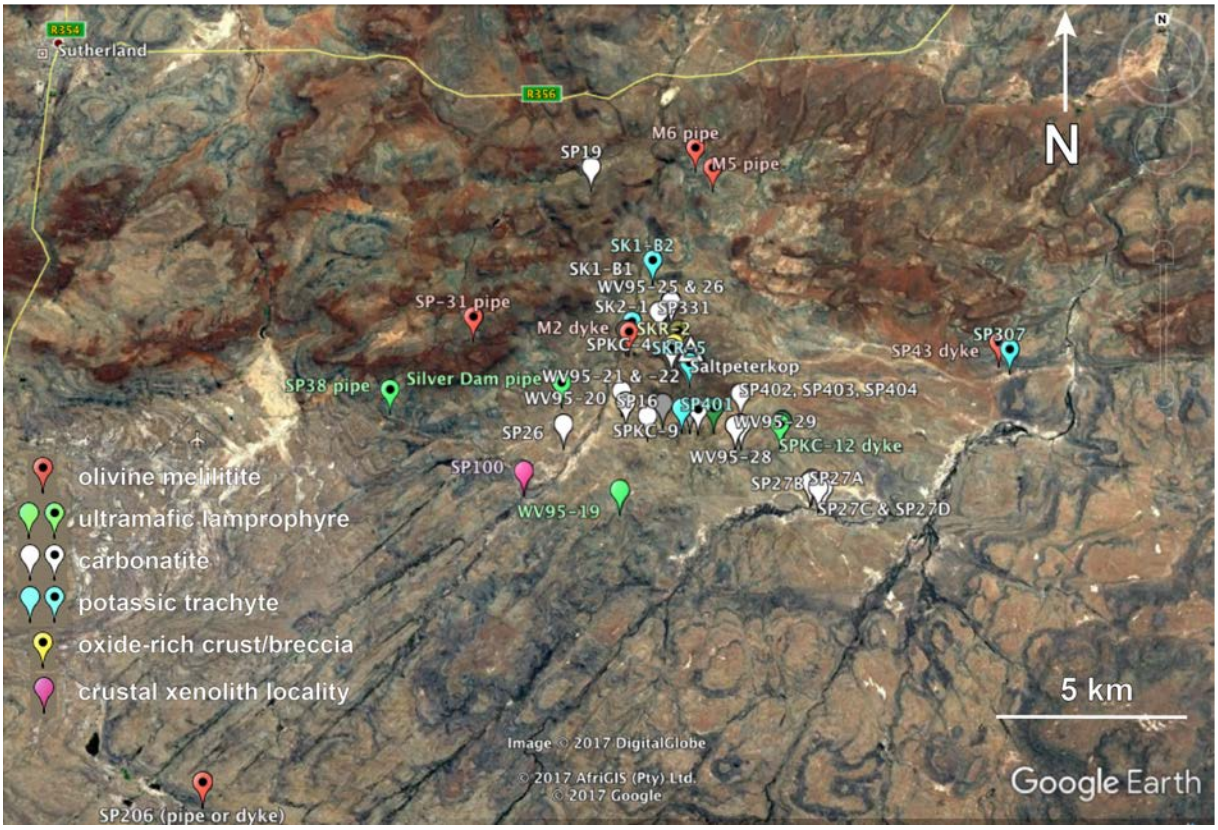

Figure 3.1. *Map of sample localities in vicinity of the Saltpeterkop carbonatite complex. Note the location of Sutherland in the extreme northwest of the map and olivine melilitite locality SP206 in the extreme southwest. Rock localities are colour coded by type (see legend) and symbols with dots indicate sampling locations with coordinates obtained by GPS. Plain symbols (without dots) represent sample locations inferred from field maps of W.J. Verwoerd and L. Chevallier. White triangle marks the location of Saltpeterkop peak. (Google Earth image)*

With regard to outcrop patterns, Fe and Mn-rich oxide-rich crusts and mineralised breccias are confined to the central ring structure, whereas potassic trachyte samples are also generally concentrated near the centre of the complex. Carbonatite samples, mainly obtained from dykes and sills, mainly come from within 5 km of the complex centre, with most samples coming from the southern portion of the complex. Olivine melilitites and ultramafic lamprophyre samples were obtained from a wider range of distances. Sampled olivine melilitite bodies include dykes, sills and pipes to the north, south, east and west of the complex, at distances of 1.9 to 16.3 km from the centre. Ultramafic lamprophyres were mainly sampled from pipe and dyke localities in the west, south and southeast of the complex, at locations up to 8 km from the centre.

3.3 Sample preparation

Whole rock powders were prepared from the freshest available samples. The samples were split using a hydraulic splitter and crushed into fragments smaller than 10mm using a jaw crusher. Rock chips from these samples were examined under the binocular microscope, and carefully selected to avoid inclusions and to exclude chips with obvious country rock inclusions/xenoliths and also to exclude, where possible, the more altered portions of the samples. The rock chips selected were placed in a SiebTechnik carbon steel swing mill and ground to a fine powder. This powder was used in all subsequent analytical analyses. Typically, 50-200 g of picked rock chips per sample were milled.

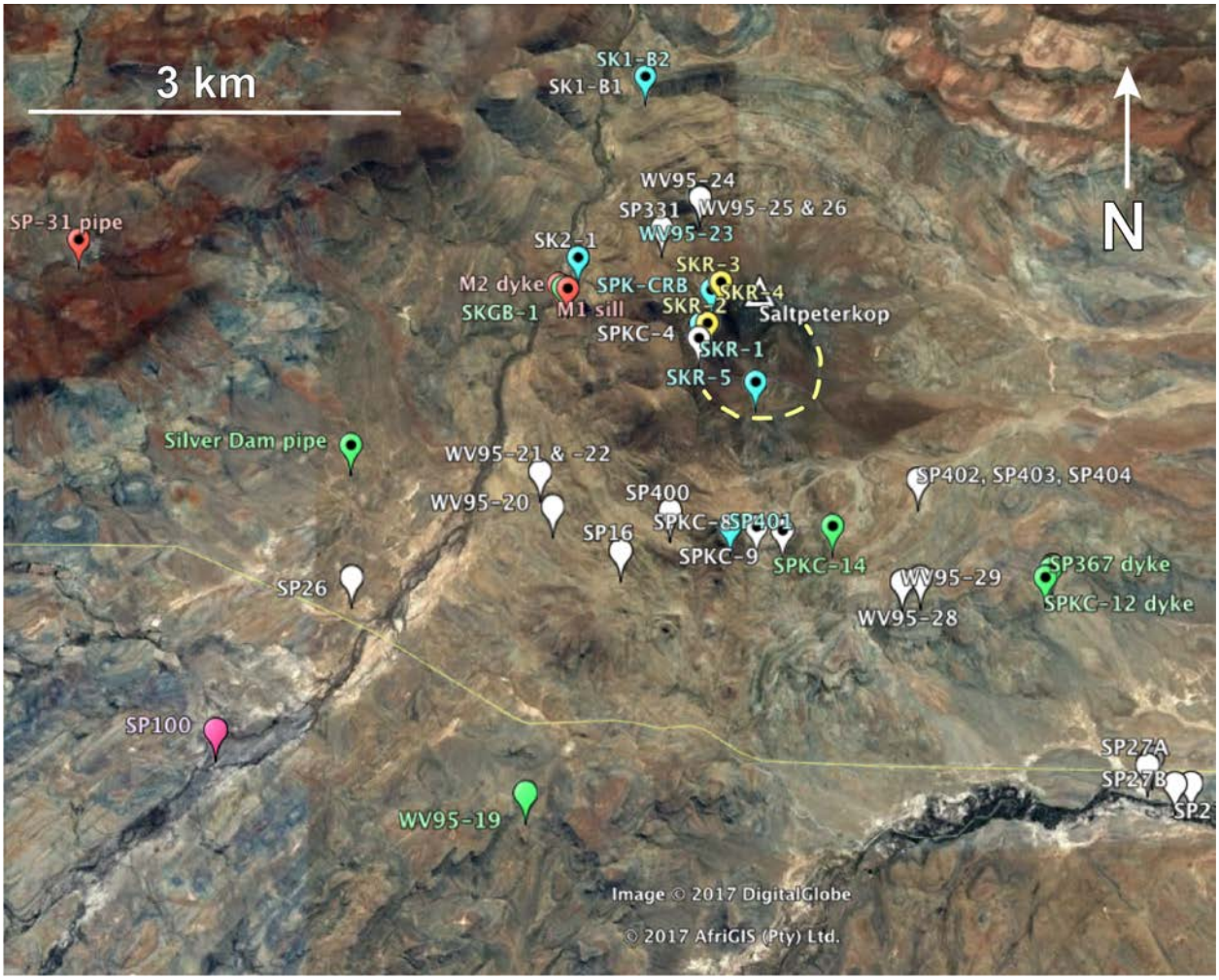

Figure 3.2. *Closeup of the centre of the Saltpeterkop complex with sampling locations. Yellow dashed circle indicates the central tuff ring structure. Symbols are the same as in Figure 3.1.*

3.4 Whole-rock geochemistry

3.4.1 X-ray fluorescence

All samples were analysed for whole-rock major oxides and trace elements. Major elements and selected trace elements were analysed using X-ray fluorescence spectrometry (XRF) at UCT. The analyses were carried out using a Panalytical Axios XRF spectrometer in the

Figure 3.3. *Photo of the SP38 ultramafic lamprophyre breccia (from breccia pipe). Clasts include rounded juvenile lapilli and angular sandstone country rock fragments. Lens cap (50 mm) for scale.*

Department of Geological Sciences, University of Cape Town. Fusion disks and pressed powder briquettes were used for XRF major and trace element measurements, respectively. The powder briquettes were made from 6g of the sample powder (mixed with 2 drops of polyvinyl alcohol as binder) and a coating of 4g of boric acid around the sides and back of the pellet. The sample and boric acid coating were then compressed with 10 tonnes of pressure to create the powder briquette. The fusion discs were generated by weighing out 2g of sample into a crucible. The crucible was then placed in an oven at 110 °C overnight, then weighed (to determine H_2O^-) and then roasted at 850 °C for four hours to determine loss on ignition (LOI) and to oxidise all Fe to Fe^{3+}. The ignited sample powder was then removed and 0.7g of the ignited sample powder was added to 6g of a mixed 57% Li tetraborate- 43% Li metaborate flux with a small amount of LiBr added as the releasing agent. The mixture was then melted in a Pt crucible over a gas flame and poured into a Pt mold (using a Claisse M4 fluxer) to form a fusion disc.

XRF major and trace element measurements were performed separately but in both cases, calibration was performed using a series of well-characterised natural rock powder standard reference materials issued by organisations such as MINTEK, the United States Geological Survey and the Geological Survey of Japan, prepared identically as samples for analysis. In all cases, measured analyte peak intensities were corrected for background. Analyte peak intensities for trace element measurements were also corrected for absorption and enhancement effects (through the use of mass attenuation coefficients) and spectral line overlaps (e.g., RbK_{β} on YK_{α}).

3.4.2 Inductively Coupled Plasma – Mass Spectrometry

Concentrations of a larger set of trace elements, including the rare earth elements (REE), were determined by inductively coupled plasma-mass spectrometry (ICP-MS) on selected samples of all rock types using a Thermo X-Series 2 quadrupole ICP-MS instrument, also in the Department of Geological Sciences. Because many of the samples in this study contain resistant oxide phases such as perovskite and pyrochlore, all samples analysed for trace elements by ICP-MS in this study were processed using high temperature-high pressure bomb digestion to ensure complete sample dissolution. Typically, 20-30 milligrams of sample was weighed out into 3 ml teflon vials and 2 ml of a 3:1 concentrated HF-HNO_3 mixture was added, then the vials were capped. The 3 ml vial was then placed inside of the teflon capsule of a steel-jacketed Parr digestion vessel along with 2 ml of ultrapure water to mitigate the pressure differential inside the smaller and larger teflon containers. These bombs were then placed in an oven at 200°C for 18-24 hours for digestion to take place. After the oven was switched off and the bombs were cool enough to handle, they were disassembled, and the inner 3 ml teflon vial was carefully opened and placed on a hotplate at 100°C to evaporate the HF-HNO_3 acid mixture. Once the samples were dry, 2 ml of concentrated nitric acid (HNO_3) was added and the resuspended sample remained on the hot plate until dry. This procedure was repeated once more with 2 ml of concentrated nitric acid. Once the sample was dry, it was diluted (typically in two stages) by a factor of 15 000 to 20 000 with a of 5% nitric acid solution containing 10 ppb of the internal standard elements Rh, In, Re and Bi. The diluted sample was placed in a 15 ml centrifuge tube for analysis.

Acquisition of solution ICP-MS trace element data was performed in peak-jumping mode. Each sample analysis consisted of 3 sets of 100 sweeps across the mass spectrum, with

dwell times on each selected atomic mass (including analytes, internal standards and interferences) of 40 milliseconds. The ion intensities obtained were converted into concentrations through calibration using a series of six synthetic calibration standards prepared from certified multielement standard solutions, spanning a concentration range of nearly three orders of magnitude to ensure that all analyte intensities in all samples fell within the calibrated range. Accuracy and precision were monitored through the analysis of the USGS rock standards COQ-1 (carbonatite; GeoREM preferred values used, http://georem.mpch-mainz.gwdg.de) and AGV-1 (andesite; values from Eggins et al., 1997) and the UCT in-house mid-ocean ridge basalt glass standard V5-40-56 (e.g., Janney et al., 2005). Errors were better than 3%, relative, and detection limits were in the lower ppb range (see Appendix 2, Table 3 for average values obtained for rock standards analysed as unknowns).

4. PETROGRAPHY OF THE SALTPETERKOP IGNEOUS ROCKS

The petrography of the igneous and related rocks of the Saltpeterkop complex is described below, divided into sections by rock type. The samples were classified on the basis of mineralogy, texture and (in the case of the carbonatites) chemical composition. The rocks are described in order of decreasing abundance as estimated from exposures in the field.

4.1 Petrography of carbonatites

Sampled Saltpeterkop carbonatites can be divided into two main types on the basis of their major element composition: *calciocarbonatites* and and *ferruginous calciocarbonatites* (based on the classification of Gittins & Harmer, 1997), *magnesiocarbonatites* and *ferrocarbonatites* were also sampled, but these are relatively minor. Texturally, the vast majority of carbonatites sampled are porphyritic alvikites (fine-grained porphyritic calcite carbonatites), with sövites being very minor.

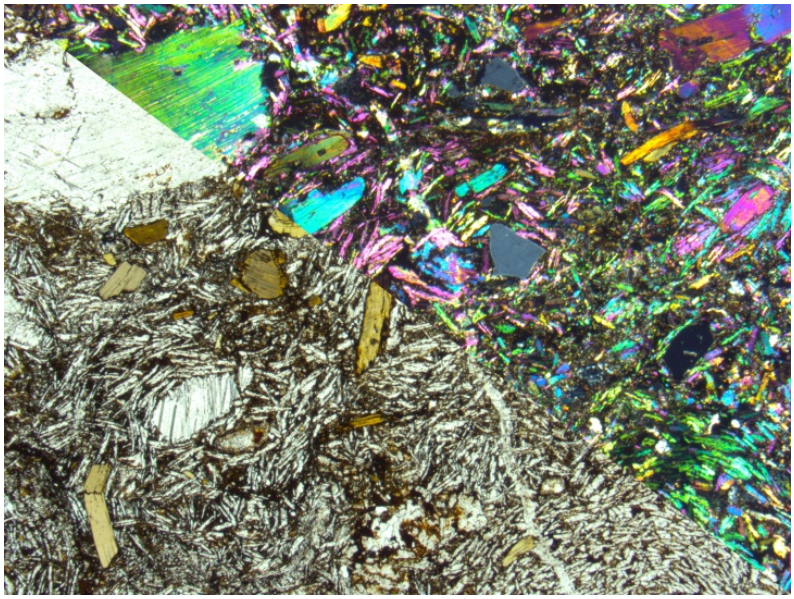

Figure 4.1. *Calciocarbonatite SP-27C in PPL (lower left) and XPL (upper right) showing phenocrysts of calcite (large, anhedral, colourless grains in PPL), biotite (brown in PPL) and potassium feldspar (1st order gray in XPL). Scale = 4mm across horizontal.*

4.1.1 Calciocarbonatites

Calciocarbonatites are defined by Gittins and Harmer (1997) as having molar CaO/[CaO + MgO + (FeO^{total} + MnO)] of greater than or equal to 0.75. At Saltpeterkop, calciocarbonatites tend to be porphyritic, with phenocrysts of (mainly anhedral) calcite, and (mainly subhedral)

biotite and potassium feldspar and with groundmasses composed of these same minerals along with (in some samples) fine-grained clinopyroxene and ubiquitous opaque oxides (mainly magnetite). Phenocrysts are highly variable in size and range up to 5 mm in maximum dimension, although most are 1 mm or less in size. The samples studied are alvikites aside from a single sövite sample (WV95-19C, of which ≈75 vol.% is composed of approximately 0.5 mm equant calcite grains). The groundmass of the alvikites is dominated by calcite (typically 0.3 to 0.1 mm) and fine oxides, with biotite and potassium feldspar as the main groundmass silicate minerals (typically in the range of 0.1 to 0.5 mm). Additionally, a couple of samples (SP-27A and SP-404) display seriate textures with no distinct groundmass and phenocryst grain size populations. A number of samples appear to have undergone significant alteration, which has resulted in recrystallization and/or loss of calcite (e.g., SPKC-4, SPKC-6, SP-402, SP-403, SP-404) along with alteration of biotite, other silicate minerals and even oxides in some cases.

In detail, phenocrysts in the calciocarbonatites tend to make up between 5 and 25 vol.%, and the phenocryst assemblages are dominated by calcite, with either biotite or potassium feldspar as the main silicate phenocryst. Potassium feldspar sometimes occurs as inclusions in both calcite and biotite, but the only inclusions seen in feldspar are opaque oxides. Calcite tends to make up 50 to 75 vol.% of the groundmass, with opaque oxides (mainly fine and dusty in appearance) of up to 25 vol.% and the remainder mainly composed of biotite and potassium feldspar, with rare clinopyroxene (difficult to identify conclusively because of its fine grain size). Groundmass calcite often tends to be aligned and lays parallel to the edges of phenocrysts (particulary well shown in SP-27C). Many of the carbonatite samples also contain angular xenoliths of local Beaufort sandstone, although such xenoliths were excluded as much as possible during sample preparation.

4.1.2 Ferruginous calciocarbonatites

Ferruginous calciocarbonatites are defined by Gittins and Harmer (1997) as having the molar ratio CaO/[CaO + MgO + (FeO^{total} + MnO)] of between 0.75 and 0.5 *as well as* molar (FeO^{total} + MnO) > molar MgO. Their higher Fe and Mn contents are reflected in the overall higher modal proportion of opaque oxides in these samples (typically >30 vol.%), although their texture and mineralogy are similar in most respects to the calciocarbonatites (i.e., mainly with porphyritic textures dominated by calcite, oxides, biotite and potassium feldspar). Phenocryst

contents in these carbonatites (0 to 40 vol.%) are more variable than in the calciocarbonatites, with a significant number of samples that have less than about 5 vol.% phenocrysts (e.g., SP-16A, SP26B, SPKC-8). Generally, calcite phenocrysts are anhedral to subhedral, whereas biotite and potassium feldspar are subhedral to euhedral.

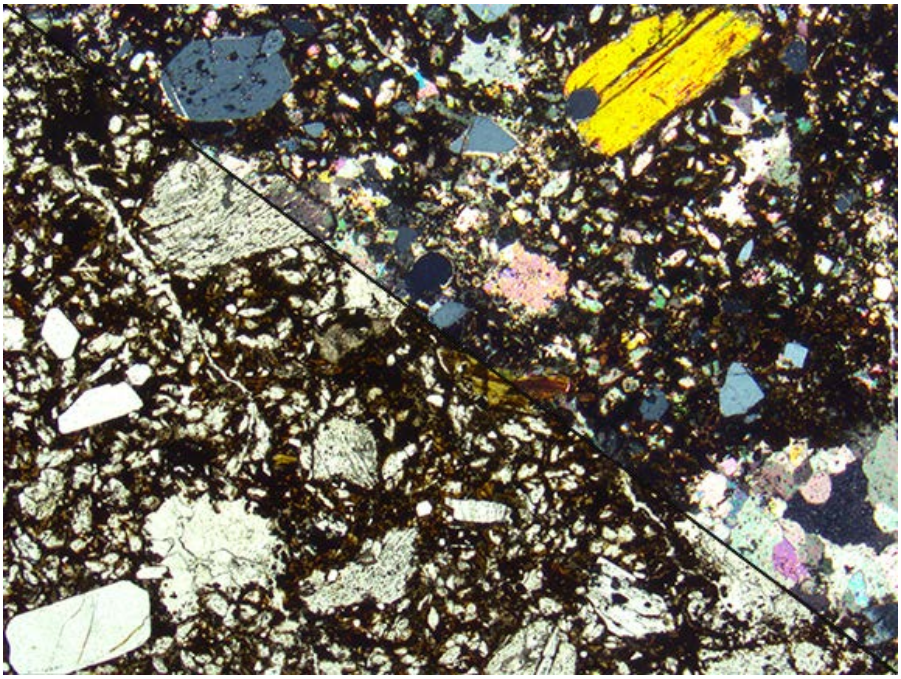

Figure 4.2. *Calciocarbonatite WV95-29 in PPL (lower left) and XPL (upper right) showing calcite, potassium feldspar and biotite phenocrysts in a groundmass of calcite and abundant fine oxide grains. Scale = 4mm across horizontal.*

The ferruginous calciocarbonatites are also more commonly highly altered and recrystallized than the calciocarbonatites, and calcite in most samples shows evidence of recrystallization. Some of these samples also contain significant quartz, which can be present as small sandstone xenoliths and xenocrysts of rounded quartz grains likely representing disaggregated sandstone (always less than 5 vol.%), but some altered ferruginous carbonatites (most notably SPKC-4) contain up to 30 vol.% quartz mainly present as irregular, patchy grains that appear to represent the result of silicification, likely as a result of hydrothermal alteration.

4.1.3 Magnesiocarbonatites and ferrocarbonatites

Gittins and Harmer (1997) classify samples that do not fall into the calciocarbonatite or ferruginous calciocarbonatite categories as either magnesiocarbonatites or ferrocarbonatites

depending on whether molar MgO or (FeO^{total} + MnO) are more abundant. Only four out of the 28 carbonatite samples in this study fall into these categories (three magnesiocarbonatites and one ferrocarbonatite). It is important to note that these magnesiocarbonatites are relatively Ca- and Fe-rich (see Fig. 5.4 in Chapter 5) and they contain calcite rather than dolomite, unlike the dolomitic magnesiocarbonatites that characterise many southern African carbonatites (e.g., Marinkas Quellan and Dicker Willem; Smithies, 1991; Cooper and Reid, 1998). The magnesiocarbonatites are poorly phyric (<5 vol.%) and relatively altered, and two of them (WV95-24 and -26) have groundmasses that contain more than 30 vol. % clay minerals, along

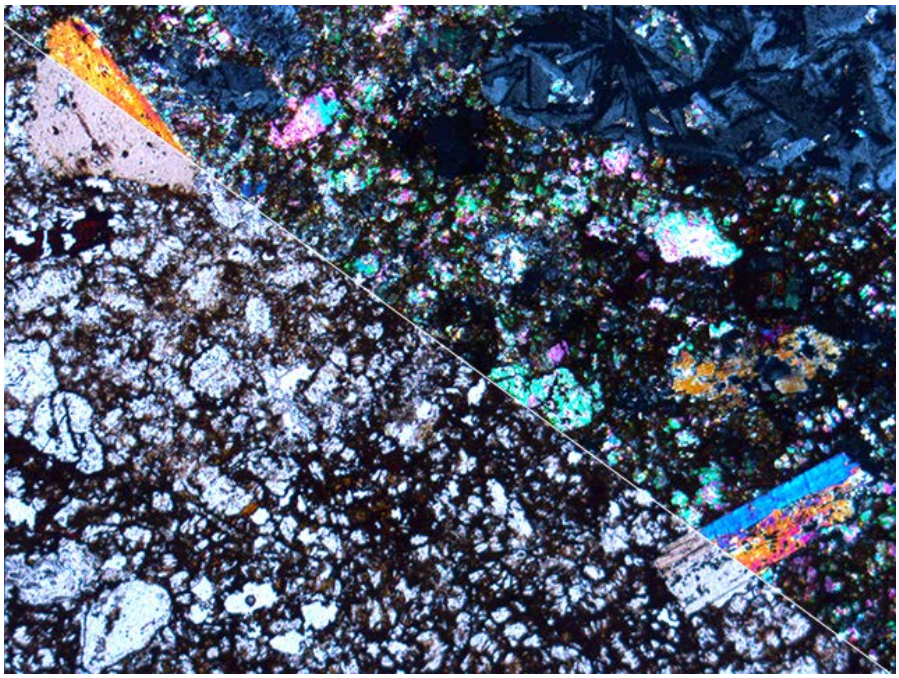

Figure 4.3. *Ferruginous calciocarbonatite SP-16A in PPL (lower left) and XPL (upper right) showing calcite, phlogopite phenocrysts, potassium feldspar microphenocrysts, abundant opaque oxides and a feldspathic crustal xenolith in the upper right. Field of view = 4 mm across horizontal*

with calcite and oxides. The lone ferrocarbonatite sample (SPKC-9) is aphyric and appears to be composed solely of calcite and oxide minerals.

4.2 Petrography of the potassic trachytes

The potassic trachytes are porphyritic igneous rocks with a fairly simple texture and mineralogy. They contain phenocrysts and glomerocrysts of potassium feldspar (typically 15-30 vol.%, sub- to euhedral, mainly 0.5 to 3 mm in size) and rare subhedral nepheline and aegirine microphenocrysts (up to 1 mm) and groundmasses composed largely of fine-grained feldspar

microlites (<0.05 mm), devitrified glass and oxides. The feldspar phenocrysts typically do not show twinning. In most samples, the groundmass shows orange staining, apparently from the oxidation and partial dissolution of magnetite and re-precipitation as haematite. Partial to complete alteration of potassium feldspar phenocrysts, mainly via replacement by clay minerals, is also common.

A small number of the potassic trachyte samples (e.g., SPK-CRB and SKM5-2) are more accurately called trachyte breccias, due to the fact that they contain large proportions (>50% in some cases) of angular xenoliths of the local Beaufort sandstone or disaggregated quartz derived from this sandstone.

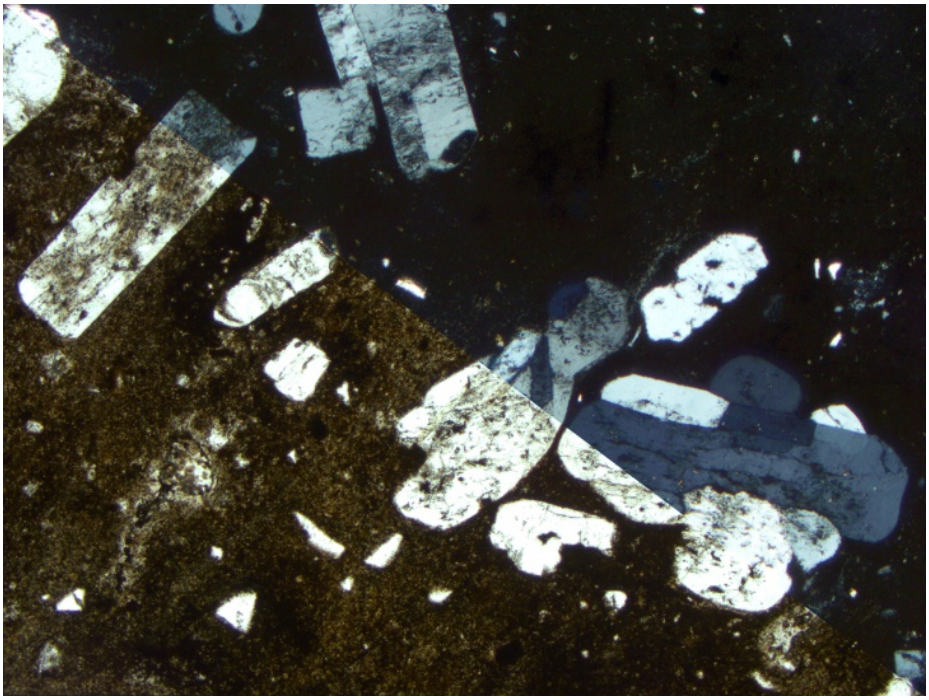

Figure 4.4. *Potassic trachyte WV95-23A with PPL and XPL showing feldspar phenocrysts with a glomeroporphyritic texture. Scale = 4mm across horizontal.*

4.3 Petrography of olivine melilitites

The olivine melilitites from the Saltpeterkop complex are all porphyritic and contain olivine as the main phenocryst phase, as well as groundmasses containing melilite, perovskite, opaque oxides and, variably, phlogopite, clinopyroxene and nepheline. However, the seven localities from which the melilitites were sampled show some significant textural and mineralogical differences. Most obviously, the phenocryst assemblage varies from being solely composed of olivine (in the "M1" sill and "M2" dyke of de Wet (1975), as well as the SP31 and

SP206 olivine melilitites of Chevallier (unpublished.)) to being composed of olivine phenocrysts plus melilite microphenocrysts (in the "M5" pipe and "M6" dyke of de Wet et al. (1985)) or olivine plus clinopyroxene phenocrysts (in the SP43 dyke of Chevallier (unpublished.)). There are also significant

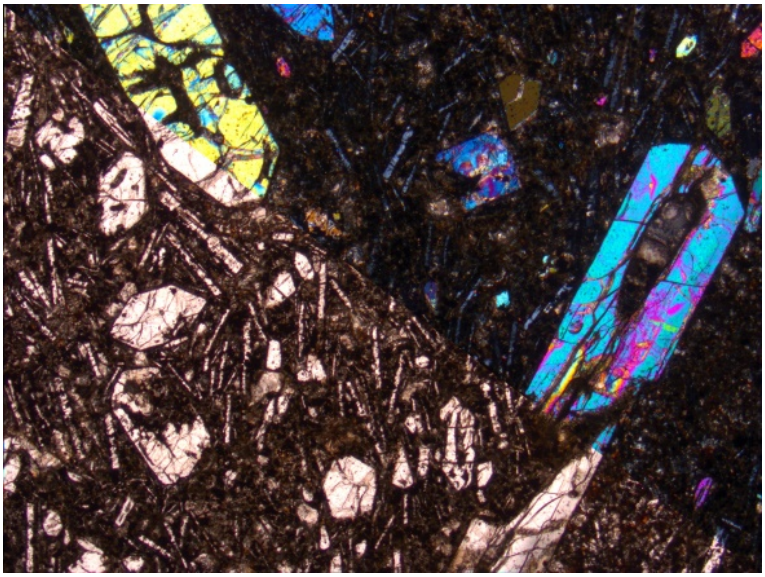

Figure 4.5*. Olivine melilitite SP-43 in PPL (lower left) and XPL (upper right) showing euhedral, skeletal olivine phenocrysts, lath-shaped melililite microphenocrysts and fine groundmass composed mainly of fine-grained olivine, perovskite and other oxide minerals. Field of view (horizontal) = 4 mm.*

differences in the groundmass mineral assemblages, particularly the variable presence of phlogopite and nepheline (see Table 4.1).

Olivine phenocrysts tend to be subhedral to euhedral and are typically less than 3 mm in size and can be as small as 0.05 mm when present as a groundmass mineral. Clinopyroxene phenocrysts (present only in the SP43 dyke) are mainly anhedral and typically are 0.3 to 0.6 mm in length. Melilite microphenocrysts are typically euhedral (tabular to lath-shaped) and smaller than 0.4 mm in length. In the groundmass, melilites are typically lath-shaped to acicular and 0.05 to 0.075 mm in length. They are often aligned to sub-aligned. Phlogopite, clinopyroxene and nepheline grains all tend to be anhedral in the groundmass, and are generally less than 0.1 mm in size. Groundmass clinopyroxene has a fibrous habit in SP43 and SP206. The freshest olivine melilitite samples come from the M5, SP31 and SP206 pipes, and to a slightly lesser extent the M6 and SP43 dykes. The M1 sill, M2 dyke and SP206 pipe are the most altered and tend to have large proportions of their olivine and most of their melilite replaced by secondary minerals.

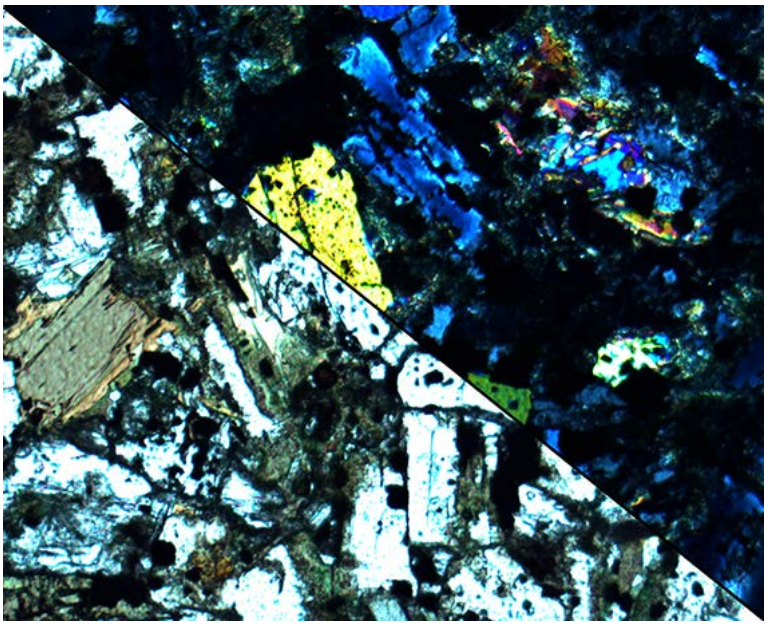

Figure 4.6. *Olivine melilitite SPK-3 (from pipe M5) in PPL (lower left) and XPL (upper right) showing olivine (colourless, anhedral, equant grains), phlogopite (brown) and melilite phenocrysts (lath-shaped with anomalous blue birefringence) set in a groundmass of olivine, nepheline, perovskite and fine opaque oxides. Field of view (horizontal) = 2 mm.*

Table 4.1. Mineral assemblages of Saltpeterkop olivine melilitites by locality

Locality	**M1 sill**	**M2 dyke**	**M5 pipe**	**M6 dyke**	**SP31 pipe**	**SP43 dyke**	**SP206 pipe**
Phenocryst assemblage	olivine	olivine	olivine melilite phlogopite	olivine melilite (micro)	olivine	olivine cpx	olivine
Groundmass assemblage	melilite cpx olivine opaques perovskite	melilite cpx opaques	olivine melilite phlogopite cpx nepheline opaques perovskite	melilite phlogopite nepheline opaques perovskite cpx	olivine melilite cpx phlogopite nepheline opaques perovskite	melilite nepheline cpx opaques perovskite	cpx melilite opaques
Samples	SKM1-1	SKM2-1	SPK-1 SPK-2 SPK-3 SKM5-1	SKM6-1	SP-31 SP31-3 SP31-4	SP-43 SP43-1 SP43-2 SP43-4	SP206-1 SP206-2 SP206-3

Abbreviations: cpx, clinopyroxene. A question mark (?) indicates that the presence of the mineral specified is suspected but not certain due to fine grain size or alteration.

4.4 Petrography of ultramafic lamprophyres

Some of the igneous rocks sampled from the Saltpeterkop complex are primitive to moderately differentiated in composition and contain significant amounts of calcite as groundmass or (less commonly) phenocryst phases along with greater modal amounts of clinopyroxene and phlogopite phenocrysts than the olivine melilitites, although their phenocryst assemblage is still olivine-dominated. They are also distinguished from the melilitites by the absence of melilite. These rocks have been termed "ultramafic lamprophyres" here due to their mineralogical similarity to rocks of this type reported in the literature (e.g., Rock, 1991; Tappe et al., 2005; 2006). Most of these samples from Saltpeterkop (e.g., SP38, WV95-19 and SPKC-12) are of a brecciated nature, making more precise rock classification problematic. These rocks are characterized by olivine (often altered) and clinopyroxene as the main phenocryst phases, and groundmasses dominated by calcite, devitrified glass, opaque oxide minerals and phlogopite, which occurs as both a microphenocryst and groundmass phase.

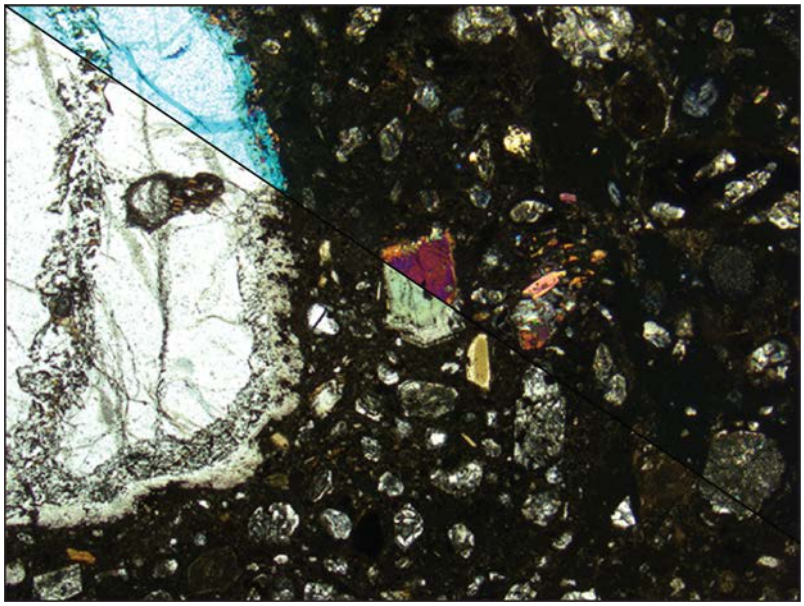

Figure 4.7. *Ultramafic lamprophyre SP-38 (from breccia pipe) in PPL (lower left) and XPL (upper right) showing olivine megacryst, zoned augite phenocryst and phlogopite and calcite microphenocrysts in a groundmass of calcite, phlogopite and oxide minerals. Scale = 5mm across horizontal.*

The ultramafic lamprophyre samples dominantly occur as volcaniclastic breccias, largely composed of juvenile lapilli, which often contain cores of fresh or altered olivine or clinopyroxene (sometimes >10 mm), and the calcite occurs both as dispersed grains within the lapilli and as fillings in the gaps between lapilli (this latter calcite often appears recrystallized

and may be secondary in origin). However, one sample of a fresh ultramafic lamprophyre dyke, with a clear igneous texture, was also obtained (SP367-1). This sample displays anhedral olivine megacrysts (grains up to 15 mm in size) and subhedral to euhedral olivine and clinopyroxene phenocrysts set in a groundmass of clinopyroxene, nepheline, calcite, opaque oxides and phlogopite. On the basis of its mineralogy, particularly the presence of nepheline (in the groundmass) it is most properly classified as a damtjernite (Tappe et al. 2005). Apart from SP367-1, which is quite fresh, the ultramafic lamprophyres are moderately to highly altered, with

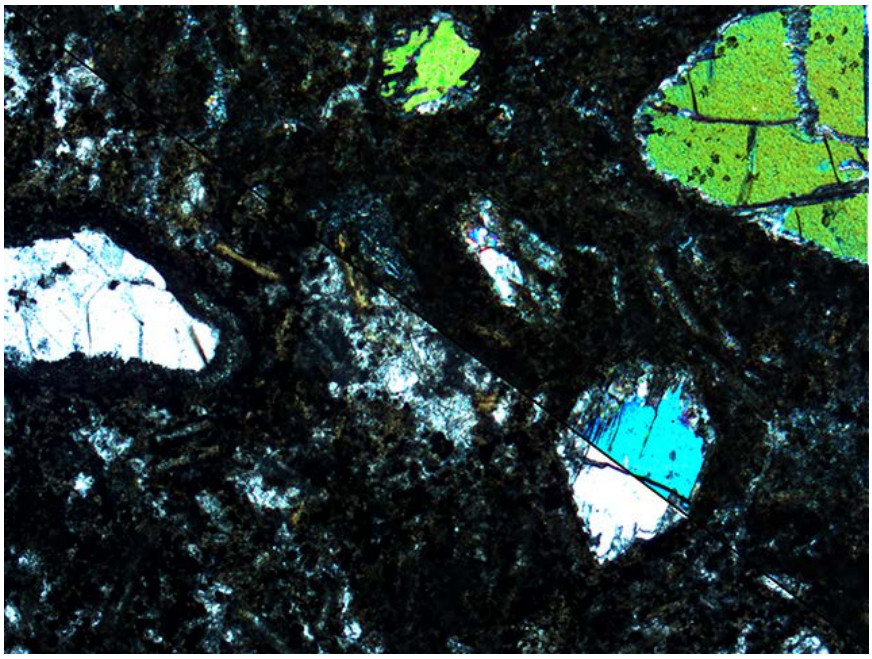

Figure 4.8. *Ultramafic lamprophyre (damtjernite) SP367-1 from dyke, shown in PPL (lower left) and XPL (upper right). It contains olivine phenocrysts (large, sub- to anhedral) and an augite phenocryst (euhedral, with cleavage) in a groundmass of calcite, phlogopite (brown), clinopyroxene, nepheline and opaque oxides. Field of view = 2 mm across horizontal.*

secondary replacement of olivine in many cases and devitrified glass in accretionary lapilli being commonly replaced by brown to green clay minerals. Some of these, with a strong green colour in outcrop, have been termed "green breccias" by Chevallier (unpublished field map) and occur at numerous locations around the Complex.

There are also a small number of moderately differentiated lamprophyres (WV95-19, SPKC-12 and SPKC-14), which have phlogopite dominating their phenocryst assemblages (with subsidiary amounts of olivine (mainly pseudomorphed) and clinopyroxene) and with calcite as a major groundmass phase. In terms of mineralogy, texture and chemical composition, these have

some similarities with both the more primitive ultramafic lamprophyres and the calciocarbonatites.

4.5. Lower crustal xenoliths from Saltpeterkop breccia pipes

The Saltpeterkop complex is hosted by sandstones and shales of the Beaufort Group. However, some insights into the nature of the continental crust beneath Saltpeterkop can be ob-

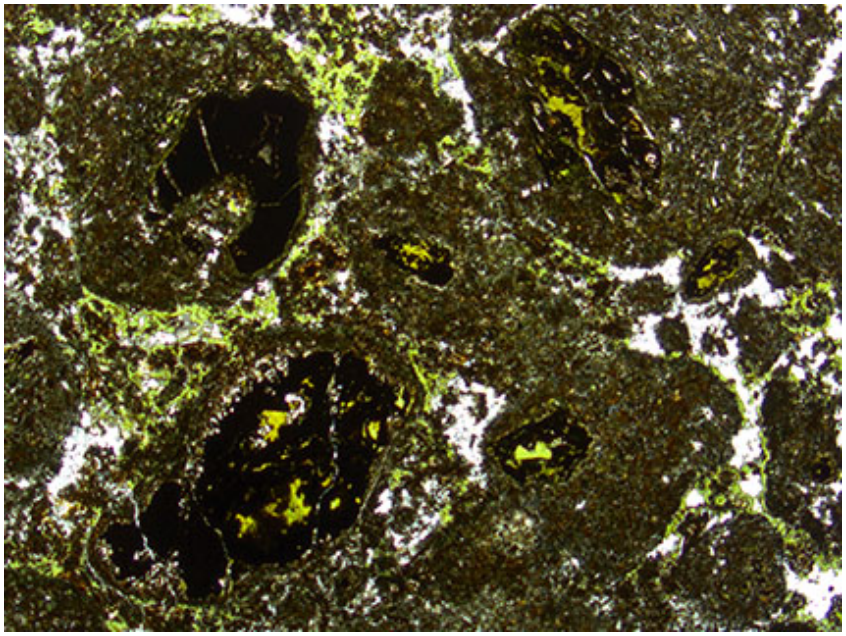

Figure 4.9. *Green, highly altered ultramafic lamprophyre breccia SKGB-1 in PPL displaying rounded juvenile lapilli (now almost entirely altered to clay minerals) with secondary mineral pseudomorphs (apparently after olivine) in their nuclei. Calcite is the light coloured mineral concentrated in the gaps between the lapilli. Field of view = 4 mm across horizontal.*

tained from the study of lower crustal xenoliths entrained in breccia pipes, such as the Silver Dam breccia pipe on farm Matjiesfontein. Several of these xenoliths were sampled and, of these, nearly all are mafic in composition. Most are dolerites or gabbros with clear igneous (and, in some cases, cumulate) textures dominated by plagioclase, clinopyroxene, oxides and (often altered) olivine. These are likely derived from dolerite sills or dykes of the Karoo igneous province present beneath the complex. Three of the xenoliths have clear metamorphic or metasomatic textures: an amphibolite, an anhydrous clinopyroxenite and an unusual phlogopite-rich clinopyroxenite xenolith with accessory olivine and ilmenite and traces of calcite and plagioclase (sample SP-100). The phlogopite in this sample is euhedral and lacks foliation. This,

combined with the presence of calcite suggests that this sample has experienced interaction with carbonatitic fluids or melts. None of the crustal xenoliths recovered in the course of this investigation contain garnet.

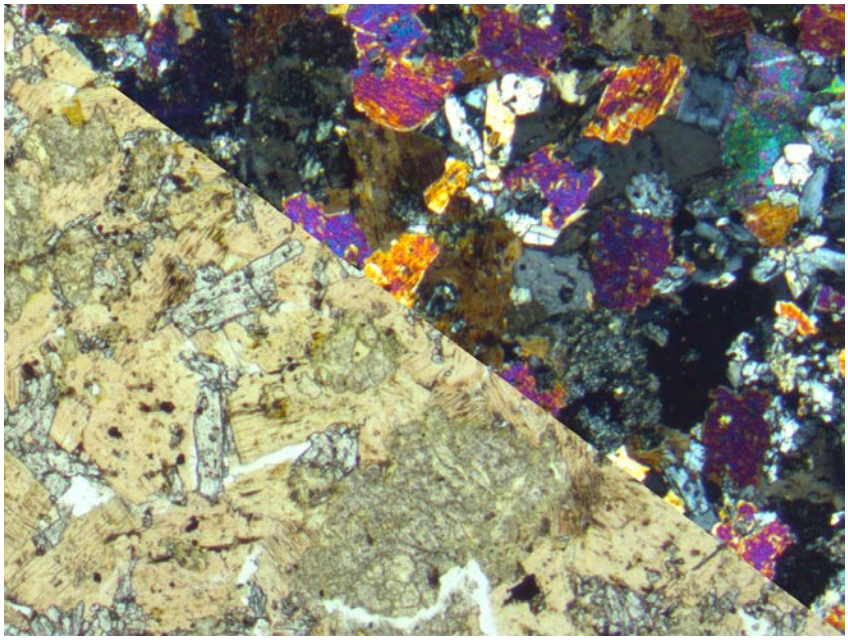

Figure 4.10. *Phlogopite-rich clinopyroxenite lower crustal xenolith SP-100 in PPL (lower left) and XPL (upper right). Aegirine-augite pyroxene is pale green, phlogopite is pale yellow, and olivine and calcite are colourless. Field of view = 4 mm across horizontal.*

4.6. Mineral chemistry of olivine melilitites and ultramafic lamprophyres

The measurement and interpretation of the major element compositions of mineral phases in the Saltpeterkop igneous rocks is outside the scope of this study. However, the petrogenetic modeling of olivine melilitites and ultramafic lamprophyres undertaken in Chapter 6 requires knowledge of the compositions of the main phases in these minerals. A limited suite of mineral compositions was published by Boctor and Yoder (1986) from a variety of South African olivine melilitites, including the M5 pipe at Saltpeterkop (W.J. Verwoerd, personal communication, 2015), and Malarkey et al. (2010) also reported major and trace elements for minerals from this pipe. Additionally, mineral data for silicate and oxide phases from a number of melilitite and ultramafic lamprophyre localities at Saltpeterkop were presented in the honours thesis of Mabaso (2017). Appendix 1, Tables 1, 2, 3 and 4 summarise the compositions of the main minerals

present in the Saltpeterkop olivine melilitites and ultramafic lamprophyres (olivine, clinopyroxene, phlogopite, melilite, nepheline, calcite, titanomagnetite, perovskite and spinel).

Olivine phenocryst and microphenocryst compositions averaged by sample fall within a fairly tight range of Mg# values from 89 to 86, higher than that for olivine megacrysts in ultramafic lamprophyres (Mg# 80-85, from SP38 and SP367). Clinopyroxene phenocryst compositions (measured on one melilitite (SP43) and two ultramafic lamprophyre localities (SP38 and SP367)) are all augitic with Mg# values between 76 and 82 and with Al_2O_3 contents of 3.7 to 5.7 wt.%. Phlogopites (measured in samples from the M5, M6 and SP31 melilitite localities and the SP38 UML locality) have Mg# values of 82 to 89 and (Si+Al) value of 7.15 to 8.0 cation formula units per 24 oxygens. This means that they are trending slightly toward the tetraferriphlogopite end-member.

5. WHOLE ROCK GEOCHEMISTRY

Approximately 75 whole-rock samples from the Saltpeterkop carbonatite complex have been analysed for major and trace elements by X-ray fluorescence (XRF), with roughly forty of these samples also being analysed by inductively coupled plasma mass spectrometry (ICP-MS) for the rare earth element and other trace element concentrations. All whole rock analyses were carried out at the University of Cape Town in the Department of Geological Sciences (see Chapter 3 for information on methods). All of these data are presented in Appendix 2, Tables 1 and 2.

The rocks sampled include (1) intrusive and hypabyssal igneous rocks (all olivine melilitites, most carbonatites and potassic trachytes and some ultramafic lamprophyres fall into this category), (2) breccias, which in most cases are from pipes and dykes and dominantly composed of igneous material (most ultramafic lamprophyres, as well as some carbonatites and potassic trachytes), as well as (3) a small number of iron and manganese oxide-rich gossan-type crusts and mineralised oxide-rich breccias that appear to be the result of extensive hydrothermal interaction. More than two thirds of all samples analysed come from locations situated outside of the main ring structure (i.e., more than 1.3 km from the centre of the complex, located approximately at 32°28'49"S, 20°50'30"E), due to the fact that nearly all samples within the ring structure itself have been strongly hydrothermal altered. The coarse volcaniclastic breccias and fine-grained bedded volcaniclastic sediments comprising the main tuff ring and crater-filling, which are composed mainly of country rock fragments, were not analysed in this study because (1) they offer little insight into the sources and petrogenesis of the SPKC and (2) they have experienced very severe hydrothermal alteration. Many of the Saltpeterkop samples analysed show significant alteration and mineral replacement. However, much of this alteration likely occurred as a result of deuteric processes occurring during and soon after emplacement and it was considered worthwhile to examine the geochemical characteristics of even moderately altered rock samples.

5.1 Overview and Classification

In some cases, such as with the olivine melilitites and ultramafic lamprophyres, the Saltpeterkop igneous rocks are more properly classified on the basis of mineralogy and

petrography (see Chapter 4) than chemical composition. Others, such as the carbonatites, are more easily classified on the basis of major element composition. Some samples, which are heavily altered and have few primary minerals remaining, are classified on the basis of texture and their geochemical similarity to less altered rock types. Due to the wide variation in rock types, relevant chemical classification criteria are described in the section describing major element data for each rock type.

In overview, with the exception of the potassic trachytes, the main rock types can be most clearly distinguished using a normalized Mg-Ca-(Fe+Mn) triangular diagram based on normalise molar proportions (Figure 5.1; Gittins & Harmer, 1997). Aside from the Fe-Mn oxide-rich crusts and mineralised breccias, the data form a roughly continuous trend from the calciocarbonatites at the extreme Ca-rich end of the range, to the olivine melilitites, which are richest in Mg and intermediate in Ca and (Fe+Mn). The ultramafic lamprophyres bridge the small gap between the melilitites and the most Fe, Mn and Mg-rich carbonatites.

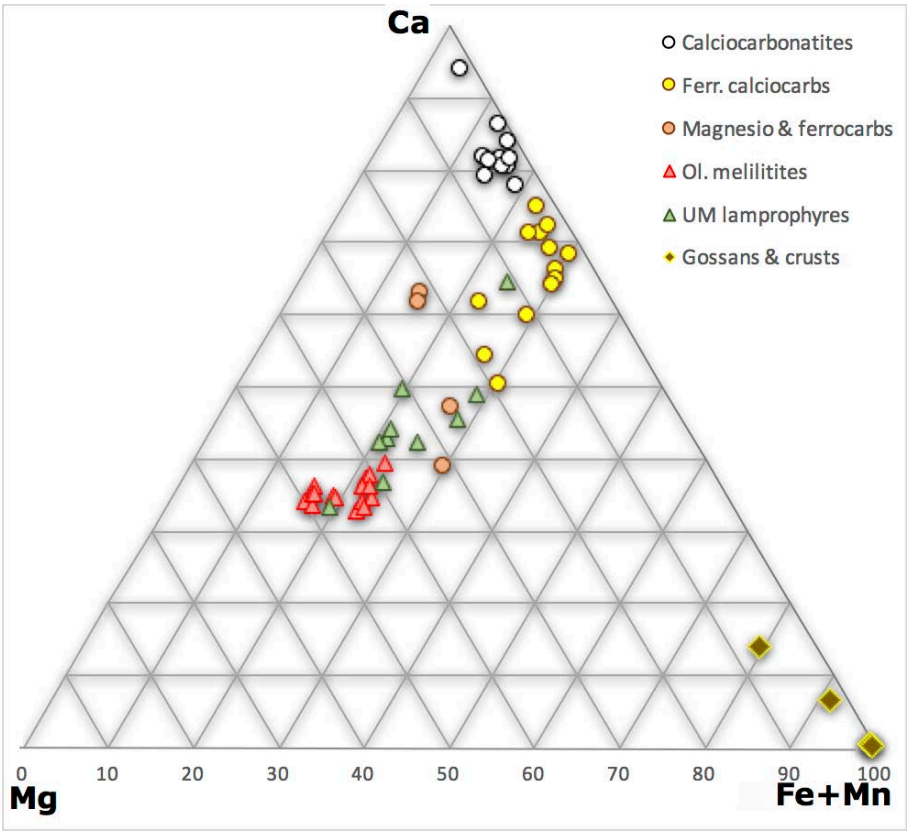

Figure 5.1. *Ca-Mg-(Fe+Mn) diagram (based on normalised molar proportions) for Saltpeterkop igneous rocks, mineralised breccias and Fe-oxide crusts showing their distinct major element compositions. Carbonatites are classified according to the criteria of Gittins and Harmer (1997). Note that potassic trachytes are not shown.*

5.2 Major Elements

Major element data for Saltpeterkop igneous rocks and mineralised breccias and Fe oxide crusts are presented in Appendix 2, Table 1. Figures 5.2, 5.3 and 5.4 show various types of classification diagrams based on major element composition that are appropriate for the carbonatites and silicate igneous rocks. Given the different chemical classification criteria for each rock type, these will be discussed separately. Figure 5.4 shows variation diagrams of SiO_2 versus major elements for all igneous rocks from Saltpeterkop that displays their wide compositional range. The Saltpeterkop igneous rocks show strong negative correlations of SiO_2 with CaO, MgO and FeO^{tot} and strong positive correlation of SiO_2 with K_2O, Al_2O_3 and Na_2O.

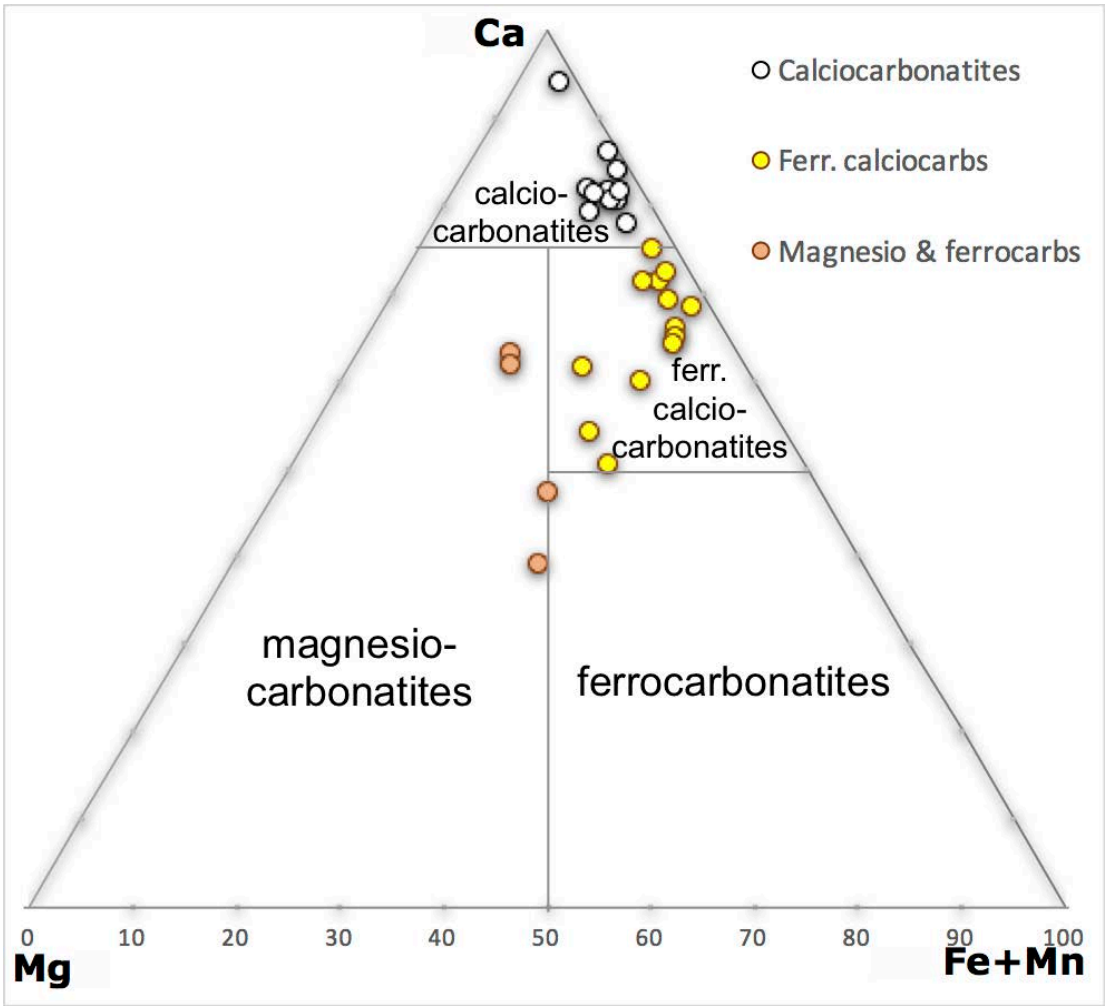

Figure 5.2. *Ca-Mg-(Fe+Mn) carbonatite classification diagram of Gittins and Harmer (1997) based on normalised molar proportions of these elements in Saltpeterkop carbonatites. Note that most samples fall into the calciocarbonatite and ferruginous calciocarbonatite fields.*

5.2.1 Carbonatites

Samples of carbonatite collected at Saltpeterkop are classified, on the basis of their major element compositions, mainly as calciocarbonatites and ferruginous calciocarbonatites according to the criteria of Gittins and Harmer (1997) with three samples falling in the magnesiocarbonatite field and one on the border between magnesiocarbonatite and ferrocarbonatite. As a group, the carbonatites are characterised by high CaO, (17.9 to 45.6 wt.%) and low SiO_2 (0.5 to 22.5 wt%,), Al_2O_3 (0.18 to 5.65 wt.%) and Na_2O (below detection to 0.81 wt.%) values. Contents of TiO_2 (0.1 to 2.4 wt.%), FeO^{tot} (1.5 to 16.0 wt.%), MgO (0.3 to 11.0 wt.%), K_2O (below detection to 3.99 wt.%) and P_2O_5 (0.06 to 7.00 wt.%) are highly variable (all of the above ranges exclude altered sample SPKC-4). There are strong positive correlations between SiO_2 and Al_2O_3 and SiO_2 and K_2O, which are likely controlled by the modal amount of potassium feldspar present in the carbonatite samples. In contrast, neither $FeO^{tot.}$, MgO, CaO nor P_2O_5 show significant correlations (positive or negative) with SiO_2 content. The one strongly altered carbonatite sample (SPKC-4), from a location within the central ring structure, has unusually high SiO_2, Al_2O_3 and K_2O contents (36.9 and 9.8 and 9.1 wt.%, respectively) along with unusually low CaO and $FeO^{tot.}$ (18.0 and 7.0 wt.%, respectively), all likely due to severe hydrothermal alteration.

5.2.2 Potassic trachytes

Silicate igneous rocks from Saltpeterkop are plotted on the silica versus total alkalis classification diagram in Figure 5.3. The rock samples identified by de Wet (1975) and Verwoerd (1990) as potassic trachytes were classified as such on the basis of their high K_2O/Na_2O ratios, they also nearly identical to petrographically similar rocks at the Dicker Willem carbonatite complex in southern Namibia classified as potassic trachytes by Cooper and Reid (2000). Saltpeterkop potassic trachytes and trachyte breccias fall mainly into the tephri-phonolite and phonolite fields of Le Bas et al. (1986), with only one patently crustally contaminated sample falling into the trachyte field. The potassic trachytes and trachyte-dominated breccia samples are characterised by distinctly high K_2O (7.0 to 12.9 wt.%), and low MgO (0.1 to 1.8 wt.%), TiO_2 (0.2 to 0.8 wt.%) and Na_2O values (0.3 to 2.2 wt.%). The oxides SiO_2 (41.0 to 73.9 wt.%), Al_2O_3 (8.3 to 16.8 wt.%), $FeO^{tot.}$ (2.7 to 11.4 wt.%), CaO (0.3 to 13.1 wt.%) and P_2O_5 (0.2 to 1.1 wt.%) are all variable. Most of these samples form good correlations on variation diagrams (Fig. 5.4), with Al_2O_3, Na_2O and K_2O being positively and FeO and CaO

being negatively correlated with SiO_2. However, a few of the trachyte breccia samples with higher SiO_2 fall off these trends due to their inclusion of large proportions of xenoliths of the local Beaufort-series sandstone (see Fig. 5.3 below).

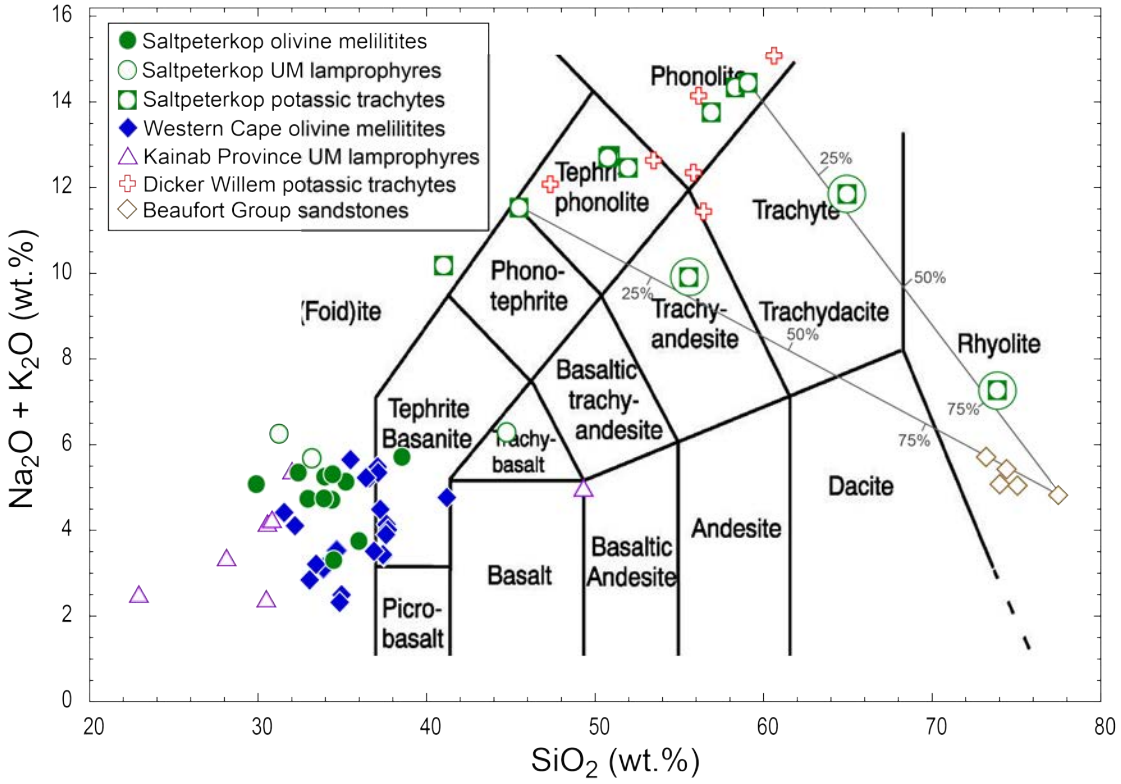

Figure 5.3. *Silica versus total alkalis classification diagram for silicate igneous rocks from Saltpeterkop (after Le Bas et al., 1986). Data plotted are not normalised volatile-free since some samples include significant calcite in their primary mineralogy. Note that trachyte samples enclosed by circles are trachyte breccias containing a large proportion of sandstone xenoliths (at least 25-75%, see gray mixing lines; Beaufort sandstone composition from Paiva, 2015). Compositionally similar rocks from southern Africa are shown for comparison: the Western Cape melilitites (Janney et al., 2002), ultramafic lamprophyres of the Kainab alkaline province, southern Namibia (Bishop and Janney, unpublished data 2015), and potassic trachytes associated with the Dicker Willem carbonatite, southern Namibia (Cooper and Reid, 2000).*

5.2.3 Olivine Melilitites

Olivine melilitite samples have Mg numbers (i.e., 100*Mg/(Mg + Fe^{2+}) in molar units assuming Fe^{3+}/Fe^{2+} = 0.15) of 66 to 79, which represent near-primary melt compositions (i.e., are close to being in equilibrium with mantle olivine of $Fo_{91\text{-}92}$; Roedder and Emslie, 1970). The samples with the highest Mg numbers (76-79) probably reflect accumulation of olivine during ascent, and those with lower Mg numbers (< 70) likely experienced some olivine fractionation.

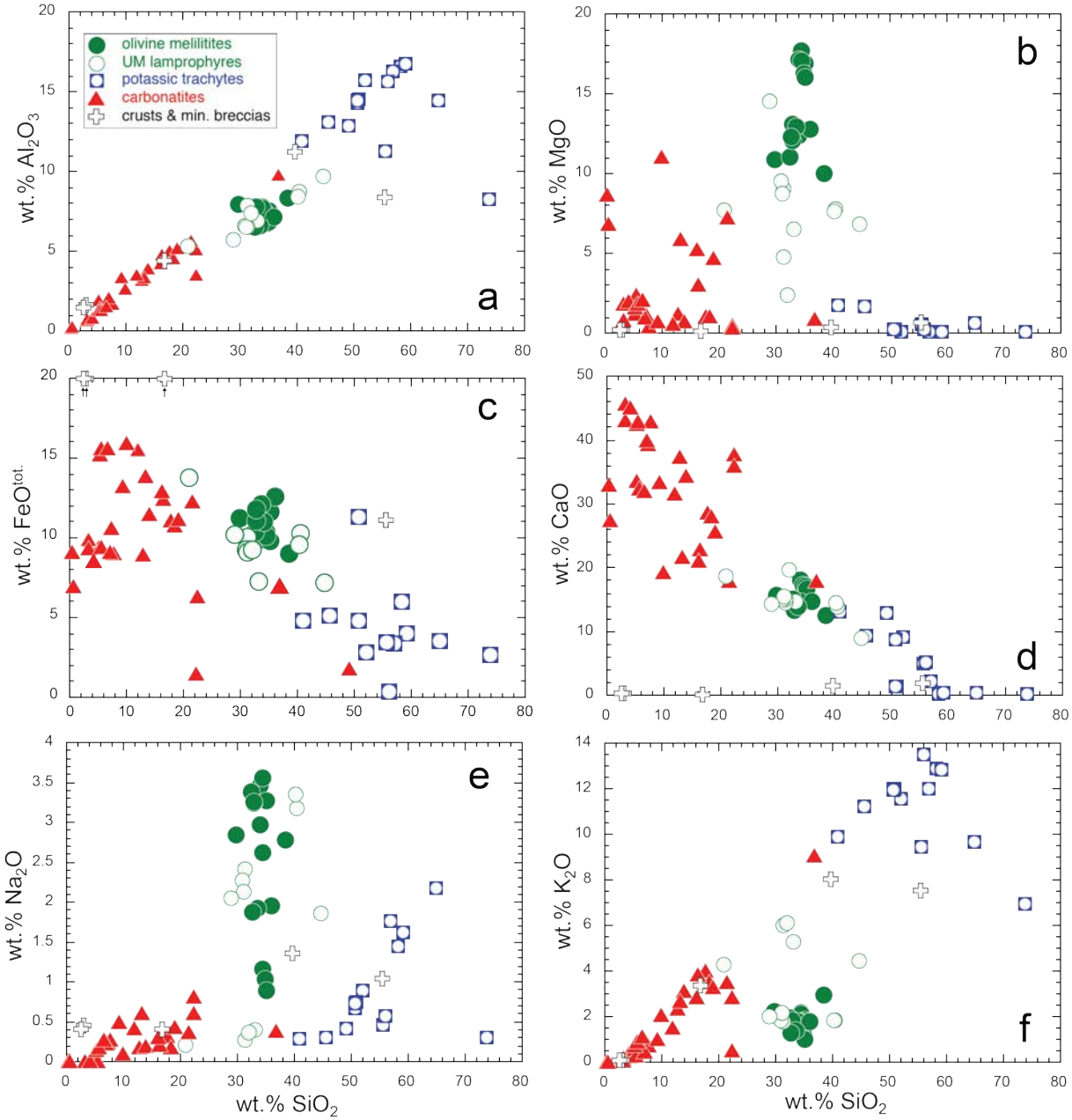

Figure 5.4. *Major element variation diagrams for Saltpeterkop igneous rocks and Fe oxide-rich crusts and mineralised breccias, all showing wt.% SiO_2 versus (a) Al_2O_3, (b) MgO, (c) $FeO^{tot.}$ (note logarithmic axis), (d) CaO, (e) Na_2O, (f) K_2O.*

Olivine melilitites are characterised by high MgO (10 to 17.8 wt.%), as well as SiO_2 (29.9 to 38.5 wt.%), $FeO^{tot.}$ (10.1 to 14.0 wt.%) and CaO contents (12.5 to 17.2 wt.%) that are intermediate between those of the trachytes and the carbonatites. Na_2O contents are high (0.9 to 3.6 wt.%) and K_2O contents are low (1.8 to 2.9 wt.%) compared to most carbonatite and potassic trachyte samples.

5.2.4 Ultramafic lamprophyres

Ultramafic lamprophyre samples have a range in Mg# of 34 to 74 and thus range from primitive to moderately differentiated compositions. It is likely however, that the value at the lower end of this range (for sample SKGB-1) is actually due to Mg loss during alteration, as this sample has far higher Cr and Ni concentrations (161 and 584 ppm, respectively) than would be expected for a lamprophyre sample with such a low Mg# value. The ultramafic lamprophyres chemically overlap with olivine melilitites in many respects, and have SiO_2, Al_2O_3, $FeO^{tot.}$, CaO, and P_2O_5 contents that are similar to, but with wider ranges than, those for the olivine melilitite samples. However, they tend to have lower TiO_2 (1.0 to 2.8 wt.%), MgO (2.4 to 14.6 wt.%, with mean = 7.8 wt.%), and distinctly higher K_2O (1.8 to 6.0 wt.%) than the melilitites. In terms of SiO_2, Al_2O_3, $FeO^{tot.}$, CaO and K_2O, some of the ultramafic lamprophyres are chemically intermediate between the carbonatites and potassic trachytes.

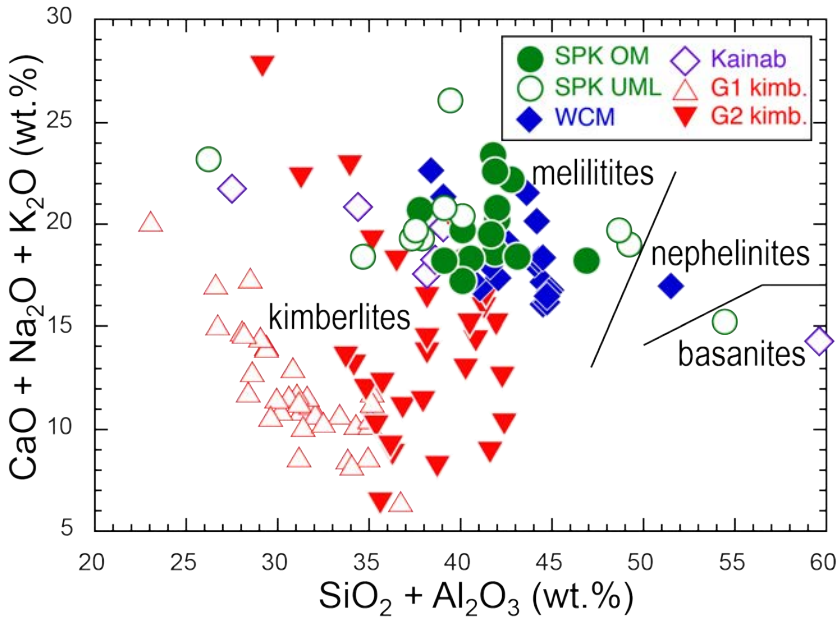

Figure 5.5. *SiO_2 + Al_2O_3 versus CaO + Na_2O +K_2O diagram for distinguishing basanites, nephelinites and melilitites from Le Bas (1989). Data are plotted as reported, not normalised volatile-free. In addition to the Saltpeterkop olivine melilitites (OM) and lamprophyres (UML), also plotted are the Western Cape melilitites (WCM, Janney et al., 2002), carbonated ultramafic lamprophyres of the Kainab Province, southern Namibia (Bishop and Janney, unpublished data 2015) and South African Group 1 (G1) and Group 2 (G2) kimberlites (le Roex et al., 2003; Becker & le Roex, 2006).*

5.3 Trace Elements

The olivine melilitites and ultramafic lamprophyres have the highest abundances of the compatible elements Ni (167 to 502 and 56 to 366 ppm, respectively) and Cr (472 to 961 ppm and 192 to 1195, respectively) of the igneous rocks from Saltpeterkop and both elements show a strong positive correlation with Mg# (Fig. 5.6) and MgO content. Carbonatites have a wide range of Ni and Cr contents from below detection to 395 ppm Ni and to 860 ppm Cr, with the data population being heavily skewed toward low values (with average values of 32 and 72 ppm for Ni and Cr, respectively). The potassic trachytes have even lower values (averages of 7 and 20 ppm, respectively), as would be expected for strongly differentiated rocks. The Fe oxide crusts and green mineralised breccias also tend to have relatively low Ni and Cr concentrations (with means of 53 and 44 ppm, respectively).

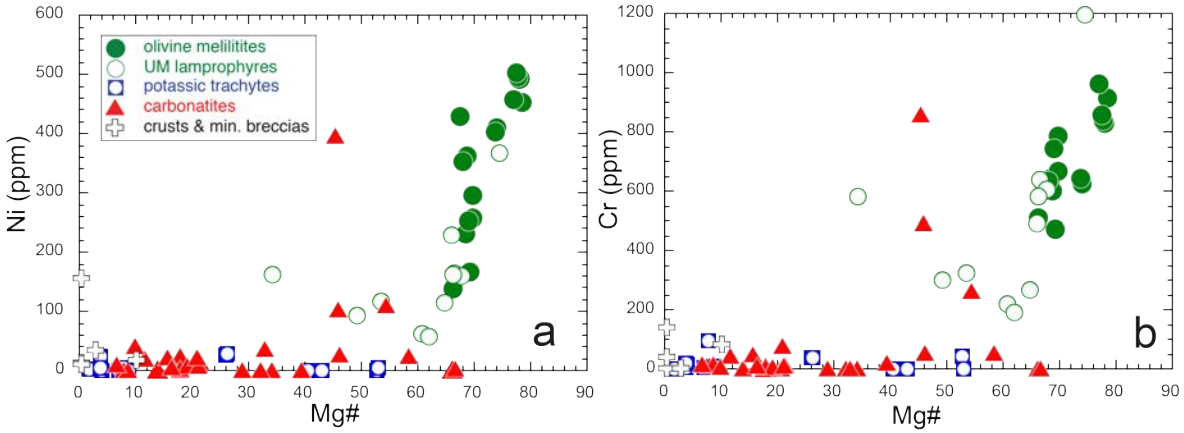

Figure 5.6. *Variations in Mg# versus (a) Ni and (b) Cr concentrations in Saltpeterkop igneous rocks and mineralised crusts and breccias.*

Overall, the carbonatites have the highest and most variable incompatible trace element concentrations of all igneous rocks (e.g., 330 to 7950 ppm Sr; 400 to 17,000 ppm Ba; 4 to 1600 ppm Nb; 26 to 387 ppm Y), although for a few elements (e.g., Nb, Y, Zr) the Fe oxide crust samples have higher abundances. The potassic trachytes have variable to high abundances of some elements, such as Zr (203 to 6315 ppm), Nb (26 to 1043 ppm) and Ba (1542 to 24,338 ppm) and low to moderate concentrations of others, such as Sr (306 to 1844 ppm). As a group, the melilitites and ultramafic lamprophyres tend to have the lowest incompatible element

concentrations (e.g., 90-320 ppm Zr, 470 to 2450 ppm Ba, 114 to 520 ppm Nb) although they are still highly enriched in these elements compared to most crustal and mantle-derived igneous

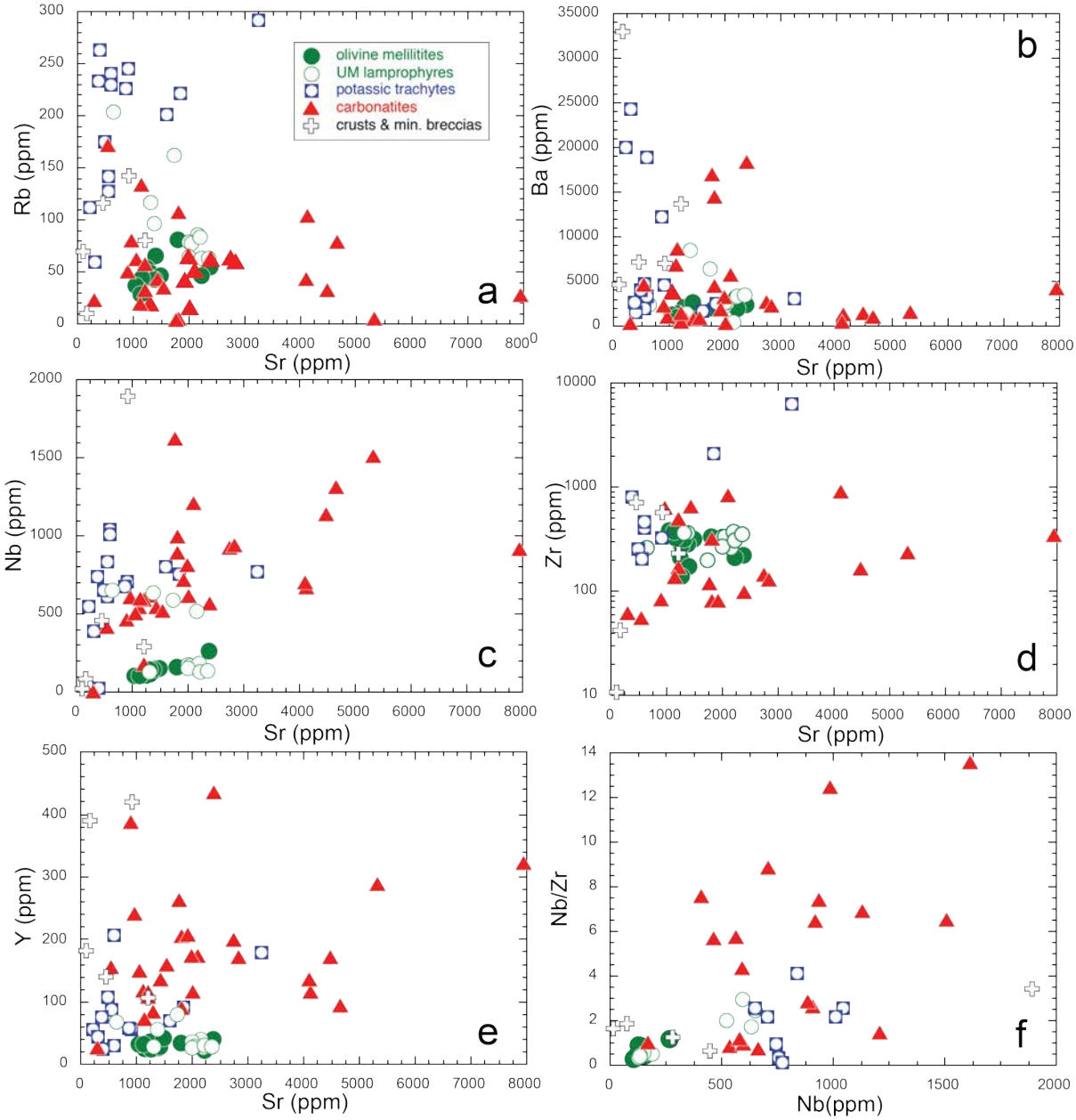

Figure 5.7. *Incompatible element-element and element-ratio plots for igneous rocks and mineralised samples from Saltpeterkop. Panels a-e: Sr vs. (a) Rb, (b) Ba, (c) Nb, (d) Zr (note logarithmic axis), (e) Y, all in ppm. Panel (f), Nb vs. Nb/Zr ratio. Note the poor correlations in general and the very large range of Nb/Zr ratios spanned by the carbonatite samples.*

rocks. Generally, the correlations on incompatible element-element diagrams (Figure 5.7) are poor, for even elements having typically similar geochemical behavior (e.g., Sr and Ba; Fig. 5.7).

5.4 Incompatible element characteristics & patterns

Chondrite-normalised rare earth and primitive mantle-normalised incompatible element patterns are shown in Figure 5.8 and Figure 5.9 respectively, the normalising factors used were those of Evensen et al. (1978) and McDonough and Sun (1995), respectively. The characteristics of each sample type is described separately.

5.4.1 Carbonatites

The carbonatites have chondrite-normalised REE patterns with moderate to strong LREE enrichment relative to the HREE (Figure 5.8) with the exception of one anomalous sample with low REE abundances (SP-27D). La abundances fall in the range from 1179 to 18,452 times chondrite and Lu from 24 to 212 times chondrite. Rare earth patterns for the carbonatite samples generally plot sub-parallel to one another, although a few samples are unusual in having concave-upward HREE patterns with positive slopes from Er to Lu. Chondrite-normalised $(La/Sm)_N$ and $(La/Yb)_N$ ratios (again, excluding SP-27D) fall in the ranges from 4.8 to 21.6 and 18 to 260, respectively.

The carbonatites have distinct negative anomalies in the high field strength elements (Zr, Hf and Ti), and alkalis (K and Rb; Figure 5.9), and show relative enrichments in Ba, Th, U and Nb on primitive mantle-normalised incompatible element diagrams (Fig. 5.9). These are typical of those seen in carbonatites elsewhere (e.g., Nelson et al., 1988; Cooper & Reid, 1998; Bizimis et al., 2003). The ferruginous calciocarbonatites are more enriched in LREE relative to elements of similar compatibility (e.g., Nb, U) than the other carbonatite varieties and they and the magnesiocarbonatites display the strongest negative anomalies in the alkalis and high field strength elements (Zr, Hf and Ti) of all the carbonatites. The calciocarbonatites have less distinct Zr and Hf anomalies, though they still have large negative Ti anomalies. The ferrocarbonatite sample SPKC-9 shows the weakest negative anomalies in alkalis and HFSEs. Anomalous, REE-poor sample SP-27D is also unique in that it has a slight negative Nb anomaly and no negative anomalies in Zr, Hf or the alkalis, and a relatively small negative Ti anomaly.

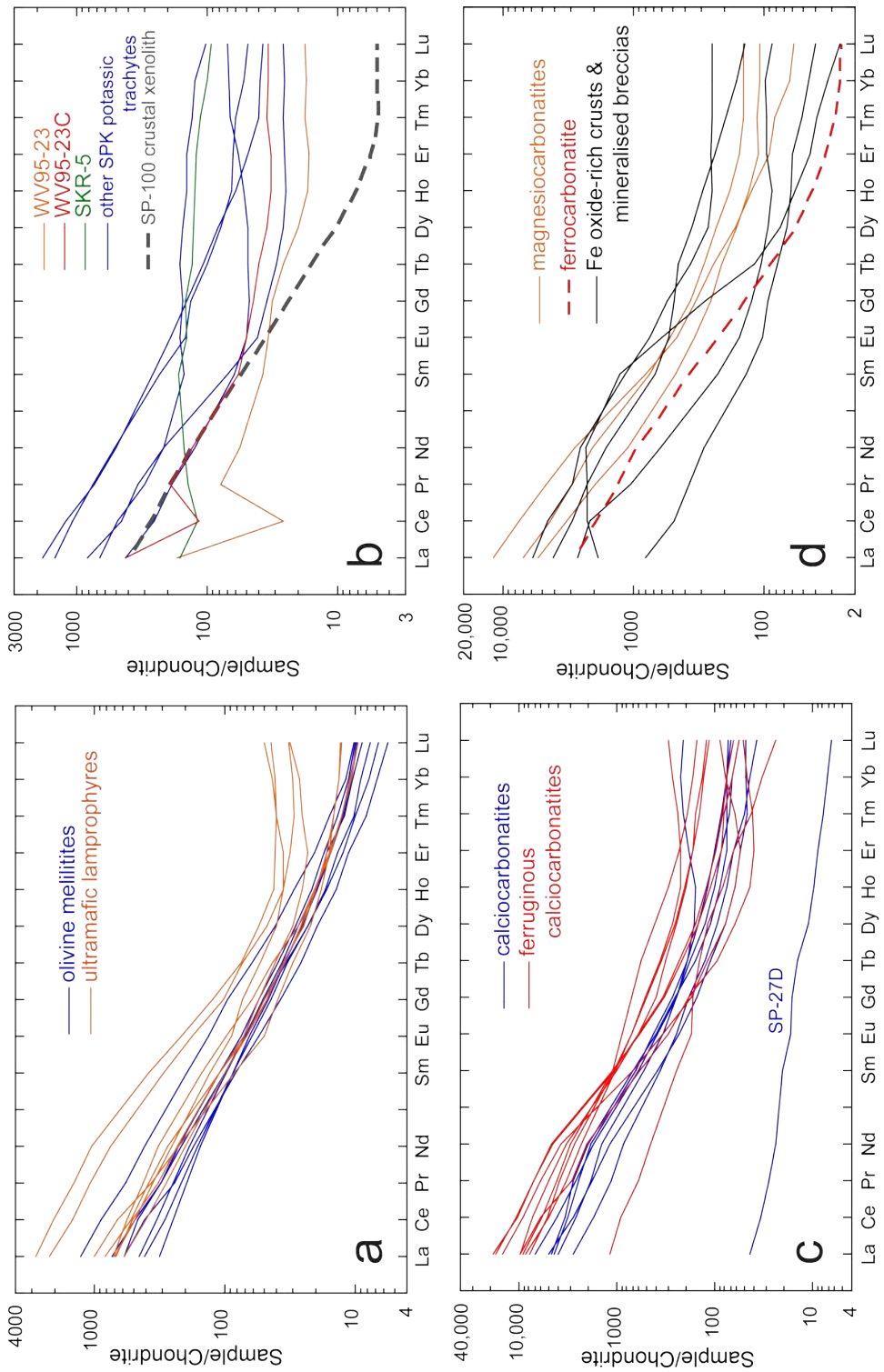

Figure 5.8. *Chondrite-normalized (Evensen et al., 1978) rare earth element patterns for Saltpeterkop igneous rocks and Fe oxide-rich crusts and mineralised breccias. Panel (a) olivine melilitites and ultramafic lamprophyres, (b) potassic trachytes and SP-100 fenitised crustal xenolith, (c) calciocarbonatites and ferruginous calciocarbonatites and (d) magnesio-carbonatites, ferrocarbonatite and Fe oxide-rich crusts and mineralised breccias.*

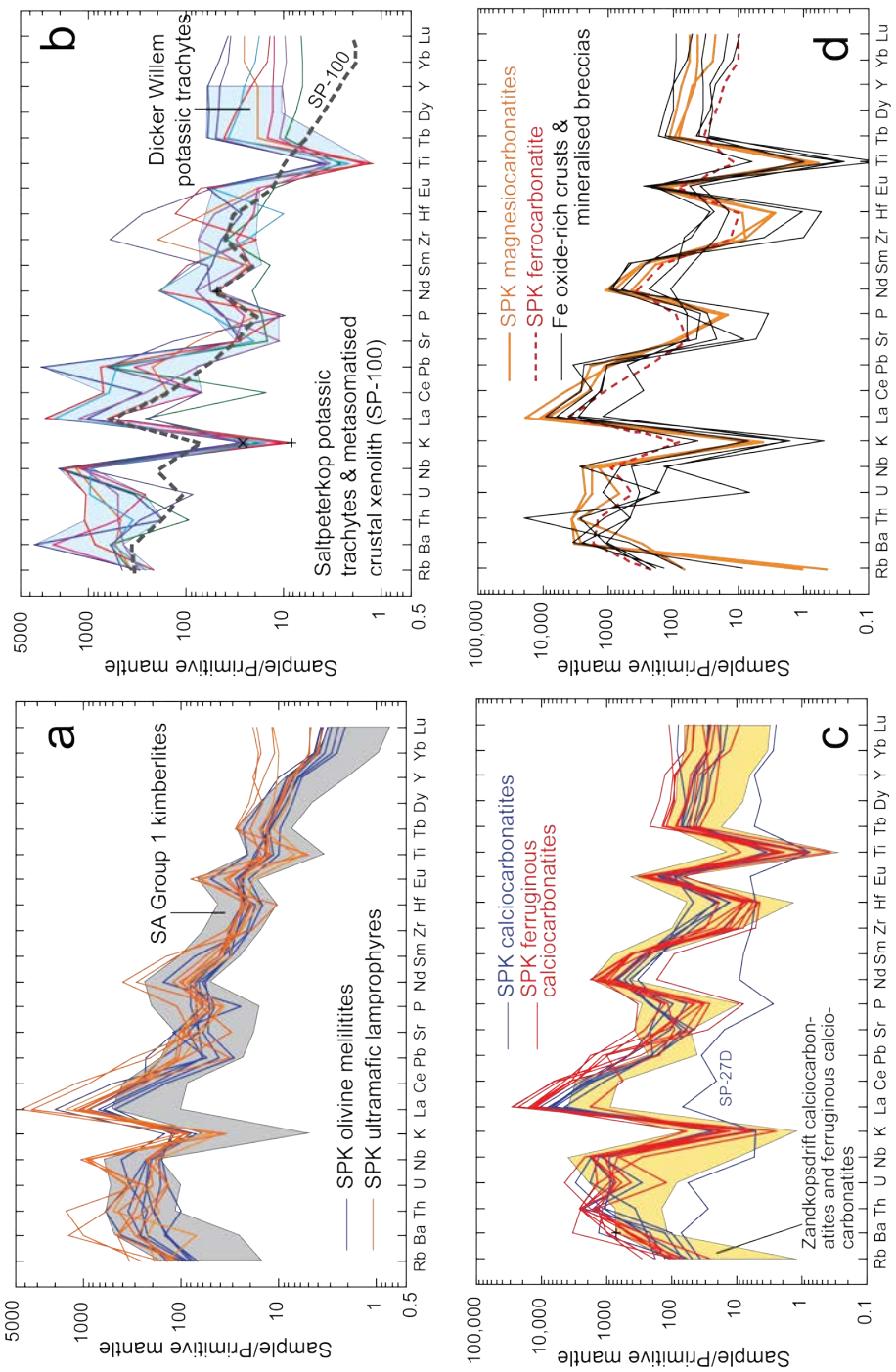

Figure 5.9. *Primitive mantle-normalised incompatible element compositions of Saltpeterkop igneous rocks and Fe-rich crusts and mineralised breccias. (a) olivine melilitites and ultramafic lamprophyres, (b) potassic trachytes and fenitised crustal xenolith, (c) calciocarbonatites and ferruginous calciocarbonatites and (d) magnesiocarbonatites, ferrocarbonatites and Fe oxide-rich crusts and Fe-mineralised breccias. Field for South African group 1 kimberlites is from le Roex et al. (2003) and Becker & le Roex (2006), field for Dicker Willem potassic trachytes is from Cooper & Reid (2000), field for Zandkopsdrift carbonatites is from Ogungbuyi & Janney (unpublished data, 2015).*

5.4.2 Potassic trachytes

The potassic trachytes are all moderately enriched in the LREE relative to the HREE, with $(La/Sm)_N$ and $(La/Yb)_N$ ratios of 4.5 to 7.2 and 5.4 to 28, respectively. Roughly half of all trachyte samples display negative Ce anomalies (Ce/Ce* = 0.22 to 0.85) suggesting alteration under oxidizing conditions (Henderson, 1984). Most of the samples show distinct concave-upward HREE patterns that are fairly flat from Dy to Lu.

In terms of the other incompatible elements, the trachytes show strong enrichments in Ba, Nb, La and Pb with highly variable U, Th and Zr contents. They also show significant negative anomalies in Rb, K, Sr and Ti (Figure 5.9). It is notable that fenitised, biotite-rich crustal xenolith SP-100 shares some attributes of the potassic trachytes (notably strong enrichments in the LREE, Nb and Ba and negative K anomaly) although it is also far more depleted in the heavy REE.

5.4.3 Olivine melilitites and ultramafic lamprophyres

REE abundances of olivine melilitite and ultramafic lamprophyre samples are generally very similar, and all are moderately LREE-enriched, with $(La/Sm)_N$ and $(La/Yb)_N$ values of 3.7 to 12 and 35.7 to 110, respectively. The melilitites have linear sub-parallel chondrite normalized REE patterns with strong HREE depletion (Figure 5.8), whereas the UML show greater variation in their REE patterns, with roughly half of the samples showing a concave-upwards pattern in the heavy REE from Dy to Lu.

Saltpeterkop olivine melilitites show enrichments in Ba, Th, U, Nb and the light REE, as well as moderate negative K anomalies and most show slight negative anomalies in Pb and Ti. They have variable negative Zr and Hf anomalies relative to elements of similar incompatibility. The ultramafic lamprophyres show general incompatible element similarities to the melilitites except that they generally have greater enrichments in Ba, Th, U, Nb and the light REE and show more pronounced negative Zr, Hf and Ti anomalies than the melilitites (Figure 5.9), as well as less pronounced HREE depletion (and flat to concave upward HREE patterns from Dy to Lu).

5.4.4 Fe oxide-rich crusts and Fe-rich mineralised breccias

The incompatible element compositions of the Fe and Mn oxide-rich crusts and mineralised breccias sampled from in and near the Saltpeterkop ring structure display strong

enrichments in Ba, Nb and the LREE and strong depletions in the alkalis and the high field strength elements (Zr, Hf and Ti). In these attributes, they strongly resemble the more differentiated carbonatite samples, especially the ferruginous calciocarbonatites and (relatively Fe-rich) magnesio-carbonatites. Some of these crust and breccia samples also display mild Ce anomalies that are likely the result of oxidative alteration.

5.5 Comparison of Saltpeterkop ultramafic alkaline igneous rocks with others from southern Africa

The Western Cape olivine melilitite province, of which Saltpeterkop is considered to be a member (Janney et al., 2002), includes three other Late Cretaceous olivine melilitite localities to the west and south: the Sutherland Commonage, Robertson and Spiegelrivier melilitites. The general resemblance of these melilitites to HIMU-type ocean island basalts has been noted previously (Janney et al., 2002). The Saltpeterkop melilitites and lamprophyres also show a strong similarity in their incompatible element concentrations and patterns to southern African Group 1 kimberlites (e.g., Becker & le Roex, 2006; Figs. 5.9 and 5.12) and to potassic ultramafic dykes and plugs from the Kainab alkaline province of southern Namibia, associated with the Cambrian Kuboos-Bremen igneous province (Miller, 2008). Major element data from these rocks are shown in Figure 5.10. along with data for Saltpeterkop melilitites and ultramafic lamprophyres. Each sample type tends to plot as a group, with the Saltpeterkop melilitites having very similar SiO_2, TiO_2, Al_2O_3, $FeO^{tot.}$, CaO and alkali contents to the Western Cape melilitites, but extending to lower MgO values. The Saltpeterkop ultramafic lamprophyres have distinctly lower TiO_2 as well as MgO and K_2O values that tend to be lower and higher, respectively, than those in the melilitites. As a group, all of the Saltpeterkop melilitites and ultramafic lamprophyre (UML) samples fall at lower MgO values than Group 1 kimberlites, and at the low end of the range for Group 2 kimberlites from southern Africa. The Saltpeterkop UML do show a close chemical resemblance (in chemical variability and average composition) to potassic, carbonated ultramafic lamprophyres from the Kainab Alkaline Province of southern Namibia, which is part of the Cambrian Kuboos-Bremen igneous province (Moore et al., 2008; Reid, 1991).

In terms of their compatible (e.g., Ni and Cr) trace element concentrations, the Saltpeterkop melilitites and ultramafic lamprophyres overlap significantly, but both groups

extend to lower values than found in the other Western Cape melilitites and they are significantly lower than those of southern African Group 1 or Group 2 kimberlites, presumably due to their range of differentiation. However, all of these rocks lie on a similar trend line of Ni and Cr

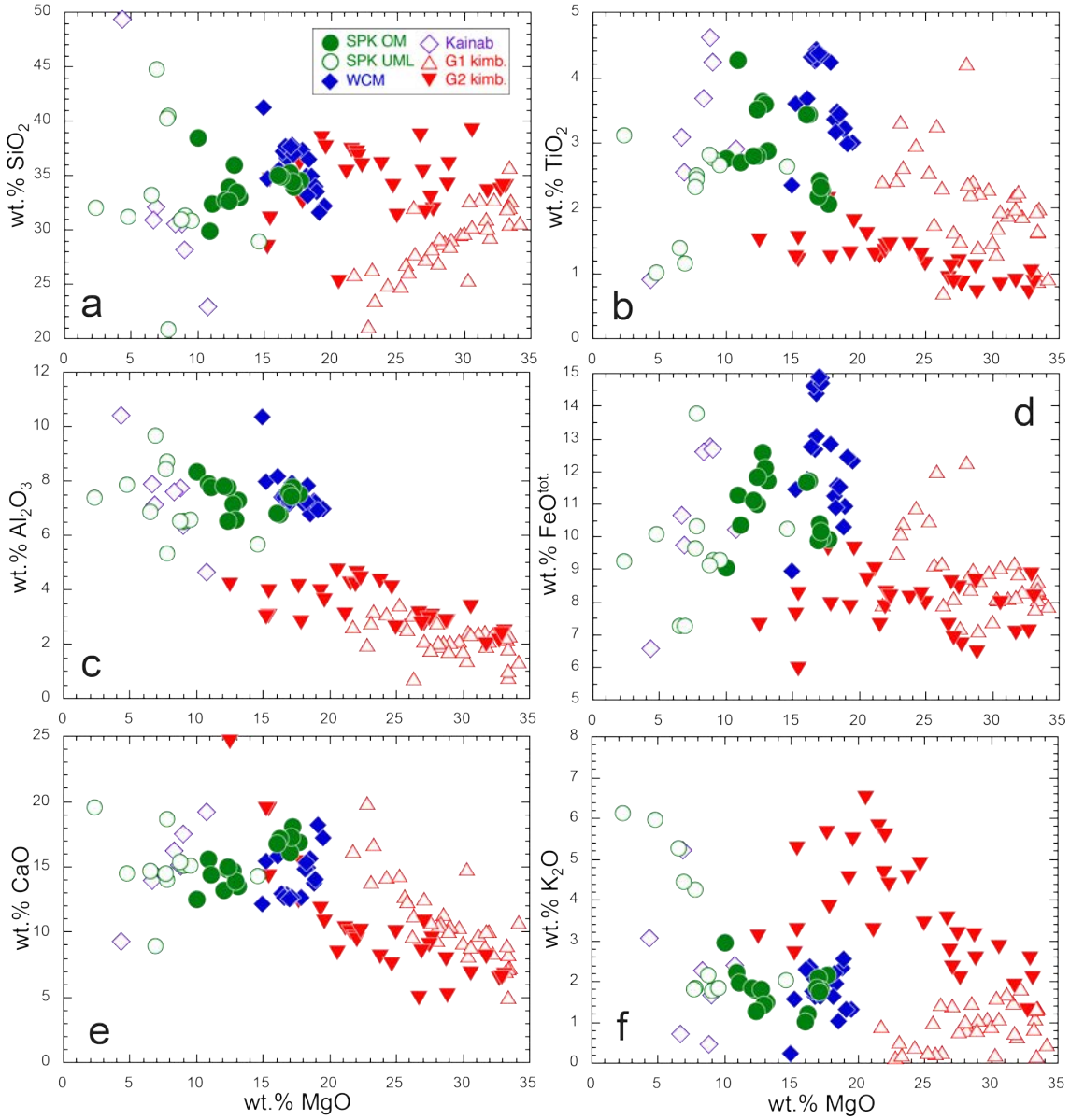

Figure 5.10. *Variation diagrams of wt.% MgO versus other major elements in olivine melilitites (OM) and ultramafic lamprophyres (UML) from Saltpeterkop compared with those from the Western Cape melilitites (WCM; Janney et al., 2002), South African Group 1 (G1) and Group 2 (G2) kimberlites (le Roex et al., 2003; Becker & le Roex, 2006 and Coe et al., 2008) and carbonated ultramafic lamprophyres of the Kainab Alkaline province, southern Namibia (Bishop and Janney, unpublished data 2015). Plots show wt.% MgO versus (a) SiO_2, (b) TiO_2, (c) Al_2O_3, (d) $FeO^{tot.}$, (e) CaO, (f) K_2O.*

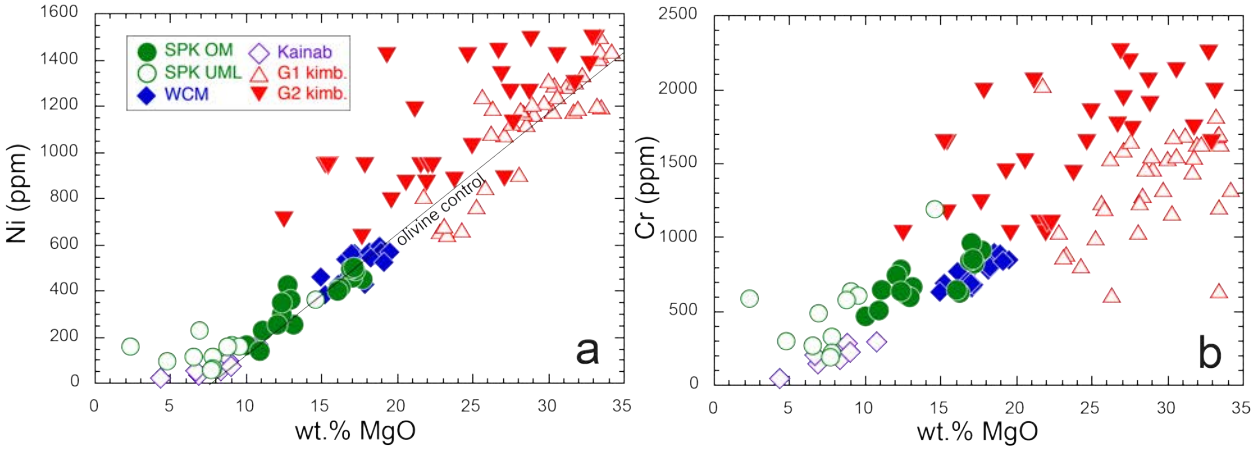

Figure 5.11. *Plots of MgO content versus (a) Ni and (b) Cr concentration for Saltpeterkop olivine melilitites (OM) ultramafic lamprophyres (UML), the Western Cape melilitites (WCM), southern African Group 1 (G1) and Group 2 (G2) kimberlites and ultramafic lamprophyres of the Kainab alkaline province, southern Namibia. Thin black line in (a), labelled "olivine control", shows the change in composition due to accumulation or fractionation of the average olivine composition measured by Mabaso (2017). Data sources are the same as in Figure 5.10.*

concentrations plotted versus MgO, indicating that their concentrations are mainly controlled by fractionation/accumulation of a similar set of minerals (presumably olivine, clinopyroxene and spinel).

In terms of incompatible element concentrations, there is a large degree of overlap between the Saltpeterkop melilitites and ultramafic lamprophyres, the other Western Cape melilitites and southern African kimberlites (particularly group 1 kimberlites). The Saltpeterkop melilitites and lamprophyres display greater enrichments in the highly incompatible elements and Pb generally (as indicated by their relatively high Ba/Nb, Th/Nb, La/Nb and low Ce/Pb ratios) than the Sutherland, Robertson or Spiegelrivier Western Cape melilitites and these enrichments are in some cases greater than in Group 1 kimberlites (e.g., Fig. 5.12). In contrast, southern African Group 2 kimberlites display strong enrichments in Rb and Ba not seen in the other rock types.

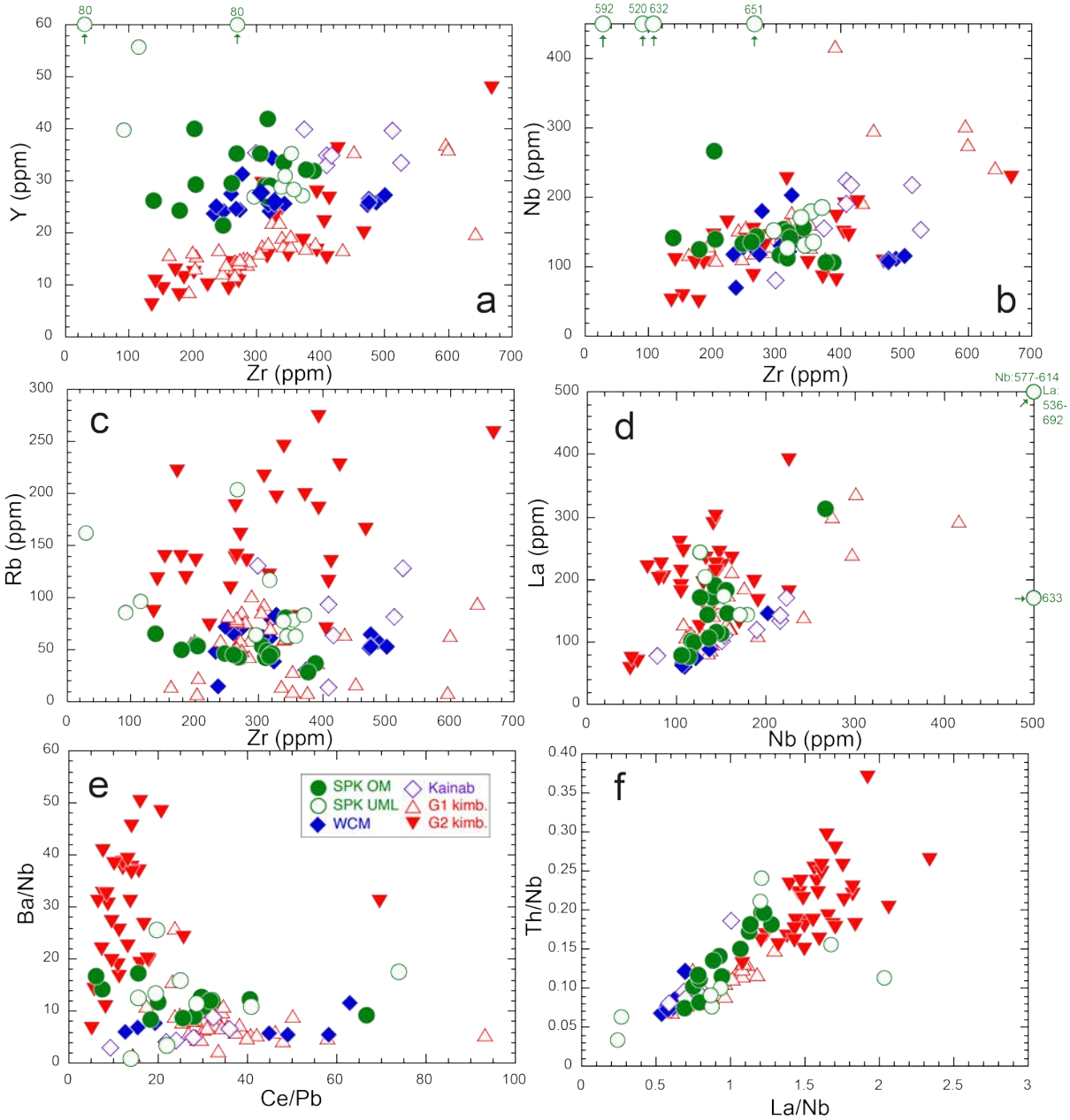

Figure 5.12. *Incompatible element concentration and ratio plots comparing the Saltpeterkop olivine melilitites (OM) and ultramafic lamprophyres (UML) with those of the Western Cape melilitites (WCM), southern African Group 1 (G1) and Group 2 (G2) kimberlites, and ultramafic lamprophyres of the Kainab Alkaline province, southern Namibia. Panels (a-c) show Zr plotted versus (a) Y, (b) Nb, (c) Rb. Panel (d) shows Nb vs. La, (e) shows Ce/Pb versus Ba/Nb ratios and (f) shows La/Nb versus Th/Nb ratios. Data sources are as in Fig. 5.10.*

6. DISCUSSION

This thesis has described four main igneous rock types at the Saltpeterkop carbonatite complex: (1) carbonatites, (2) potassic trachytes, (3) olivine melilitites and (4) ultramafic lamprophyres. It has also described crusts and mineralised breccias rich in iron and manganese oxides. However, as the rock samples in this last category likely represent extreme extents of hydrothermal alteration and/or supergene enrichment processes, they will not be discussed further here.

The main aim of this chapter is to address several questions regarding the origin and petrogenesis of the Saltpeterkop igneous rocks:

(a) What constraints can be placed on the source composition, source mineralogy and conditions of melting in the origin of the olivine melilitites and ultramafic lamprophyres?

(b) Can the more differentiated olivine melilitites and ultramafic lamprophyres be related to the more primitive ones by simple fractional crystallization? If so, what mineral assemblage(s) were likely involved. Also, do the ultramafic lamprophyres appear to be derived from the olivine melilitites (or vice versa) by fractional crystallization?

(c) What constraints can be placed on the petrogenesis carbonatites at Saltpeterkop? Can they be plausibly related to one or more of the other magma types? Which differentiation processes (e.g, liquid immiscibility, fractional crystallization) appear to be most important in this evolution?

(d) What constraints can be placed on the petrogenesis of the potassic trachytes at Saltpeterkop? Is there evidence to support their derivation from fenitised continental crust, as has been proposed for other southern African carbonatites (e.g., Cooper & Reid, 2000)?

(e) What were the most important processes leading to rare earth element enrichment in the Saltpeterkop complex?

6.1 Constraints on the differentiation of the olivine melilitites and ultramafic lamprophyres

The olivine melilitites and ultramafic lamprophyres span significant ranges of Mg# values (78.5 to 66.4 and 74.4 to 49.3, respectively, excluding the altered lamprophyre breccia SKGB-1). These ranges indicate that not all of these samples can represent primary magmas and so some amount of differentiation must have taken place. This could include accumulation processes (i.e., incorporation of previously crystallized material) as well as conventional fractional crystallization. The crystallization sequence in the melilitites was modeled in three stages, from those with the highest to the lowest Mg# values, with the daughter composition from the previous stage serving as the parent for the following stage. Mineral compositions used were those of Mabaso (2017) and Boctor and Yoder (1986), please see Appendix 1, Tables 1, 2, 3 and 4 for details regarding the mineral data used. The evolution of the ultramafic lamprophyres was similarly modeled in two stages.

Least-squares fractionation models were calculated using the Solver module in MS Excel. The Solver uses iterative calculations to minimize mismatch between the model result and a true sample composition. The least squares models are based on mixing equations like the one below:

$$(SiO_2)_{parent} = (SiO_2)_{daughter}*F + (SiO_2)_{min1}*X + (SiO_2)_{min2}*Y + (SiO_2)_{min3}*Z +... \quad (1)$$

where F is the proportion of (daughter) magma remaining at the end of the crystallization step and X, Y, and Z are the relative proportions of minerals 1, 2, 3, etc. that crystallized from the parent magma. F, X, Y, and Z etc. are all fractional values between 0 and 1 and their sum must equal 1.

This equation is calculated for every major oxide (e.g., SiO_2, TiO_2, Al_2O_3 etc.), for all possible mineral assemblages with the stipulation that, in every model, the values for F, X, Y, Z, etc. must be the same for every oxide (i.e., as these represent the proportions of daughter melt and fractionating minerals). The mismatch between the modeled parent composition and the actual parent composition for each oxide (e.g., residual SiO_2 = wt.% SiO_2 for modeled parent - wt.% SiO_2 for actual parent) is called the *residual* and the mixing proportions F, X, Y, Z, etc. are determined iteratively by the Solver so as to minimise the sum of the squares of residuals (also called the *residual sum of squares* or RSS) for all oxides:

RSS = (residual wt.% $SiO2)^2$ + (residual wt.% $TiO2)^2$ + (residual wt.% $Al2O3)^2$ + (residual wt.% $FeO^{tot.})^2$ + (residual wt.% $MnO)^2$ + (residual wt.% $MgO)^2$ + (residual wt.% $CaO)^2$+ (residual wt.% $Na_2O)^2$ + (residual wt.% $K_2O)^2$ (2)

6.1.1. Olivine melilitites least squares fractionation results

The models for the olivine melilitites are based upon the following conditions and assumptions:

(1) Olivine melilitite whole-rock compositions were normalised so that the values of SiO_2, TiO_2, Al_2O_3, $FeO^{tot.}$, MnO, MgO, CaO, Na_2O and K_2O summed to 100 wt.% (i.e., no P_2O_5 or volatiles are included). This was done to avoid complications due to the facts that (1) H_2O and CO_2 are not measured separately, (2) the possibility that some volatiles in whole-rock sample compositions may have resulted from alteration, and (3) because no P2O5-bearing minerals were measured (such as apatite or monazite).

(2) All minerals were re-normalised so that the values of SiO_2, TiO_2, Al_2O_3, $FeO^{tot.}$, MnO, MgO, CaO, Na_2O and K_2O summed to 100 wt.%. Elements that were not determined (e.g., Na_2O and K_2O in olivine, OH in phlogopite) were assumed to be 0.

(3) For each crystallization stage in the olivine melilitite modeling, the same potential mineral assemblage was used (olivine, clinopyroxene, melilite, titanomagnetite, perovskite, phlogopite and nepheline) but the mineral compositions used, where possible, were those measured in the parent (preferred) or daughter (if mineral compositions from parent are unavailable), or from another sample with roughly similar composition (if mineral compositions from neither parent nor daughter are available), or finally, from a relevant published source if no primary data were available. This latter case was only true for the mineral nepheline, which was not measured by Mabaso (2017)). The nepheline composition used was from Boctor and Yoder (1986), from a melilitite from the M5 pipe.

The models outlined above indicate that the variably differentiated melilitites can be derived from one another by fractional crystallization of assemblages consisting mainly of

olivine, melilite, clinopyroxene, phlogopite and oxide minerals, with melilite being most important in the earlier stages and clinopyroxene initially not being involved, but becoming increasingly important in the later stages. The RSS values of these models are between 1.8 and 2.5, which represent reasonable model fits.

Table 6.1. Example of least squares fractionation calculation (ol. melilitite stage 1)

	%	Fraction	SiO2	TiO2	Al2O3	FeO	MnO	MgO	CaO	Na2O	K2O	Total
Daughter												
SP31-3	**46.8**	0.47	38.11	3.73	7.44	12.72	0.21	17.49	18.22	0.96	1.12	100.0
olivine	14.3	0.08	40.61	0.06	0.25	10.45	0.22	47.73	0.67	0.00	0.00	100.00
clinopyroxene	0.0	0.00	51.56	0.91	3.18	5.84	0.11	15.46	22.25	0.66	0.01	100.0
melilite	47.0	0.25	43.10	0.07	6.23	2.38	0.05	9.97	35.43	2.59	0.19	100.0
Ti-magnetite	7.4	0.04	0.08	12.12	8.19	72.12	0.79	6.61	0.10	0.00	0.00	100.00
Perovskite	1.6	0.01	0.00	58.88	0.66	1.48	0.00	0.03	38.95	0.00	0.00	100.00
Phlogopite	28.7	0.15	42.79	1.38	13.26	5.71	0.07	27.40	0.02	0.12	9.24	100.00
Nepheline	1.0	0.01	42.84	0.00	33.53	0.17	0.00	0.08	0.21	22.97	0.20	100.00
SUM	100.0	1										
calculated			38.46	2.97	7.58	11.07	0.17	18.75	17.78	1.24	1.98	100.00
SKM6-1			37.45	2.24	8.20	10.78	0.19	19.21	18.33	1.26	2.34	100.00
Parent												
sum of squares	2.6338	residuals	-1.00	-0.73	0.62	-0.29	0.02	0.45	0.55	0.02	0.36	

Column labeled "Fraction" gives the fractional values of daughter melt plus minerals in the fractionating assemblage (all summing to 1.0). Column labelled "%" gives the fraction of liquid remaining in percent, and, separately, the percentage of all minerals in the crystallizing assemblage (where sum of all minerals = 100%). All compositional data are given in weight percent. Bottom row gives the residuals (mismatches) for all oxides, as well as the value of the sum of residuals squared

However, the fractionation assemblages calculated by the least-squares models are not always consistent with the petrographic evidence. For example, olivine only makes up 14 to 23% of the crystallising assemblage in any of the three steps, which seems implausibly low given that olivine is by far the most abundant phenocryst in every melilitite sample and often a dominant groundmass phase as well. Additionally, taken at face value, the models indicate that the most differentiated melilitite, SKM2-1 (Mg# = 66.4) could represent 86% crystallization of the most primitive melilitite, SKM6-1 (Mg# = 78.5), which seems an unrealistically high extent of crystallization for such a limited change of Mg# values. To some extent, this high value may be due to the likelihood that SKM6-1 (with Mg# = 78.5) represents the product of olivine accumulation and is therefore not a true liquid composition.

Table 6.2. Summary of results of least squares fractional crystallization models for olivine melilitites

					----------All values shown in %----------							
	Parent	Mg#	Daughter	Mg#	F	ol	cpx	mel	phlog	neph	Ti-mag	pv	RSS
(1)	SKM6-1	78.5	SP31-3	73.8	**46.8**	14.3	0.0	47.0	28.7	1.0	7.4	1.6	**2.63**
(2)	SP31-3	73.8	SP43-2	69.7	**40.5**	23.1	10.5	42.0	11.8	0.0	9.0	3.5	**2.50**
(3)	SP43-2	69.7	SKM2-1	66.4	**78.0**	20.8	51.9	8.7	18.7	0.0	0.0	0.0	**1.78**

Abbreviations: F, percentage of liquid remaining (after crystallization step), ol, olivine, cpx, clinopyroxene, mel, melilite, phlog, phlogopite, neph, nepheline, Ti-mag, titanomagnetite, pv, perovskite, RSS, residual sum of squares. Values given for minerals are their percentage in the fractionating assemblage. Please see text for explanation.

These issues show some of the weaknesses of the least squares modeling technique. The program tunes the results to minimize the RSS, regardless of whether the assemblage chosen is plausible based on the petrographic evidence. A combination of melilite (which contains much more Ca relative to Mg, Fe and Si than cpx) along with olivine (Mg-rich), Fe-Ti oxides (Fe- and Ti-rich) and phlogopite (Al- and K-rich) can be used by the model preferentially to clinopyroxene because this mixture of minerals can be tuned to minimize the residuals more effectively than with clinopyroxene (which has significant SiO_2, TiO_2, Al_2O_3, FeO, MgO and CaO in fixed proportions that cannot be independently tuned). Additionally, the program weights residuals of the different oxides equally, so that a residual mismatch of 0.4 wt.% in SiO_2 counts the same as a residual mismatch of 0.4% in K_2O, despite the fact that the rocks contain roughly 40 wt.% SiO_2 but only 1 to 3 wt.% K_2O. Because of this, the relative mismatch for the minor oxides (e.g., TiO2 and especially Na_2O and K_2O) is much larger than for the major oxides (e.g., SiO_2, Al_2O_3, FeO, MgO and CaO). All of this means that, while these results are useful in showing that the different melilitite samples can be related by fractional crystallization, it must be understood that these models are likely not correct in detail and should not be interpreted to precisely reflect crystallization history.

6.1.2. Olivine melilitites - equlibrium olivine fractionation modeling

An alternative technique for estimating the extent of fractionation for mildly differentated rocks is the technique of iteratively adding increments of olivine in equilibrium with the sample's bulk composition until a primary magma composition (i.e., Mg# = 73) is attained. Limiting the crystallizing assemblage to only olivine is, admittedly, an oversimplification but it is clear that

Table 6.3. Calculated extents of olivine fractionation/accumulation in SPK olivine melilitites

OM locality	Avg. % ol crystallization
M1 sill	8
M2 dyke	16
M5 pipe	-7
M6 pipe	-10
SP-31 pipe	-1
SP-43 dyke	9
SP-206 dyke?	14

Percent fractionation of olivine is indicated by positive numbers, accumulation is indicated by negative numbers. Data are averaged by locality. Values were calculated by iteratively adding (or subtracting in the case of samples with Mg# > 73) 1% increments of olivine in equilibrium with the magma composition until a Mg# value of 73 was achieved, assuming Fe-Mg partitioning of Roedder & Emslie (1970).

(1) olivine is by far the dominant phenocryst in these samples and therefore is likely the dominant fractionating phase and (2) this method provides a useful independent alternative constraint to the least squares modeling. Using this method, the compositions of the olivine melilitites appear to represent up to 16% fractional crystallization and up to 10% olivine accumulation relative to an ideal primary magma with Mg# = 73, in equilibrium with mantle olivine of Mg# = 91 (Table 6.2 above). This gives a much smaller and more plausible figure of only 26% total variation in (olivine) crystallization from SKM6-1 to SKM2-1, compared to the 86% total crystallization estimated by the least squares method.

6.1.3. Ultramafic lamprophyre least squares results

Fractional crystallization was modeled in the ultramafic lamprophyres using an approach similar to that applied to the olivine melilitites. It is important to note that the ultramafic lamprophyres have some differences in mineralogy to the melilitites. The most significant of these are that the lamprophyres contain significant calcite, and for this reason has higher "loss on ignition" values (the % weight lost upon heating the sample to 850°C in a furnace for 4 hours) than the melilitites. The large amounts of calcite present mean that CO_2 cannot be avoided as an important component of the rocks. Therefore, these models include CO_2. Of less importance, the lamprophyres do not appear to contain melilite so this mineral was not included in the lamprophyre models.

The following assumptions/model parameters were used for the ultramafic lamprophyres:
1) In the parent and daughter magmas, the LOI value is attributed entirely to CO2. These whole rock compositions are still normalised to 100% on a H2O-free and P2O5-free basis.
2) For calcite, the missing percentage (100% - mineral total) is assumed to be CO2.
3) Because no oxide minerals (Ti-magnetite & perovskite) were measured in the lamprophyres, the compositions of these minerals used were those from intermediate composition olivine melilitites.

Table 6.4. Summary of least squares fractional crystallization results for ultramafic lamprophyres

Parent	Mg#	Daughter	Mg#	F	ol	cpx	phlog	neph	Ti-mag	cc	RSS
SP367-1	74.4	SP38-1	66.6	**61.6**	40.8	0.0	22.1	3.0	8.0	26.2	0.32
SP38-1	66.6	SPKC-12	49.3	**70.0**	39.8	13.0	0.0	17.3	1.1	28.8	9.4

Please see text and Table 6.2 caption for explanation. Abbreviations as in Table 6.2 with addition of cc, calcite.

The transition from the most primitive to the most evolved ultramafic lamprophyres can therefore be explained as the result of fractional crystallization of a mineral assemblage dominated by olivine and calcite, with variable amounts of clinopyroxene, phlogopite, nepheline and titanomagnetite. The large RSS value in fractionation step 2 (SP38-1 to SPKC-12; RSS = 9.4) is likely at least partly due to the large difference in sample compositions and the fact that the mineral compositions used are likely far from being in equilibrium with the parent and daughter compositions. The addition of CO2 (and thus the use of 10 oxides instead of 9 as with the melilitites) also may contribute to the higher RSS values.

6.1.4. Are the olivine melilitites and ultramafic lamprophyres related by fractional crystallization?

It seems extremely unlikely that the olivine melilitites are related to the ultramafic lamprophyres by simple fractional crystallization. The most direct evidence supporting this statement is that the most primitive olivine melilitites (from the M6 pipe) and the most primitive ultramafic lamprophyre (the SP367 dyke) are similarly primitive, with Mg# values of 78.5 and 74.4, respectively. There is, therefore, no evidence to suggest that the generally higher K_2O and

lower SiO_2, CaO and Na_2O of the ultramafic lamprophyres are caused by fractional crystallization of an olivine melilitite parent (or that the melilitites are derived from a lamprophyre parent). Rather, the major element differences and trace element similarities between the melilitites and lamprophyres would seem to suggest that both are derived from sources with similar incompatible element compositions, but with source mineralogies and conditions of melt generation that were significantly different. This conclusion is supported by the seminal experimental work on the petrogenesis of olivine melilitites by Brey and coworkers Brey and co-workers (Brey and Green, 1977; Brey, 1978, Brey et al., 1983)

6.2. Conditions of melt generation and source mineralogy & composition

A wide range of experimental and analytical studies (e.g., Brey et al., 1978; Ringwood et al., 1992; Kesson et al., 1994; Wilson et al., 1995; Wyllie and Lee, 1999; Tappe et al., 2006) have concluded that olivine melilitites, ultramafic lamprophyres and similar magmas, including group 1 kimberlites, are the product of low degrees of partial melting of carbonated peridotite sources, with melting occurring largely or entirely in the garnet stability field.

6.2.1. Constraints on degrees and depths of melt generation

The rare earth elements are particularly useful for constraining degrees and depths of melt generation because they are a group of incompatible elements with identical valence state and smoothly varying ionic radius, which controls their incompatibility during melting. While any modeling of melting processes based on the REE are dependent on assumptions of source composition, source variations are most likely to affect the lighter REE, whereas variations in the degree of partial melting are likely to have a greater influence on the middle to heavy REE (McKenzie & O'Nions, 1991). Additionally, the relative abundances of the heavy REE in mantle-derived igneous rocks are strongly affected by the presence (or absence) of garnet in the source lithology. The heavy REE are compatible in garnet, meaning that magmas generated from a mantle source with residual garnet will have lower HREE abundances for any given degree of partial melting than a melt generated from a garnet-free but otherwise identical source. Since the presence of garnet in mantle peridotite is a function of pressure (garnet being the stable Al-bearing mantle phase at depths greater than about 70 km), the relative depletion of the heavy REE can be used to infer, in a relative sense, the average depth of melting of a mantle-derived

igneous rock. However, it is important to note that this approach can be invalidated if melts are derived from lithologically heterogeneous mantle sources containing rock types such as garnet pyroxenite or eclogite. These garnet-pyroxene-dominated rocks are stable to considerably lower pressures than garnet peridotite (Hirschmann and Stolper, 1996) and, therefore, can generate HREE-depletions in magmas generated at depths shallower than the stability field for garnet-bearing peridotite.

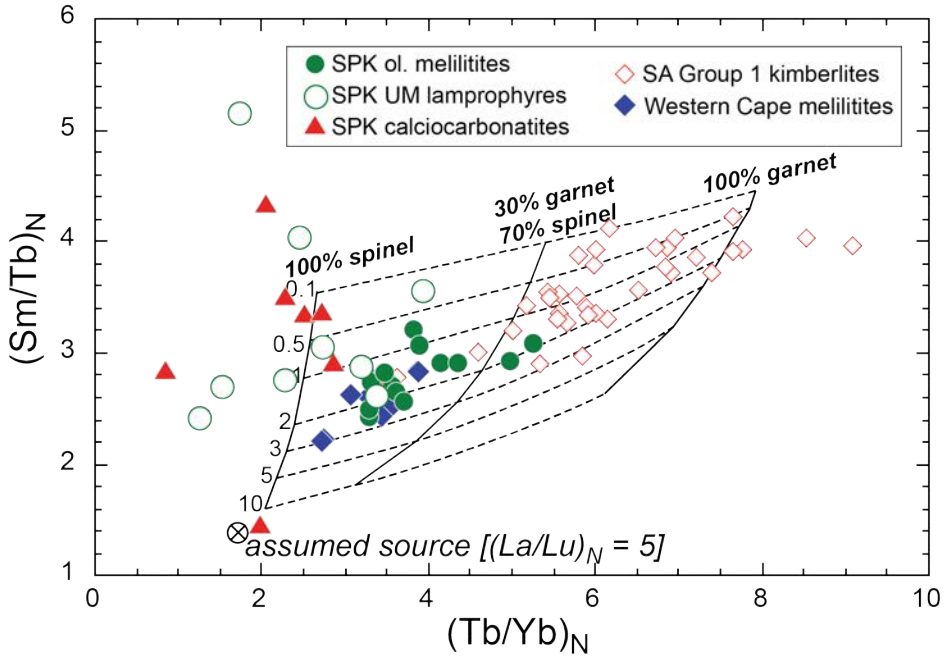

Figure 6.1. *Chondrite-normalised Tb/Yb versus Sm/Tb ratios for Saltpeterkop olivine melilitites, ultramafic lamprophyres, and calciocarbonatites compared with data for the Western Cape melilitites, and South African group 1 kimberlites (data from same sources as cited in Fig. 5.10). Melting grid shows compositions of melts of assumed source composition calculated for different degrees of partial melting (0.1 to 10%) of a peridotite mantle source having variable relative proportions of spinel and garnet. Assumed modal and melt contribution proportions of olivine/orthopyroxene/clinoproxene/(spinel + garnet) were 0.5/0.3/0.1/0.1 and 0.25/0.25/0.25/0.25. Partition coefficients used are given in Appendix 3, Table 1.*

Figure 6.1 shows a plot of chondrite-normalised Tb/Yb versus Sm/Tb ratios, with a grid of hypothetical melt compositions generated by varying degrees of partial melting (0.1 to 10%) from a series of mantle sources (spinel peridotitie (i.e., garnet-free), 30% garnet-/70% spinel-peridotite and 100% garnet peridotite) from a hypothetical, moderately enriched mantle source with a linear REE pattern having $(La/Lu)_N = 5$. This composition was chosen so as to be able to generate melts straddling the range from the Saltpeterkop ultramafic lamprophyres to southern

African group 1 kimberlites. Variations in degree of partial melting of any given mantle source tend to produce larger variations in $(Sm/Tb)_N$ ratios than in $(Tb/Yb)_N$, whereas changes in the spinel/garnet ratio of the mantle source, for any given degree of partial melting, produce much larger changes in $(Tb/Yb)_N$ than $(Sm/Tb)_N$. Obviously, the source composition selected is fairly arbitrary and the melting grid is only meant to be a relative guide to show the effects of different degrees of melting at different average depths for a single given source composition.

The olivine melilitites from Saltpeterkop form a sub-horizontal array on Figure 6.1 suggesting that they were generated by roughly similar degrees of melting from sources with variable modal proportions of garnet (e.g., being generated by 1 to 3% partial melting overall and with ≈10% to ≈50% of this melting occurring in the presence of garnet peridotite assuming the source composition shown). If the melilitites' sources were only peridotitic (i.e., did not contain significant pyroxenite), then this suggests that they were generated by melting over a significant range of depths. It may be significant that the garnet signature in the other Western Cape melilitites overlaps with that of the Saltpeterkop melilitites, but is significantly less overall (i.e., with only ≈5 to 20% of melting occurring in the presence of garnet peridotite, assuming the given source composition), whereas South African group 1 kimberlites show a much greater garnet signature overall as well as appearing to have been generated by slightly lower degrees of partial melting. Therefore, the Saltpeterkop olivine melilitites appear to be transitional in their conditions of melting between group 1 kimberlites and the other Western Cape melilitites, which is not surprising given that they lie more toward the continental interior than the other localities.

In contrast to the melilitites, the ultramafic lamprophyres and calciocarbonatites plot at relatively low $(Tb/Yb)_N$ ratios and moderate to high $(Sm/Tb)_N$ ratios, suggesting much weaker garnet signatures as well as degrees of partial melting that are comparable or lower than those that generated the melilitites, although it is also likely that the source of these carbonate-rich rocks had higher LREE enrichment, and therefore Sm/Tb ratios, than those of the melilitites. It is important to point out that the lamprophyres and calciocarbonatites include samples that are significantly more differentiated than the melilitites and so must be treated with caution due to the possibility that fractional crystallization or other processes unrelated to partial melting may have affected their REE patterns/LREE enrichments. Indeed, the lamprophyres and calciocarbonatites with the highest $(Sm/Tb)_N$ ratios are also among the most differentiated in these groups. Nevertheless, even for the most primitive of these rock types, a smaller overall

proportion of the melting that generated them appears to have occurred in the presence of garnet-bearing mantle lithologies. Additionally, several authors have pointed out that lamprophyres and carbonatites are likely to be derived from highly metasomatised mantle sources, which likely have source mineralogies distinct from those of the alkali basalt clan igneous rocks (such as olivine melilitites), and would likely yield significantly different melt compositions than spinel or garnet lherzolite for a given degree or depth of melting (e.g., Lee & Wyllie, 2000; Pilet et al., 2008; Rosenthal et al., 2009). Therefore, better constraints on the source mineralogy of the ultramafic magmas (lamprophyres and melilitites) and the more primitive carbonatites are needed.

6.2.2. Constraints on the role of exotic minerals in the mantle source of the Saltpeterkop Complex

The presence of 'exotic' minerals (i.e., phases not commonly occurring in mantle peridotite, but which may be introduced by metasomatism) have been frequently invoked to explain the trace element characteristics of highly alkaline basalts and other low-degree mantle melts (e.g., Rogers et al., 1992; Class & Goldstein, 1997). The exotic minerals (i.e., phases other than olivine, pyroxene, garnet and spinel) most likely to be present in the mantle source(s) of the Saltpeterkop complex are carbonate (calcite or dolomite) as well as phlogopite and ilmenite. The prevalence of carbonatite requires a carbonate-rich mantle source (Wyllie & Lee, 1998) and phlogopite and ilmenite are common in a wide range of southern African mantle xenoliths (e.g., Gregoire et al., 2002; 2003) occurring far more commonly in southern African mantle xenoliths than other exotic phases such as rutile, amphibole, or zircon (e.g., Dawson & Smith, 1977; Erlank et al., 1987).

Carbonate minerals are consumed very rapidly during melting, and so are extremely unlikely to remain in the residue to cause trace element fractionations (Dasgupta & Hirschmann, 2006). In contrast, phlogopite and ilmenite, while consumed more rapidly than pyroxenes, garnet, spinel and olivine, can potentially remain in the residue following low degrees (<5%) of partial melting and so are much more likely to affect the trace element compositions of such low-degree melts produced (Foley et al., 1999). The possible role of phlogopite and ilmenite in the generation of the incompatible element compositions of the more primitive magmas from Saltpeterkop (olivine melilitites, ultramafic lamprophyres and calciocarbonatites) are examined

in Figure 6.2. Panel (a) shows the average, primitive-mantle normalised incompatible element patterns for the three sample groups from Saltpeterkop along with the group 1 kimberlite source composition from le Roex et al. (2003), hereafter termed the "G1 source".

Using the G1 source composition from le Roex et al. (2003), the composition of small-degree melts (0.1%, 0.5%, 1% and 2%) generated from (1) normal mantle peridotite, (2) phlogopite-bearing peridotite and (3) ilmenite-bearing peridotite were calculated and are shown in Figure 6.2 panels b, c and d. Use of the of the G1 source composition for the primitive Saltpeterkop magmas is an assumption, but seems plausible based on (1) the physical proximity of the Saltpeterkop Complex to southern African group 1 kimberlites (which occur roughly 150 km to the northeast), and (2) the overall major and trace element similarities between southern African kimberlites and the Saltpeterkop melilitites and lamprophyres (e.g., Figs. 5.9 and 5.10).

In general, there is fairly good agreement between the mean olivine melilitite and ultramafic lamprophyre compositions and the 0.5% and 1% melts of a "normal" peridotitic G1 source, including mild depletions in K and enrichments in Nb, Th and Ba relative to other highly incompatible elements. The only significant departure is a depletion in Rb relative to Ba in both igneous rock types, which is significantly more pronounced than in the melts of the G1 source. There is much poorer agreement between the patterns for the calculated melts and the mean calciocarbonatite composition, which, in addition to having much higher overall REE concentrations, has very strong negative K, Zr, and Hf anomalies, much lower Nb/La ratios and strong depletions in Rb and Ba relative to Nb and Th compared to melts of the kimberlite source.

Addition of 1% modal phlogopite to the melting assemblage results in very little change to the shape of the calculated melts of the G1 source except for greater depletions in Ba and especially Rb and K relative to other highly incompatible elements, such as Nb and Th. This causes the incompatible element patters of the 0.5 to 1% partial melts of the phlogopite-bearing G1 mantle source to match more closely those of the Saltpeterkop carbonatites and especially the olivine melilitites and lamprophyres compared to the phlogopite-free source over the elemental range from Nb to Rb. It should be noted, though, that the strong negative K anomalies in melts of the phlogopite-bearing peridotite are significantly greater than those seen in the olivine melilitites and lamprophyres, and yet are less than that seen in the average calciocarbonatite. In contrast, addition of 1% ilmenite to the melting assemblage results in significantly poorer agreement between the primitive Saltpeterkop igneous rocks and melts of the G1 source due to

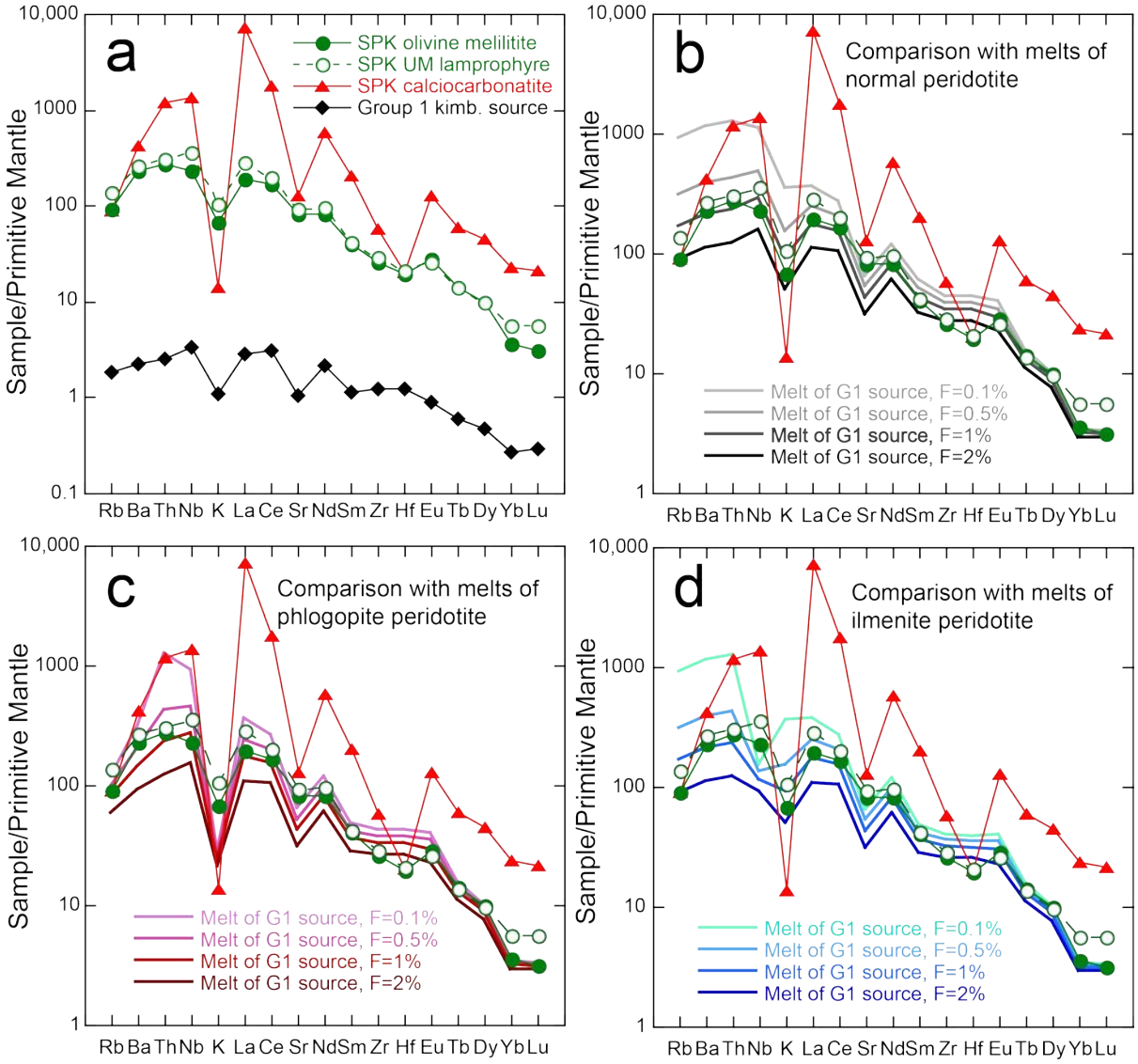

Figure 6.2. *(Panel a) Primitive mantle-normalised incompatible element diagrams showing the mean compositions of Saltpeterkop olivine melilitites, ultramafic lamprophyres and calciocarbonatites, as well as the Group 1 kimberlite source of le Roex et al. (2003). Panels (b-d) show the compositions of these three types of Saltpeterkop igneous rocks superimposed upon the compositions of equilibrium partial melts calculated from the Group 1 kimberlite source assuming (b) normal peridotite mineralogy (olivine, pyroxene, garnet and spinel only), (c) phlogopite-bearing peridotite (1% modal phlogopite added to the same modal assemblage as used in panel (b)) and ilmenite-bearing peridotite (1% modal ilmenite added to the same modal assemblage as used in (b)). Assumed modal proportions and melt contributions for the normal peridotite assemblage in (b) are 0.63/0.23/0.12/0.005/0.015 and 0.2/0.2/0.5/.025/0.075 for olivine, orthopyroxene, clinopyroxene, garnet and spinel, respectively. For panels (c) and (d), the modal proportions and melt contributions for phlogopite and ilmenite were both assumed to be 0.01 and 0.1, respectively, with the other modal contents and melt contributions adjusted proportionally. Partition coefficients used for these calculations are given in Appendix 3, Table 1.*

the relative depletions in Nb relative to elements of nominally similar incompatibility such as Th and La, caused by the strong compatibility of Nb in ilmenite (Zack and Brumm, 1998). Such depletions in Nb are not seen in the mantle-derived Saltpeterkop igneous rocks. On the basis of these models, it seems likely that the only exotic phase to have been residual to melting during the generation of the primitive Saltpeterkop igneous rocks was phlogopite. None of the calculated melt compositions does a particularly good job of matching the entire incompatible element pattern of the mean calciocarbonatite, likely indicating that the generation of this rock involved processes in addition to melting (such as significant fractional crystallization and/or immiscible liquid separation) that are also responsible for its incompatible element composition.

6.3 Petrogenesis of the Saltpeterkop carbonatites

The Saltpeterkop Complex is unusual in that it displays a nearly continuous range of compositions, from carbonatites through carbonated lamprophyres and ultramafic silicate rocks, that is distinct from that seen in most other carbonatite complexes. This is in contrast to many other carbonatite complexes (e.g., Spitskop, Dicker Willem, and the Damaraland intrusive complexes; Cooper & Reid, 1998; Harmer, 1999; le Roex and Lanyon, 1998) that display a much greater compositional gap between carbonatites and associated silicate igneous rocks.

A useful contrast to Saltpeterkop is provided by the carbonatite complex located on the island of Brava in the Cape Verdes oceanic island chain (Weidendorfer et al., 2016). This complex displays large compositional gaps between carbonatite and associated silicate rock types on a triangular plot of normalised molar Na_2O+K_2O, $CaO+MgO+FeO$ and $SiO_2+TiO_2+Al_2O_3$ (Figure 6.3). The main gap is between the magnesio- and calciocarbonatites falling near the $CaO+MgO+FeO$ corner, and the associated pyroxenites, ijolites, nephelinites, nepheline syenites, etc. that extend from the midpoint of the $[CaO+MgO+FeO]$-$[SiO_2+TiO_2+Al_2O_3]$ join, to a point on the $[SiO_2+TiO_2+Al_2O_3]$-$[Na_2O+K_2O]$ join (Fig. 6.3).

Weidendorfer et al. (2016) interpreted this distribution, based on the experimental work of Kjarsgaard & Peterson (1991) and Brooker and Kjarsgaard (2011), to be the result of separation of immiscible SiO_2 & Al_2O_3-rich silicate melts and alkali-rich carbonate melts. Subsequently, the initial carbonatites experience separation of an alkali carbonate fluid/melt

(which presumably is highly mobile and fenitises the surrounding crust during ascent) to leave the carbonatites rich in Ca and Mg and poor in Na and K.

In contrast, the lack of compositional gaps in the igneous rocks from Saltpeterkop do not appear to support a dominant role for liquid immiscibility in their generation. Rather, the main compositional variation of the Saltpeterkop complex carbonatites, lamprophyres and melilitites appearst to be plausibly explainable by variable extents of fractionation of mainly calcite/dolomite, olivine, clinopyroxene, phlogopite and oxide minerals, along with some

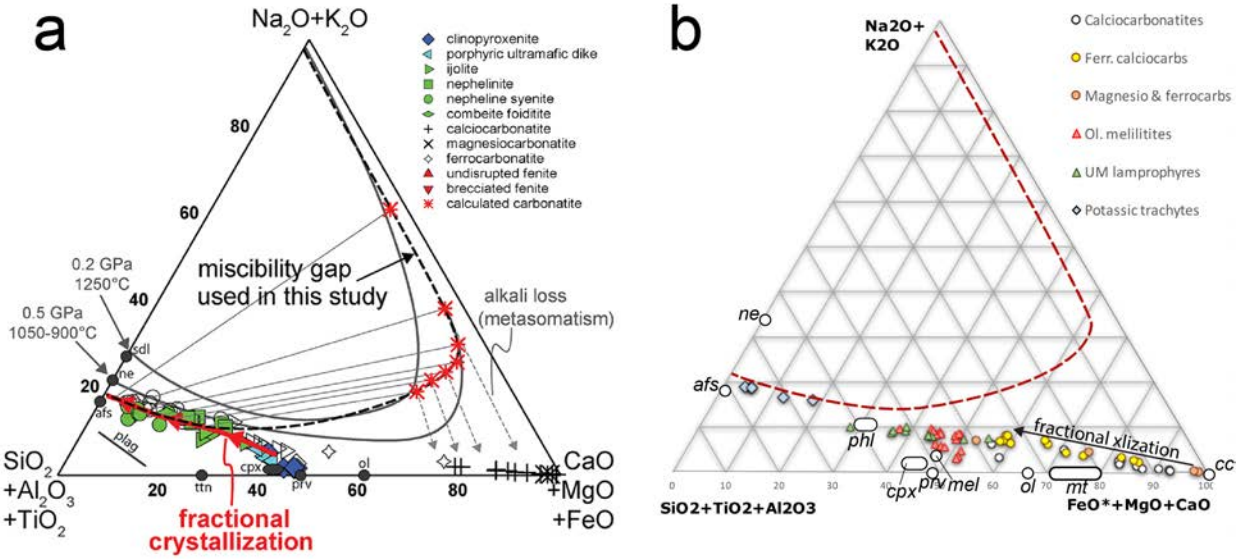

Figure 6.3. *A comparison of igneous rock compositions from (a) the carbonatite complex on the the island of Brava in the Cape Verdes chain (Weidendorfer et al., 2016) and (b) the Saltpeterkop Complex, on the basis of normalised molar oxide contents. Note the large compositional gaps between the Brava carbonatites and associated silicate rocks and the relative lack of such gaps in the data from the Saltpeterkop Complex (however there is a gap between the olivine melilitites and UMLs and the unaltered calciocarbonatites, filled with ferruginous calciocarbonatites derived by fractional crystallization, see vector). In both diagrams are shown the compositions of minerals occurring in the carbonatites and associated silicate rocks. Abbreviations: afs, alkali feldspar, cc, calcite, cpx, clinopyroxene, mel, melilite, mt, magnetite, ne, nepheline, ol, olivine, phl, phlogopite, prv, perovskite, ttn, titanite. The red dashed curve in panel (b) is the miscibility gap used in the Weidendorfer et al. (2016) study (same as black dashed curve in panel a).*

contribution from variations in source composition, mineralogy and degree/depth of melting. There is additionally no petrographic evidence observed in Saltpeterkop igneous rocks that would be indicative of separation of immiscible liquids (e.g., presence of carbonate segregations in ultramafic silicate igneous rocks, such as reported by le Roex and Lanyon, 1998).

On the basis of this evidence, it seems most plausible that the Saltpeterkop carbonatites were derived mainly by fractional crystallization processes from a more primitive magma. Whether this magma was purely carbonatitic in nature, or a carbonated silicate magma similar to the more primitive ultramafic lamprophyres at Saltpeterkop, is impossible to say with the available data. The latter possiblity, however, appears to be supported by the fairly strong trace element similarities between some of the ultramafic lamprophyres and the calciocarbonatites (e.g., Figs 5.7, 5.8 and 5.9). Given the evidence presented in section 6.1 for the primitive nature of the melilitites, it does not seem likely that the magmas from which these rocks formed, which appear relatively carbonate-poor, represent the silicate complement to the carbonatites. Rather, it seems likely that if the carbonatites formed from carbonated silicate melts, that there are likely accumulations of fractionated silicate minerals, constituting intrusive cumulate rocks such as as pyroxenites, ijolites and syenites, remaining unexposed at depth beneath the Saltpeterkop complex. Such rocks are common at deeply eroded intrusive carbonatite complexes (e.g., Marinkas Quellen, Dicker Willem, Spitskop; Smithies, 1991; Cooper & Reid, 1998; Harmer, 1999) but they have not been found at at Saltpeterkop, likely because this complex has not experienced similar deep levels of erosion (e.g., de Wet, 1975; Verwoerd, 1990).

6.4 Origin and evolution of the Saltpeterkop potassic trachytes

Along with the carbonatites, the potassic trachytes make up the most voluminous igneous rock types in the Saltpeterkop complex. These are also, by far, the most siliceous and potassic igneous rocks present and, because of this, they are difficult to plausibly derive by closed-system fractionation processes (such as fractional crystallization) from a parent composed of carbonatite, melilitite or ultramafic lamprophyre. Potassic trachytes and their coarse-grained intrusive equivalents are not uncommon at other carbonatite complexes in Africa (e.g., Toror Hills; Dicker Willem; Sutherland, 1965; Cooper & Reid, 2000) and they have been proposed to represent melts of local middle to upper crust that has been fenitised by interaction with immiscible alkali-rich carbonatitic fluids released from an intruding carbonatite or hybrid carbonate-silicate magma (Cooper & Reid, 2000). Such fenitisation could lead to crustal melting by both the solidus-lowering effect of the addition of alkali- and volatile-rich components, as well as heat, from the infiltrating fluid.

One way to evaluate the possible role of the melting of crustal fenites in the origin of the potassic trachytes at Saltpeterkop is through the modeling of the major and trace element composition of fenitised crustal rocks from the site. A number of mid- and upper-crustal xenoliths have been recovered from breccia pipes at Saltpeterkop, including amphibolites and clinopyroxenites, as well as dolerites and gabbros presumably of Karoo origin. Most of these xenoliths show little to no clear evidence of fenitisation, but one exception is an extraordinary mafic crustal xenolith, SP-100, that is composed mainly of subequal portions of euhedral biotite (≈40%) and aegirine-augite clinopyroxene (≈40%) with minor olivine, ilmenite and a trace of calcite and plagioclase feldspar (Fig 4.10). The presence of plagioclase, calcite and the euhedral texture of the biotite suggest that this sample represents a mafic crustal xenolith that had interacted with a hydrous, potassic carbonated melt or fluid. A mafic rock with such a potassium-rich composition (e.g., 4.2 wt.% K_2O) seems to represent a plausible source rock for potassic trachyte melts.

To test this hypothesis, the compositions of partial melts of SP-100 have been modeled using THERMOCALC (Powell et al., 1998), based on the whole-rock major element composition of the sample and the calculated mineralogy (which is very close to the observed mineralogy), for melts produced at a pressure of 7 kb (equivalent to ≈ 20 km or mid-crustal depth; Nguuri et al., 2001) at temperatures of 800°, 1000°C and 1200°C. The modeling employed the activity-composition models of White et al. (2014) and Green et al. (2016), and was based on the thermodynamic mineral stability data of Holland and Powell (2011). A summary of the melting model results is given below:

Table 6.5 Modeling results for melting of the SP-100 fenitised xenolith

	prior to melting	800°C	1000°C	1200°C
F	0	0.092	0.144	0.359
Cpx	0.421	0.361	0.357	0.278
Bi	0.454	0.456	0.427	0.371
Ol	0.100	0.163	0.200	0.330
Ilm	0.025	0.020	0.015	0.021

This table gives the fraction of melt present at varying temperatures, as well as the modal mineral proportions in the residual solid, all at 7 kb. Results were obtained using THERMOCALC, incorporating the activity-composition model of White et al. (2014) and Green

et al. (2016) and the thermodynamic mineral data set of Holland and Powell (2011). Abbreviations: cpx, clinopyroxene, bi, biotite, ol, olivine, ilm, ilmenite.

The composition of the calculated melts of SP-100 (Table 6.6) range from 50 to 75 wt.% SiO_2, similar to the trachytes measured, but they have K_2O and Al_2O_3 values that are below that of the range measured in the trachytes. A comparison of the major element compositions of the model melt compositions and the actual potassic trachytes is shown in Figure 6.4. The calculated melts are not a close match for the trachyte samples, but it is plausible that such melts, modified by fractional crystallisation plus significant assimilation of Beaufort Group sedimentary rocks, could generate compositions similar to those of the trachytes observed.

Table 6.6. Compositions of melts of SP-100 generated at different temperatures

Temp.	800°C	1000°C	1200°C
SiO_2	74.63	55.52	50.82
TiO_2	0.00	0.00	0.00
Al_2O_3	6.93	9.28	7.29
FeO^T	5.73	13.08	13.56
MgO	3.86	7.65	10.33
CaO	3.51	6.27	11.38
Na_2O	1.46	0.49	0.16
K_2O	3.89	7.71	6.46

Melt compositions were determined from calculated mineral compositions, mineral modes and melt fractions obtained from the THERMOCALC model described in Table 6.5 and the text.

The plausibility of this model can also be tested by comparing the trace element compositions of calculated melts of SP-100 with that of actual potassic trachyte samples from Saltpeterkop. This is shown in Figure 6.5, where primitive mantle-normalised incompatible element patterns for 10%, 20% and 40% equlibrium melts of SP-100 are shown, plotted along with the patterns for Salpeterkop potassic trachyte samples. The modal and melt contribution values for the different minerals used to calculated the melt compositions were obtained from the melting model (e.g., the values in Table 6.5). The calculated melts closely resemble the actual potassic trachyte compositions, particularly in reproducing the strong negative anomalies in Ti and K (caused by residual ilmenite and phlogopite), and the depletion in Rb relative to Th and Nb (also due to residual phlogopite), as well as depletions in Sr (inherited from the SP-100 source). The major and trace element evidence, therefore, strongly supports the model of Cooper

and Reid (2000) that melts of metasomatised/fenitised crust, such as that represented by the SP-100 xenolith, subsequently modified by assimilation-fractional crystallization processes, are the main source for the potassic trachytes.

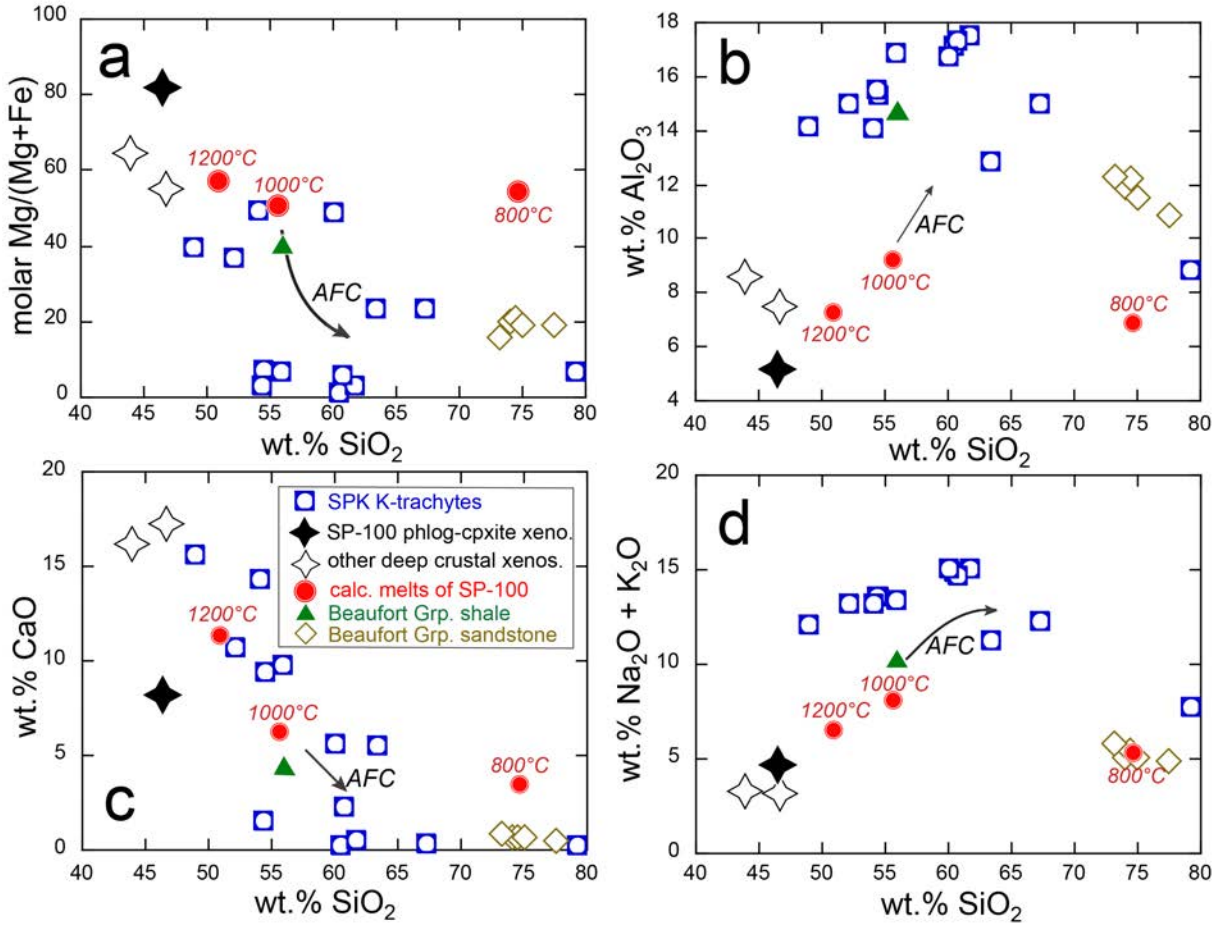

Figure 6.4. *Plots of wt.% SiO2 versus (a) Mg#, (b) wt.% Al_2O_3, (c) wt.% CaO, (d) wt.% total alkalis (Na_2O + K_2O). The compositions of Saltpeterkop potassic trachytes are shown along with those for lower to mid-crustal xenoliths, as well as Beaufort Group (upper crustal) sandstone (Paiva, 2015) and shale (this study). Schematic vectors for the effects of upper crustal assimilation-fractional crystallization (AFC) are shown for reference.*

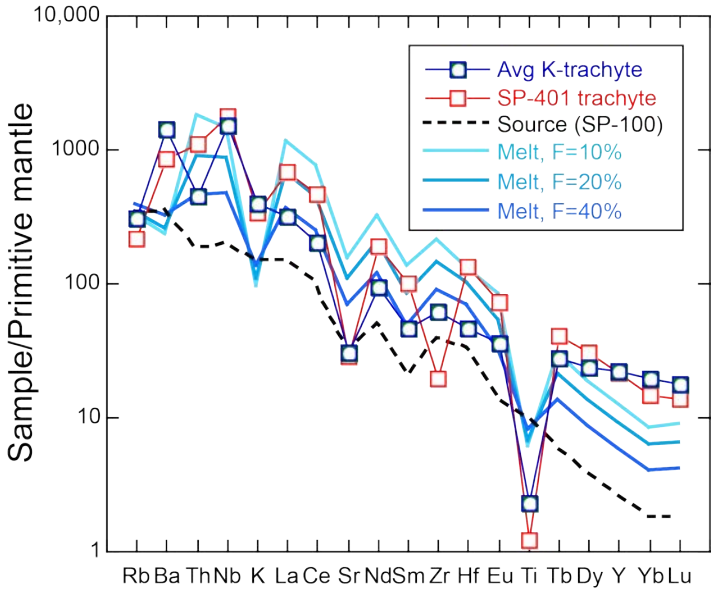

Figure 6.5. *Primitive mantle-normalised incompatible element diagram showing the average Saltpeterkop potassic trachyte composition, the fenitised, phlogopite-rich lower/mid-crustal xenolith SP-100, and calculated 10%, 20% and 40% equlibrium partial melts of this xenolith (using modal and melt-contribution values from the melting model) and potassic trachyte sample SP-401, which provides the closest match to the calculated melt compositions (aside from a negative Zr anomaly which is not reproduced in the calculated melts). Partition coefficients used are listed in Appendix 3 Table 1.*

6.5 Rare earth element enrichment processes and evolution of the Saltpeterkop complex.

Carbonatites host a range of economically valuable metals and the most significant of these are the rare earth elements. It is therefore important to understand the processes that led to the variable enrichment of these elements in the different igneous rocks of the Saltpeterkop Complex. To do this, it is instructive to see to what extent the rare earth elements have been enriched relative to other elements of similar magmatic incompatibility. This provides clues as to whether the distribution of rare earth elements was largely controlled by magmatic processes, or whether other processes, such as mineralisation, alteration or crustal contamination were also important. Figure 6.6 shows a plot of Nb/La versus Nd/Pb ratios. These element pairs have similar incompatibility during mantle melting and fractional crystallization of mafic phases, yet both ratios show large (tenfold to hundredfold) variations in the Saltpeterkop igneous rocks. The main variation is between the differentiated carbonatites (particularly the ferruginous calciocarbonatites) and the potassic trachytes, which extend toward low and high Nb/La ratios and high and low Nd/Pb ratios, respectively (Figure 6.6). The most likely explanation for these

trace element fractionations are, on the part of the carbonatites, extensive fractionational crystallization leading to extreme enrichment in the REE, possibly combined with the fractionation of Nb-rich phases such as pyrochlore (which had been found by de Wet (1975) and Verwoerd et al. (1995) but that has not been petrographically identified in this study), leading to low Nb/La and high Nd/Pb values. On the part of the potassic trachytes, the assimilation of deep continental crust that has been fenitised by Nb-rich alkaline carbonatitic fluids is likely the cause of the high Nb/La and low Nb/Pb ratios. High Pb concentrations in this crust may have been derived from the carbonatitic fluid, or may have been present in the crust prior to fenitisation.

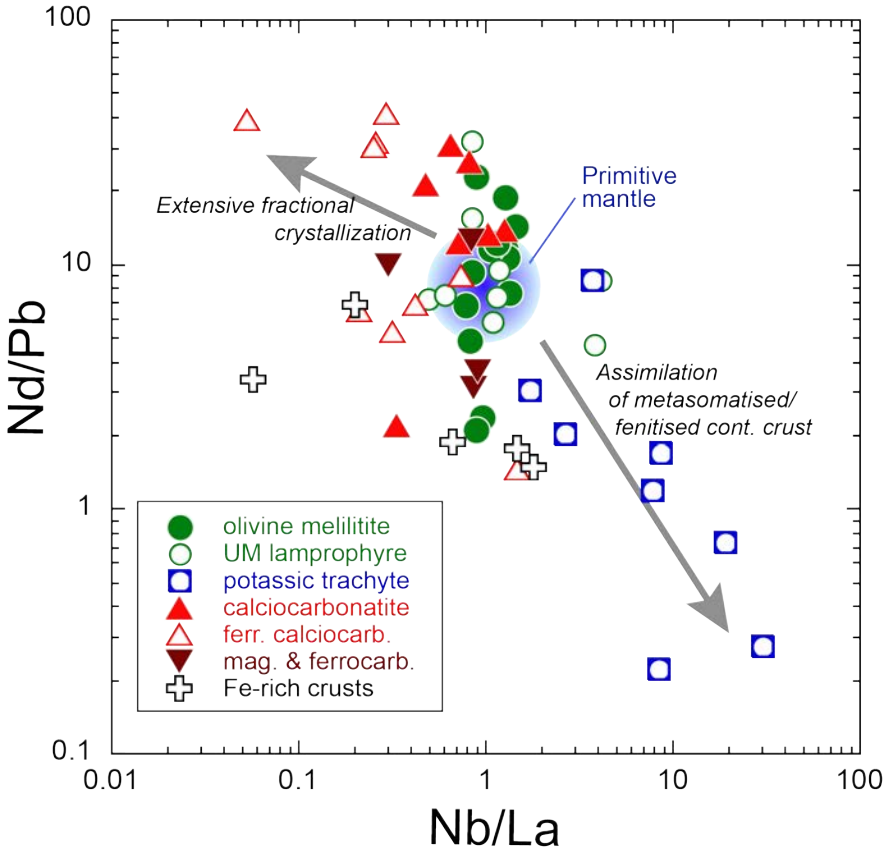

Figure 6.6. *Log-log plot of Nb/La versus Nd/Pb ratios in Saltpeterkop igneous rocks and iron-rich crusts. The primitive mantle composition (Sun & McDonough, 1995) is shown along with schematic vectors for fractional crystallization and crustal assimilation.*

The total rare earth element contents in the Saltpeterkop carbonatites vary from 0.01 to 1.7 wt.% total rare earth oxides (TREO), with an average value of 0.76 wt.%. This maximum value is significantly lower than that at other carbonatite complexes that have been explored for their economic rare earth element potential (e.g., Zandkopsdrift, with maximum grades in excess of 10 wt.%; Harper et al., 2015). However, it should be noted that the purpose of this study was

to characterise the geochemistry and petrogeneses of the main rock types at Saltpeterkop and that therefore, to accomplish this, the freshest available material as preferentially sampled and analysed. It is therefore possible that weathered material may exist that has considerably higher REE contents than that sampled. Indeed, at Zandkopsdrift, it is the supergene weathered cap zone of the complex that has the highest REE contents, whereas fresh carbonatite obtained by coring has average REE contents of only 0.6 wt.% TREO, slightly lower than for Saltpeterkop (Ogungbuyi et al., unpublished data 2015).

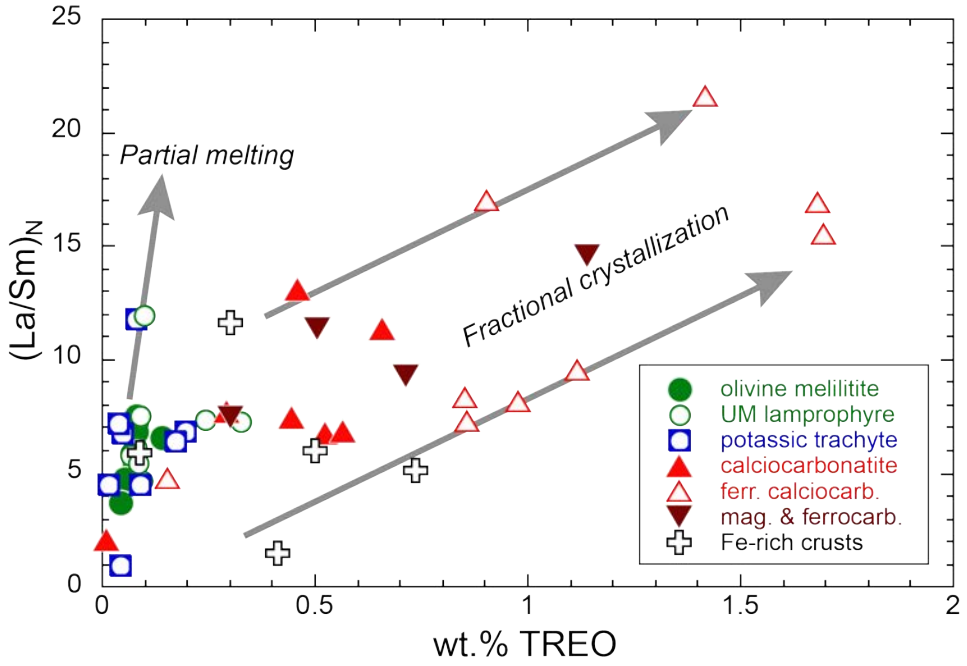

Figure 6.7. *Plot of weight % total rare earth oxides (TREO; sum of REE (La-Lu) concentrations expressed as weight percent oxides) versus chondrite-normalised La/Sm ratio for Saltpeterkop igneous rocks and Fe-rich crusts. Chondrite normalising values used are from Evensen et al. (1978). Schematic vectors represent the expected trends produced by variable extents of partial melting and fractional crystallization.*

Even though the extent of REE enrichment in the Saltpeterkop carbonatites is not extreme, it is important to understand the processes that have caused it. Allegre et al. (1977) found that partial melting and fractional crystallization processes produced distinct sloped trends on plots of incompatible element abundance versus the ratio of highly to moderately incompatible elements, with the steeper trend (of rapidly increasing incompatible element ratio for a given increase in incompatible element abundance) being the result of partial melting and

the shallower trend being the result of fractional crystallization. These trends can be seen clearly in the Saltpeterkop data on a plot of wt.% TREO versus chondrite- normalised La/Sm ratio. The primitive silicate igneous rocks (especially the olivine melilitites and ultramafic lamprophyres) primarily define the partial melting trend. In contrast, the carbonatites largely define the fractional crystallization trend, with the calciocarbonatites falling on the left side (low TREO values) of the diagram and the ferruginous calciocarbonatites falling on the right-hand side (high TREO values) of the diagram. This agrees with evidence previously mentioned for the ferruginous calcio- carbonatites representing, as a group, the most differentiated carbonatites and that the fractionation processes responsible for their REE enrichment had, at most, only a moderate effect on their extent of light rare earth element enrichment.

7. CONCLUSIONS

This thesis provides the first detailed geochemical description of the igneous rocks (and mineralised crusts) of the Saltpeterkop Carbonatite Complex. This complex includes a relatively wide range of rock types, including an important group, the ultramafic lamprophyres, that had not previously been recognised from this locality. It is possible that the diversity of rock types observed, and the absence of some rock types that are important in other carbonatite complexes (e.g., nepheline syenites and ijolites) is a result of the minimal extent of erosion that the complex has experienced and such rocks may exist at deeper levels. Indeed, the question of whether such rocks are present or absent at Saltpeterkop remains one of the more important unanswered questions with regard to the structure and petrologic evolution of the complex.

In describing and interpreting this wide variety of rock types, it has only been possible to sketch out their petrogeneses in broad strokes. It will require future studies to provide detailed models for their derivation. However, a basic model for the origin and evolution of the complex can be outlined:

(1) The lithospheric mantle beneath Saltpeterkop is infiltrated by hydrous, carbonated melts, resulting in it becoming modally metasomatised by the introduction of calcite and/or dolomite, phlogopite and possibly other metasomatic minerals.

(2) Due to an unknown cause, the local lithosphere is heated, causing low-degree partial melting of the metasomatised mantle beneath Saltpeterkop.

(3) Variably carbonated silicate and possibly carbonatitic magmas are generated by this melting. Some of these melts are emplaced directly as dykes and diatremes of olivine melilitite and ultramafic lamprophyre. Some of these experience variable degrees of crystal fractionation and/or accumulation (particularly of olivine) on the way to the surface.

(4) Given the variety of intrusive rocks exposed at the surface, it remains unclear what is the nature of the main volume of igneous rock emplaced at depth beneath Saltpeterkop. There is little petrographic or major & trace element evidence for the carbonatites, melilitites and ultramafic lamprophyres being derived from a common parental magma, but limited isotopic constraints (Janney, personal communication, 2018) suggests that

all of these magma types are derived from a similar, narrow range of mantle source compositions.

(5) A hydrous, potassic carbonatitic fluid or magma metasomatises the surrounding deep continental crust. The heat from the crystallizing magma and the solidus-lowering effect of the volatile addition causes a significant amount of the metasomatised or fenitised crust to undergo partial melting. Fractional crystallization of these melts, combined with assimilation of upper crustal Beaufort Group sedimentary rocks were the main processes involved in the petrogenesis of the potassic trachytes.

(6) The remaining, alkali-poor carbonatites undergo further fractional crystallization and relatively primitive to highly differentiated carbonatites are emplaced as dykes and sills.

(7) Fe-rich crusts are derived from extensive hydrothermal alteration of late-stage Fe-rich carbonatites (ferruginous calciocarbonatites and ferrocarbonatites).

Although this model plausibly explains most of the features of the Saltpeterkop complex, several questions require further detailed work and modeling, and application of other techniques such as radiogenic isotope measurements and geophysical characterisation:

(a) What is the relationship between the sources of the ultramafic lamprophyres, the olivine melilitites, in terms of composition, mineralogy and depth?

(b) What is the nature of the magma parental to the carbonatites? Is it itself carbonatitic or rather a carbonated silicate magma? Are there deep intrusive cumulates of mafic silicates that are complementary to the shallow intrusive carbonatitic dykes and sills?

(c) What is responsible for the updoming of the Beaufort group sediments beneath Saltpeterkop? What is/are the sizes, shapes and compositional natures of the intrusive body or bodies present, and how deeply seated are they?

It is likely that further study of the Saltpeterkop Complex will provide significant new insights into the origin and evolution of carbonatite complexes in southern Africa.

8. REFERENCES CITED

Andersen, T. (1986) Magmatic fluids in the Fen carbonatite complex, SE Norway. Contributions to Mineralogy and Petrology 93, 491-503.

Allègre, C. J., Treuil, M., Minster, J. F., Minster, B., & Albarède, F. (1977). Systematic use of trace element in igneous process. *Contributions to Mineralogy and Petrology* **60**, 57-75.

Becker, M., & le Roex, A.P., (2006). Geochemistry of South African on- and off-craton, Group I and Group II kimberlites: petrogenesis and source region evolution. Journal of Petrology **47**, 673–703.

Becker, M., le Roex, A. P., & Class, C. (2007). Geochemistry and petrogenesis of South African transitional kimberlites located on and off the Kaapvaal Craton. *South African Journal of Geology* **110**, 631-646.

Behn, M. D., Conrad, C. P., & Silver, P. G. (2004). Detection of upper mantle flow associated with the African Superplume. *Earth and Planetary Science Letters* **224**, 259-274.

Berger, V.I., Singer, D.A. & Orris, G.J. (2009) Carbonatites of the World, Explored Deposits of Nb and REE－Database and Grade and Tonnage Models. Open-File Report 2009-1139, U.S. Department of the Interior/U.S. Geological Survey, p 20.

Bhushan, S.K. (2015). Geology of the Kamthai rare earth deposit. *Journal of the Geological Society of India* **85**,537-546.

Bishop, J. (2015) *A snapshot of the early Cambrian mantle: petrogenesis and geochemical investigation of the Grünau intrusives, Southern Namibia*, unpublished BSc (Honours) thesis, University of Cape Town, 37 pp.

Bizimis, M., Salters, V. J., & Dawson, J. B. (2003). The brevity of carbonatite sources in the mantle: evidence from Hf isotopes. *Contributions to Mineralogy and Petrology* **145**, 281-300.

Boctor, N.Z. and Yoder, H.S., 1986. Petrology of some melilite-bearing rocks from Cape Province, Republic of South Africa; relationship to kimberlites. *American Journal of Science* **286**, 513-539.

Brey, G. (1978). Origin of olivine melilitites—chemical and experimental constraints. *Journal of Volcanology and Geothermal Research* **3**, 61-88.

Brey, G. & Green, D. H. (1977). Systematic study of liquidus phase relations in olivine melilitite + H_2O + CO_2 at high pressures and petrogenesis of an olivine melilitite magma. *Contributions to Mineralogy and Petrology* **61**, 141-162.

Brey, G., Brice, W. R., Ellis, D. J., Green, D. H., Harris, K. L. & Ryabchikov, I. D. (1983). Pyroxene-carbonate reactions in the upper mantle. *Earth and Planetary Science Letters* **62**, 63-74.

Brooker, R. A. & Kjarsgaard, B. A. (2010). Silicate–carbonate liquid immiscibility and phase relations in the system SiO2–Na2O–Al2O3–CaO–CO2 at 0· 1–2· 5 GPa with applications to carbonatite genesis. *Journal of Petrology* **52**, 1281-1305.

Castor, S. B. & Hedrick, J. B. (2006). Rare earth elements. In Industrial Minerals volume, 7th edition: Society for Mining, Metallurgy, and Exploration, Littleton, Colorado, 769-792.

Castor, S. B. (2008). The Mountain Pass rare-earth carbonatite and associated ultrapotassic rocks, California. *The Canadian Mineralogist* **46,** 779-806.

Chakhmouradian, A. R., & Zaitsev, A. N. (2012). Rare earth mineralization in igneous rocks: sources and processes. *Elements* **8**, 347-353.

Chevallier, L. (1997). Distribution and tectonics of South African Cretaceous kimberlites: implications for dynamics of the mantle, *Russian Geology and Geophysics* **38**, 509-517.

Class, C. & Goldstein, S. L. (1997). Plume-lithosphere interactions in the ocean basins: constraints from the source mineralogy. *Earth and Planetary Science Letters* **150**, 245-260.

Coe, N., le Roex, A., Gurney, J., Pearson, D. G., & Nowell, G. (2008). Petrogenesis of the Swartruggens and Star Group II kimberlite dyke swarms, South Africa: constraints from whole rock geochemistry. *Contributions to Mineralogy and Petrology* **156**, 627.

Cooper, A. F., & Reid, D. L. (2000). The association of potassic trachytes and carbonatites at the Dicker Willem Complex, southwest Namibia: coexisting, immiscible, but not cogenetic magmas. *Contributions to Mineralogy and Petrology* **139**, 570-583.

Cooper, A. F., & Reid, D. L. (1998). Nepheline sövites as parental magmas in carbonatite complexes: evidence from Dicker Willem, southwest Namibia. *Journal of Petrology* **39**, 2123-2136.

Dasgupta, R. & Hirschmann, M.M., (2006). Melting in the Earth's deep upper mantle caused by carbon dioxide. *Nature* **440**, 659.

Dawson, J.B. & Smith, J.V., (1977). The MARID (mica-amphibole-rutile-ilmenite-diopside) suite of xenoliths in kimberlite. *Geochimica et Cosmochimica Acta* **41**, 309-323.

de Wet, J. J. (1975). Carbonatites and related rocks at Saltpetre Kop, Sutherland, Cape Province. *Annals, University of Stellenbosch* (Series A1) **1**, 193-232.

Dingle, R.V. and Gentle, R.I. (1972). Early Tertiary volcanic rocks on the Agulhas Bank, South African continental shelf. *Geological Magazine* **109**,137-146.

Duncan, R.A., Hargraves, R.B. and Brey, G.P. (1978). Age, palaeomagnetism and chemistry of melilite basalts in the Southern Cape, South Africa. *Geological Magazine* **115**,317-327.

Duncan, A.R. and Marsh, J.S. (2006) The Karoo Igneous Province, in Johnson, M.R., Annhaeusser, C.R. & Thomas, R.J. (eds.) The Geology of South Africa, The Geological Society of South Africa, pp. 501-520.

Garnero, E. J., and McNamara, A. K. (2008). Structure and dynamics of Earth's lower mantle. *Science* **320**, 626-628.

Eggins, S. M., J. D. Woodhead, L. P. J. Kinsley, G. E. Mortimer, P. Sylvester, M. T. McCulloch, J. M. Hergt, and M. R. Handler (1997) A simple method for the precise determination of≥ 40 trace elements in geological samples by ICPMS using enriched isotope internal standardisation. *Chemical Geology* **134**, 311-326.

Eggler, D. H. (1978). The effect of CO_2 upon partial melting of peridotite in the system Na_2O-CaO-Al_2O_3-MgO-SiO_2-CO_2 to 35 kb, with an analysis of melting in a peridotite-H_2O-CO_2 system. *American Journal of Science* **278**, 305-343.

Erlank, A. J., Waters, F. G., Hawkesworth, C. J., Haggerty, S. E., Allsopp, H. L., Rickard, R. S. & Menzies, M. (1987). Evidence for mantle metasomatism in peridotite nodules from the Kimberley pipes, South Africa. In: Menzies, M. & Hawkesworth, C. J. (eds) Mantle Metasomatism. London: Academic Press, pp. 229-311.

Evensen, N. M., Hamilton, P. J. and O'nions, R. K. (1978). Rare-earth abundances in chondritic meteorites. *Geochimica et Cosmochimica Acta* **42**, 1199-1212.

Foley, S. F., Musselwhite, D. S. and Van de Laan, S. R. (1999). Melt compositions from ultramafic vein assemblages in the lithospheric mantle: a comparison of cratonic and non-cratonic settings. In Proceedings of the 7th International Kimberlite Conference. J.J. Gurney, J.L. Gurney, S.H. Richardson and M. Pascoe (eds.) Cape Town: Red Roof Design, p. 238–246.

Foley, S. F., Barth, M. G., and Jenner, G. A. (2000). Rutile/melt partition coefficients for trace elements and an assessment of the influence of rutile on the trace element characteristics of subduction zone magmas. *Geochimica et Cosmochimica Acta* **64**, 933-938.

Garnero, E. J., and McNamara, A. K. (2008). Structure and dynamics of Earth's lower mantle. *Science* **320**, 626-628.

Gittins, J., and Harmer, R. E. (1997). What is ferrocarbonatite? A revised classification. *Journal of African Earth Sciences* **25**, 159-168.

Green, E. C. R., White, R. W., Diener, J. F. A., Powell, R., Holland, T. J. B., and Palin, R. M. (2016). Activity–composition relations for the calculation of partial melting equilibria in metabasic rocks. *Journal of Metamorphic Geology* **34**, 845-869.

Gregoire, M., Bell, D. R. and le Roex, A. P. (2002). Trace element geochemistry of glimmerite and MARID mantle xenoliths: their relationship to kimberlite and to phlogopite-bearing peridotite revisited. *Contributions to Mineralogy and Petrology* **142**, 603-625.

Gregoire, M., Bell, D. R. and le Roex, A. P. (2003). Garnet lherzolites from the Kaapvaal Craton (South Africa): trace element evidence for a metasomatic history. *Journal of Petrology* **44**, 629-657.

Hammouda, T., Chantel, J., Manthilake, G., Guignard, J., and Crichton, W. (2014). Hot mantle geotherms stabilize calcic carbonatite magmas up to the surface. *Geology* **42**, 911-914.

Harmer, R. E. (1999). The petrogenetic association of carbonatite and alkaline magmatism: constraints from the Spitskop Complex, South Africa. *Journal of Petrology*, **40**, 525-548.

Harmer, R.E., and Nex, P.A.M. (2016) Rare earth deposits of Africa. *Episodes* **39**, 381-406.

Harper, F., Wiid, G., Siegfried, P., Brown, J., Hall, M., Njowa, G, Vivier, J., Zietsman, R., Duke, V. (2015) *National Instrument 43-101 Independent Technical Report on the Results of a Preliminary Feasibility Study on the Zandkopsdrift Rare Earth Element and Manganese By-product Project in the Northern Cape Province of South Africa*, Venmyn Deloitte Independent pre-feasibility study prepared for Frontier Rare Earths, Ltd, Reference number: VMD1722 V11, 226 pp.

Hartnady, C. J. H., and le Roex, A. P. (1985). Southern Ocean hotspot tracks and the Cenozoic absolute motion of the African, Antarctic, and South American plates. *Earth and Planetary Science* Letters **75**, 245-257.

Henderson, P.A. (1984), General geochemical properties and abundances of the rare earth elements, in Henderson, P.A. (ed.) Rare Earth Element Geochemistry, *Developments in Geochemistry* **2**, 1-29.

Hirschmann, M. M., & Stolper, E. M. (1996). A possible role for garnet pyroxenite in the origin of the "garnet signature" in MORB. *Contributions to Mineralogy and Petrology* **124**, 185-208.

Hoatson, D. M., Jaireth, S., & Miezitis, Y. (2011). The major rare-earth-element deposits of Australia: geological setting, exploration, and resources. *Geoscience Australia.*

Holland, T. J. B., & Powell, R. (2011). An improved and extended internally consistent thermodynamic dataset for phases of petrological interest, involving a new equation of state for solids. *Journal of Metamorphic Geology* **29**, 333-383.

Hornig-Kjarsgaard, I. (1998). Rare earth elements in sövitic carbonatites and their mineral phases. *Journal of Petrology* **39**, 2105-2121.

Ionov, D. A., Dupuy, C., O'Reilly, S. Y., Kopylova, M. G., and Genshaft, Y. S. (1993). Carbonated peridotite xenoliths from Spitsbergen: implications for trace element signature of mantle carbonate metasomatism. *Earth and Planetary Science Letters* **119**, 283-297.

Janney, P. E., le Roex, A. P., Carlson, R. W. and Viljoen, K. S. (2002). A chemical and multi-isotopic study of olivine melilitites and associated rocks from the Western Cape, South Africa: implications for the sources of group 1 kimberlites and constraints on the origin of the HIMU component in Africa. *Journal of Petrology* **43**, 2339-2370.

Janney, P. E., le Roex, A. P., and Carlson, R. W. (2005). Hafnium isotope and trace element constraints on the nature of mantle heterogeneity beneath the central Southwest Indian Ridge (13 E to 47 E). *Journal of Petrology* **46**, 2427-2464.

Jelsma, H., Barnett, W., Richards, S., and Lister, G. (2009). Tectonic setting of kimberlites. *Lithos* **112**, 155-165.

Jordens, A., Cheng, Y. P., and Waters, K. E. (2013). A review of the beneficiation of rare earth element bearing minerals. *Minerals Engineering* **41**, 97-114.

Kesson, S. E., Ringwood, A. E., & Hibberson, W. O. (1994). Kimberlite melting relations revisited. *Earth and Planetary Science Letters* **121**, 261-262.

King, S. D., and Ritsema, J. (2000). African hot spot volcanism: small-scale convection in the upper mantle beneath cratons. *Science* **290**, 1137-1140.

Kjarsgaard, B., and Peterson, T. (1991) Nephelinite-carbonatite liquid immiscibility at Shombole volcano, East Africa: petrographic and experimental evidence. *Mineralogy and Petrology* **43**, 293-314.

La Tourrette, T., Hervig, R. L., and Holloway, J. R. (1995). Trace element partitioning between amphibole, phlogopite, and basanite melt. *Earth and Planetary Science Letters* **135**, 13-30.

Le Bas, M.J., Le Maitre, R.W., Streckeisen, and A., Zanettin, B. (1986): A chemical classifi cation of volcanic rocks based on the total alkali-silica diagram. *Journal of Petrology* **27**, 745-750.

Le Bas, M.J., (1989). Nephelinitic and basnitic rocks. *Journal of Petrology* **30**, 1299-1312.

Lee, W. J., and Wyllie, P. J. (1997). Liquid immiscibility between nephelinite and carbonatite from 1.0 to 2.5 GPa compared with mantle melt compositions. *Contributions to Mineralogy and Petrology* **127**, 1-16.

Lee, W. J., and Wyllie, P. J. (1998). Processes of carbonatite formation by liquid immiscibility and differentiation, elucidated by model systems. *Journal of Petrology* **39**, 2005-2013.

Lee, W.J. and Wyllie, P.J., (2000). The system CaO-MgO-SiO 2-CO 2 at 1 GPa, metasomatic wehrlites, and primary carbonatite magmas. *Contributions to Mineralogy and Petrology* **138**, 214-228

le Roex, A. P., and Lanyon, R. (1998). Isotope and trace element geochemistry of Cretaceous Damaraland lamprophyres and carbonatites, northwestern Namibia: Evidence for plume—lithosphere interactions. *Journal of Petrology* **39**, 1117-1146.

le Roex, A. P., Bell, D. R., and Davis, P. (2003). Petrogenesis of group I kimberlites from Kimberley, South Africa: evidence from bulk-rock geochemistry. *Journal of Petrology* **44**, 2261-2286.

Le Roux, P.J., le Roex, A.P., Schilling, J.G., Shimizu, N., Perkins, W.W. and Pearce, N.J.G., (2002). Mantle heterogeneity beneath the southern Mid-Atlantic Ridge: trace element evidence for contamination of ambient asthenospheric mantle. *Earth and Planetary Science Letters* ***203***, 479-498.

Mabaso, S. (2017) *Mineral chemistry study of olivine melilitites at Saltpeterkop*, unpublished BSc (Honours) thesis, University of Cape Town, 48 pp.

Malarkey, J., Pearson, D. G., Kjarsgaard, B. A., Davidson, J. P., Nowell, G. M., Ottley, C. J. and Stammer, J. (2010). From source to crust: Tracing magmatic evolution in a kimberlite and a melilitite using microsample geochemistry. *Earth and Planetary Science Letters* **299**, 80-90.

McDonough, W. F., and Sun, S. S. (1995). The composition of the Earth. *Chemical geology* **120**, 223-253.

McIver, J.R. and Ferguson, J. (1979). Kimberlitic, Melilititic, Trachytic and Carbonatitte Eruptives at Saltpetre Kop, Sutherland, South Africa. In: Meyer H.O.A. & Boyd F.R. (eds.) Kimberlites, Diatremes, and Diamonds: Their Geology, Petrology, and Geochemistry, Washington, DC: American Geophysical Union, pp. 111-128.

McKenzie, D., and O'Nions, R. K. (1991). Partial melt distributions from inversion of rare earth element concentrations. *Journal of Petrology* **32**, 1021-1091.

Miller, R.M., (2008) The Geology of Namibia*, Geological Survey of Namibia* **3**, 1564 pp.

Mitchell, R. H. (2005) Carbonatites and carbonatites and carbonatites. *The Canadian Mineralogist* **43**, 2049-2068.

Moore, A. E., and Verwoerd, W. J. (1985). The olivine melilitite-"kimberlite"-carbonatite suite of Namaqualand and Bushmanland, South Africa. *Transactions of the Geological Society of South Africa* **88**, 281-294.

Moore, A., Blenkinsop, T., and Cotterill, F., (2008). Controls on post-Gondwana alkaline volcanism in Southern Africa. *Earth and Planetary Science Letters* **268**, 151-164.

Nelson, D. R., Chivas, A. R., Chappell, B. W., and McCulloch, M. T. (1988). Geochemical and isotopic systematics in carbonatites and implications for the evolution of ocean-island sources. *Geochimica et Cosmochimica Acta* **52**, 1-17.

Newton, A.R. (1987). The fracture pattern around the Sutherland diatreme, Cape Province, from remote sensing. *South African Journal of Geology* **90**,99-106.

Nguuri, T. K., Gore, J., James, D. E., Webb, S. J., Wright, C., Zengeni, T. G., Gwavava, O. & Snoke, J. A. (2001). Crustal structure beneath southern Africa and its implications for the formation and evolution of the Kaapvaal and Zimbabwe cratons. *Geophysical Research Letters* **28**, 2501-2504.

O'Connor, J. M., Jokat, W., le Roex, A. P., Class, C., Wijbrans, J. R., Keßling, S., and Nebel, O. (2012). Hotspot trails in the South Atlantic controlled by plume and plate tectonic processes. *Nature Geoscience* **5**,735.

Paiva, F. (2015) *Fluvial Facies Architecture and Provenance History of the Abrahamskraal-Teekloof Formation Transition (Lower Beaufort Group) in the Main Karoo Basin*, MSc thesis, University of Cape Town, 98 pp.

Phillips, D., Kiviets, G.B., Biddulph, M.G. and Madav, M.K. (2000). Cenozoic volcanism. in Partridge, T.C., Maud, R.R., The Cenozoic of Southern Africa, *Oxford Monographs on Geology and Geophysics* **40**,182-197.

Pilet, S., Baker, M.B. and Stolper, E.M., 2008. Metasomatized lithosphere and the origin of alkaline lavas. *Science* **320**, 916-919.

Powell, R., Holland, T. J. B. H., and Worley, B. (1998). Calculating phase diagrams involving solid solutions via non- linear equations, with examples using THERMOCALC. *Journal of Metamorphic Geology* **16**, 577-588.

Reid, D. L. (1991). Alkaline rocks in the Kuboos-Bremen igneous province, southern Namibia: the Kanabeam multiple ring complex. *Communications of the Geological Survey Namibia* **7**, 3-13.

Ringwood, A. E., Kesson, S. E., Hibberson, W., & Ware, N. (1992). Origin of kimberlites and related magmas. *Earth and Planetary Science Letters* **113**, 521-538.

Rock, N.M.S. (1991) Lamprophyres, Springer, pp 552.

Roedder, E. and Emslie, R. (1970) Olivine-liquid equilibrium. *Contributions to Mineralogy and Petrology* **29**, 275–289.

Rogers, N. W., Hawkesworth, C. J. and Palacz, Z. A. (1992). Phlogopite in the generation of olivine-melilitites from Namaqualand, South Africa, and its implications for element fractionation processes in the upper mantle. *Lithos* **28**, 347-365.

Rogers, A. W., and Du Toit, A. L. (1903). Annual Report of the Geological Commission for the Cape of Good Hope for 1903, Government Printers, Cape Town.

Rogers, A. W., and Du Toit, A. L. (1904). The Sutherland volcanic pipes and their relationship to other vents in South Africa. *Transactions of the South African Philosophical Society* **15**, 61-83.

Rosenthal, A., Foley, S.F., Pearson, D.G., Nowell, G.M. and Tappe, S., (2009). Petrogenesis of strongly alkaline primitive volcanic rocks at the propagating tip of the western branch of the East African Rift. *Earth and Planetary Science Letters* **284**, 236-248.

Schmidt, K. H., Bottazzi, P., Vannucci, R., and Mengel, K. (1999). Trace element partitioning between phlogopite, clinopyroxene and leucite lamproite melt. *Earth and Planetary Science Letters* **168**, 287-299.

Smithies, R. H. (1991). *The geochemical evolution of three alkaline complexes in the Kuboos-Bremen igneous province, southern Namibia*, PhD dissertation, Rhodes University.

Tappe, S., Foley, S. F., Jenner, G. A., and Kjarsgaard, B. A. (2005). Integrating ultramafic lamprophyres into the IUGS classification of igneous rocks: rationale and implications. *Journal of Petrology* **46**, 1893-1900.

Tappe, S., Foley, S. F., Jenner, G. A., Heaman, L. M., Kjarsgaard, B. A., Romer, R. L., Stracke, A., Joyce, N. & Hoefs, J. (2006). Genesis of ultramafic lamprophyres and carbonatites at Aillik Bay, Labrador: a consequence of incipient lithospheric thinning beneath the North Atlantic craton. *Journal of Petrology* **47**, 1261-1315.

Verwoerd, W.J. (1967). The Carbonatites of South Africa and South West Africa: A Nuclear Raw Materials Investigation. Government Printer, South Africa.

Verwoerd, W. J., Viljoen, J. H. A. and Viljoen, K. S. (1990). Olivine Melilitite Excursion (GeoCongress 90 Field Guide). Johannesburg: Geological Society of South Africa, pp 60.

Verwoerd, W.J. (1990). The Salpeterkop ring structure, Cape Province, *South Africa. Tectonophysics* **171**, 275-285.

Verwoerd, W.J., Viljoen, E.A. and Chevallier, L. (1995). Rare metal mineralization at the Salpeterkop carbonatite complex, Western Cape Province, *South Africa. Journal of African Earth Sciences* **21**, 171-186.

Verwoerd, W. J. & De Beer, C. H. (2006). Cretaceous and Tertiary igneous events, in Johnson, M. R., Anhauesser, C. R., & Thomas, R. J. (eds) The Geology of South Africa: Johannesburg, Geological Society of South Africa, 573-583.

Viljoen, K. S. (1988). *Petrology of the Sutherland Commonage melilitite intrusives* MSc dissertation, University of Cape Town.

Wall, F. and Zaitsev, A.N. eds. (2004). Phoscorites and carbonatites from mantle to mine: the key example of the Kola Alkaline Province. The Mineralogical Society of Great Britain and Ireland **10**.

Wall, F. (2004) An illustration of the evolution and alteration of carbonatites using REE, Sr-rich carbonatites at Nkwomba Hill, Zambia. In N.V. Vladykin & A.P. Vinogradova (eds.) Deep Seated Magmatism: Its Sources and Their Relation to Plume Processes, pp 48-67.

Weidendorfer, D., Schmidt, M. W., and Mattsson, H. B. (2016). Fractional crystallization of Si-undersaturated alkaline magmas leading to unmixing of carbonatites on Brava Island (Cape Verde) and a general model of carbonatite genesis in alkaline magma suites. *Contributions to Mineralogy and Petrology* **171**, 43.

White, R. W., Powell, R., Holland, T. J. B., Johnson, T. E., and Green, E. C. R. (2014). New mineral activity–composition relations for thermodynamic calculations in metapelitic systems. *Journal of Metamorphic Geology* **32**, 261-286.

Wilson, M., Rosenbaum, J.M., and Dunworth, E.A. (1995). Melilitites: partial melts of thermal boundary layers?. *Contributions to Mineralogy and Petrology* **119**, 181-196.

Woolley, A. R. (2001). Alkaline rocks and carbonatites of the world: Africa. Geological Society of London.

Wyllie, P. J., and Lee, W. J. (1998). Model system controls on conditions for formation of magnesiocarbonatite and calciocarbonatite magmas from the mantle. *Journal of Petrology* **39**, 1885-1893.

Wyllie, P. J. and Lee, W.-J. (1999). Kimberlites, carbonatites, peridotites and silicate---carbonate liquid immiscibility explained in parts of the system CaO-(Na_2O + K_2O)-(MgO + FeO)-(SiO_2 + Al_2O_3)-CO_2. In: Gurney, J. J., Gurney, J. L., Pascoe, M. D. & Richardson, S.H. (eds) Proceedings of the Seventh International Kimberlite Conference. Cape Town: Red Roof Design, pp. 923-932.

Yardley, B. (2011) Metasomatism. Encyclopedia of Astrobiology. Springer Berlin Heildelberg, pp 1022-1022.

Zack, T. and Brumm, R. (1998). Ilmenite/liquid partition coefficients of 26 trace elements determined through ilmenite/clinopyroxene partitioning in garnet pyroxene. In: *7th International Kimberlite Conference Extended Abstracts*, 986-988.

APPENDICES

APPENDIX 1. MINERAL COMPOSITIONS FOR SALTPETERKOP MELILITITES & LAMPROPHYRES

Table 1. Olivine compositions

Sample	SKM2-1	SPK-2	SKM6-1	SP-31	SP43-2	SP206-1	SP367-1
SiO_2	39.74	40.52	40.57	40.25	40.49	39.97	40.28
TiO_2	0.04	0.06	0.04	0.03	0.03	0.03	0.02
Al_2O_3	0.05	0.25	0.04	0.04	0.04	0.06	0.05
Cr_2O_3	0.02	0.03	0.02	0.03	0.03	0.04	0.05
$FeO^{tot.}$	13.11	10.43	11.07	12.68	13.03	12.87	12.12
MnO	0.27	0.22	0.24	0.19	0.21	0.15	0.14
MgO	46.06	47.62	47.37	46.49	46.21	46.60	47.01
CaO	0.55	0.66	0.74	0.27	0.39	0.24	0.20
NiO	0.16	0.25	0.24	0.31	0.22	0.35	0.30
Total	100.02	100.05	100.34	100.30	100.65	100.32	100.18
Mg#	86.2	89.0	88.4	86.7	86.3	86.6	87.4

All data from Mabaso (2017).

Table 2. Clinopyroxene, melilite and nepheline compositions

Mineral	CPX	CPX	CPX	Melilite	Melilite	Nepheline
Sample	SP43-2	SP367-1	SP38-1	SPK-2	SP43-2	M5
SiO_2	50.79	49.83	50.09	43.06	43.44	42.23
TiO_2	1.03	1.50	1.44	0.07	0.09	b.d.
Al_2O_3	3.71	5.66	5.74	6.22	6.05	33.05
Cr_2O_3	0.07	b.d.	0.23	n.d.	n.d.	n.d.
$FeO^{tot.}$	7.76	5.83	6.63	2.38	3.03	0.17
MnO	0.17	0.10	0.11	0.05	0.06	n.d.
MgO	13.50	14.52	14.11	9.96	9.33	0.08
CaO	21.67	21.19	20.56	35.39	34.17	0.21
Na_2O	1.20	1.11	1.28	2.59	3.02	22.64
K_2O	0.02	0.01	0.01	0.19	0.14	0.2
Total	99.90	99.74	100.18	99.91	99.33	98.58
Mg#	75.6	81.6	79.1	88.2	84.6	-

All data from Mabaso (2017) except for nepheline, which is from Boctor & Yoder (1986)

APPENDIX 1 continued

Table 3. Phlogopite and calcite compositions

Mineral	Phlog.	Phlog.	Phlog.	Phlog.	Calcite
Sample	SPK-2	SP-31	SKM6-1	SP-38	SP367-1
SiO_2	40.08	34.82	36.39	37.55	0.03
TiO_2	1.29	6.04	5.18	4.32	0.00
Al_2O_3	12.42	13.94	12.66	15.89	0.00
Cr_2O_3	0.00	0.02	0.01	b.d.	n.d.
$FeO^{tot.}$	5.35	7.56	8.01	8.12	0.23
MnO	0.07	0.10	0.11	0.07	0.03
MgO	25.67	19.34	20.41	20.74	0.25
CaO	0.02	0.28	0.05	0.02	52.94
Na_2O	0.11	0.26	0.35	0.53	0.17
K_2O	8.65	7.53	8.07	8.92	0.01
F	0.96	2.13	1.75	0.53	n.d.
Total	94.63	92.01	93.00	96.68	53.63
Mg#	89.5	82.0	81.9	82.0	

All data from Mabaso (2017). Note that analysis does not include water (OH) or carbon dioxide (CO_2), hence the low totals.

Table 4. Oxide mineral compositions

Mineral	Timgt	Timgt	Timgt	Timgt	Timgt	Perov.	Perov.	Perov.	Spinel	Spinel	Spinel
Sample	SKM-2	SP206-1	SPK-2	SP-31	SP43-2	SKM2-1	SP206-1	SPK-2	SP206-1	SP-31	SPK43-2
SiO_2	0.09	0.73	0.09	0.04	0.22	0.06	0.01	b.d.	0.08	0.01	0.10
TiO_2	12.07	23.02	11.98	14.66	14.71	59.16	58.71	58.37	5.72	3.33	2.34
Al_2O_3	4.69	6.79	9.47	3.78	4.25	0.32	0.42	0.65	20.12	16.53	25.10
Cr_2O_3	0.50	0.05	0.01	5.64	0.32	b.d.	b.d.	b.d.	29.81	32.20	31.76
$FeO^{tot.}$	74.33	61.09	69.36	68.71	73.75	1.32	1.44	1.47	32.81	37.08	25.10
MnO	1.53	0.88	0.73	0.85	0.64	b.d.	b.d.	b.d.	0.32	0.92	0.46
MgO	5.51	5.60	7.48	6.63	5.18	0.05	0.02	0.03	11.77	8.91	14.96
CaO	0.20	0.26	0.05	0.06	0.10	38.28	38.57	38.61	0.02	0.04	0.01
NiO	0.06	0.13	0.21	0.08	0.07	0.04	0.02	0.02	0.24	0.00	0.19
Total	98.98	98.54	99.37	100.45	99.26	99.24	99.20	99.16	100.87	99.01	100.01

All data from Mabaso (2017). Abbreviations: Timgt, titanomagnetite, Perov, perovskite.

APPENDIX 2. CONCENTRATION DATA FOR SALTPETERKOP WHOLE ROCK SAMPLES

Table 1. Major and trace element data for Saltpeterkop rock samples obtained by XRF

Rock type	Calciocarbonatites							
Sample	SP-19A	SP-27A	SP-27C	SP-27D	SP-402	SP-403	SP-404	WV95-22
SiO_2	7.26	7.70	5.22	22.33	3.28	3.32	5.51	7.16
TiO_2	0.19	0.56	0.70	0.15	0.15	0.20	0.52	0.15
Al_2O_3	1.78	1.69	1.92	3.49	0.61	0.69	1.45	2.06
$Fe_2O_3^{tot.}$	11.78	10.09	10.50	1.69	11.06	10.39	10.50	10.18
MnO	1.63	0.77	0.75	0.78	1.09	0.83	0.73	1.44
MgO	1.13	0.39	1.21	0.48	0.80	1.86	2.40	0.99
CaO	39.23	42.95	42.45	37.79	43.08	45.66	42.85	39.96
Na_2O	0.24	0.27	0.02	0.81	0.00	0.00	b.d.	0.22
K_2O	0.88	0.75	0.54	0.48	0.15	0.08	0.27	0.44
P_2O_5	1.20	4.13	3.05	0.06	2.87	2.87	4.25	2.00
SO_3	0.36	0.06	0.04	0.06	0.50	0.04	0.06	0.04
H_2O-	0.42	0.41	0.69	0.24	0.61	0.29	0.35	0.89
LOI	29.30	29.60	30.52	29.53	32.80	34.17	31.06	32.18
Sum	95.40	99.37	97.64	97.90	97.02	100.42	99.94	97.71
Sc	29	38	35	30	42	39	40	31
V	225	232	218	20	136	108	158	121
Cr	<5	9	<5	20	<5	<5	<5	6
Co	7	9	27	<5	6	5	11	28
Ni	<5	<5	12	<5	<5	<5	<5	23
Cu	10	11	9	5	8	6	8	10
Zn	569	347	267	16	295	252	234	193
Rb	52	16	103	23	19	19	43	32
Sr	2116	2013	4138	321	1125	1314	1435	4486
Y	174	116	115	26	118	84	135	171
Zr	179	334	647	71	134	107	333	n.a.
Nb	1211	611	665	<5	542	618	542	1135
Mo	<5	467	5	<5	59	<5	7	<5
Ba	5693	359	1208	327	6887	728	658	1407
Pb	51	25	20	8	21	26	28	53
Th	118	95	22	3	123	116	251	82
U	106	89	77	<5	44	24	36	57
F	11461	5091	8221	424	2722	3714	6391	2330
S	1283	463	407	539	1672	376	447	392
Cl	144	1405	170	118	176	182	207	134

Major oxides are given in weight percent. Trace element abundances are all given in parts per million by weight. H2O- is the wt.% lost upon heating to 110°C for 8 h, LOI is the weight lost upon heating to

APPENDIX 2, Table 1 continued.

Rock type	Calciocarbonatites, cont'd.			Ferruginous calciocarbonatites				
Sample	WV95-28	WV95-29	SPKC-6	SP-16A	SP-16C	SP-26A	SP-26B	SP-27B
SiO_2	12.79	4.28	22.47	14.03	17.78	5.27	5.67	6.76
TiO_2	0.40	0.47	0.61	0.17	0.18	0.14	0.17	0.18
Al_2O_3	3.20	0.84	5.09	3.89	4.99	1.30	1.30	1.54
$Fe_2O_3^{tot.}$	9.95	9.52	7.08	12.80	12.39	16.96	17.42	17.41
MnO	0.62	0.67	0.48	1.94	1.81	3.91	3.59	3.52
MgO	1.21	2.00	0.30	0.75	1.02	1.64	1.82	2.06
CaO	37.39	45.10	35.88	34.34	28.59	33.59	32.38	31.94
Na_2O	0.18	0.00	0.60	0.19	0.32	0.15	0.18	0.27
K_2O	2.36	0.29	2.84	3.14	3.99	0.75	0.90	1.12
P_2O_5	4.76	4.74	6.40	0.54	1.01	1.14	0.93	0.96
SO_3	0.09	0.01	0.05	0.06	0.17	0.03	0.02	0.02
H_2O-	0.50	0.29	1.26	0.55	0.38	0.88	1.15	0.92
LOI	26.01	31.85	13.89	24.75	24.01	29.17	29.03	28.48
Sum	99.45	100.06	96.96	97.14	96.66	94.95	94.57	95.21
Sc	61	40	29	39	45	33	30	30
V	196	168	152	190	208	177	192	222
Cr	10	<5	17	44	48	7	6	9
Co	17	6	5	19	18	15	14	14
Ni	15	<5	<5	20	23	<5	8	6
Cu	19	9	15	14	26	16	14	12
Zn	161	169	203	528	483	473	583	604
Rb	80	33	43	50	63	65	64	60
Sr	981	1229	4109	921	1059	1995	2753	2834
Y	239	107	135	387	150	172	199	171
Zr	359	220	1447	32	n.a.	n.a.	152	n.a.
Nb	602	586	699	464	502	810	924	939
Mo	<5	10	144	77	80	93	70	73
Ba	1023	478	375	2186	3771	3182	2651	2178
Pb	24	24	26	135	51	64	60	57
Th	172	85	106	199	192	134	137	121
U	23	30	116	37	75	32	48	47
F	2200	4928	60871	2432	2711	4152	4663	5237
S	556	317	414	440	827	387	325	311
Cl	200	198	283	138	131	152	145	132

850°C for 4 h. Abbreviations: "b.d.", below detection (typically < 0.01 wt.%), "n.a.", not analysed. For some samples with very high Sr/Zr ratios, the correction of ZrKα intensities for SrKβ spectral overlap

APPENDIX 2, Table 1 continued.

Rock Type	Ferruginous calciocarbonatites, cont'd.							
Sample	SP-331A	WV95-20	WV95-21	WV95-25	SPKC-4	SPKC-8	SPKC-13	SK1-B1
SiO_2	13.32	11.98	18.42	16.45	36.93	9.29	16.31	19.09
TiO_2	0.38	0.11	0.07	0.17	0.46	0.47	2.37	1.74
Al_2O_3	3.33	3.51	4.55	4.80	9.80	3.35	4.20	5.19
$Fe_2O_3^{tot.}$	15.46	17.32	12.03	13.88	7.76	14.72	14.37	12.43
MnO	3.09	2.12	3.33	1.93	0.69	1.91	0.66	1.03
MgO	5.87	0.56	1.05	3.00	0.90	0.72	5.26	4.66
CaO	21.69	31.61	27.97	22.88	17.96	33.44	21.15	25.63
Na_2O	0.60	0.41	0.18	0.21	0.39	0.50	0.31	0.43
K_2O	2.68	1.54	3.49	3.84	9.09	1.01	2.86	3.31
P_2O_5	7.00	1.24	0.66	0.69	0.16	2.65	3.35	2.34
SO_3	0.06	0.02	0.02	0.95	0.23	0.03	0.04	0.08
H_2O-	0.61	0.78	0.91	0.74	0.21	1.34	5.72	1.13
LOI	19.95	26.01	22.94	20.56	12.22	27.89	21.14	20.00
Sum	94.03	97.20	95.62	90.09	96.84	97.33	97.93	97.14
Sc	33	30	57	38	18	32	61	31
V	284	191	149	384	165	283	284	267
Cr	55	15	10	<5	77	7	860	493
Co	12	9	<5	14	14	29	67	33
Ni	26	10	6	36	22	41	395	102
Cu	94	14	11	29	21	14	57	35
Zn	987	638	517	737	632	489	305	213
Rb	28	35	58	62	172	5	78	107
Sr	7948	1566	1225	2390	555	5339	4661	1814
Y	322	158	116	435	154	288	93	89
Zr	351	70	210	93	47	226	806	51
Nb	912	520	174	568	414	1513	1313	889
Mo	245	102	115	37	29	75	33	29
Ba	4131	818	1465	18339	4554	1528	969	4409
Pb	182	56	43	212	102	109	42	19
Th	201	154	280	282	128	186	179	219
U	110	54	59	55	10	173	75	35
F	5451	6127	11661	20440	18884	3330	4738	3883
S	424	320	322	3237	864	362	419	448
Cl	121	173	158	128	135	181	544	154

was deemed to be insufficiently precise and "n.a." is given for Zr in these cases. Data for SPK-1, -2 and -3 only are from Janney et al. (2002).

APPENDIX 2, Table 1 continued.

RockType	Magnesio- and ferrocarbonatites				Potassic trachytes			
Sample	SP-400	WV95-24	WV95-26	SPKC-9	SP-401	SP307-4	WV95-23	WV95-23A
SiO_2	0.49	9.90	0.64	21.53	41.00	56.07	58.30	51.95
TiO_2	0.12	0.16	0.18	2.25	0.24	0.68	0.53	0.27
Al_2O_3	0.18	2.66	0.27	5.65	11.91	15.64	16.58	15.72
$Fe_2O_3^{tot.}$	10.14	17.74	7.80	13.65	5.37	0.48	6.71	3.21
MnO	1.66	2.86	1.42	0.75	0.49	0.06	0.04	0.09
MgO	8.70	11.04	6.85	7.21	1.79	0.24	0.05	0.12
CaO	32.97	19.22	27.33	17.94	13.13	5.26	0.28	9.15
Na_2O	0.00	0.11	0.00	0.37	0.29	0.58	1.44	0.89
K_2O	0.00	2.08	0.02	3.53	9.90	13.51	12.91	11.58
P_2O_5	0.29	0.34	0.35	1.77	0.23	0.92	0.35	0.38
SO_3	0.80	0.04	0.81	0.41	0.21	0.09	0.04	0.06
H_2O-	0.72	0.57	0.79	2.76	0.82	0.26	0.23	0.26
LOI	38.18	29.65	45.35	19.72	13.41	4.45	1.39	3.91
Sum	94.25	96.39	91.82	97.55	98.80	98.25	98.85	97.59
Sc	53	40	59	34	19	15	5	11
V	363	172	275	286	121	55	126	81
Cr	<5	55	<5	264	<5	46	<5	6
Co	6	15	5	40	<5	<5	2	<5
Ni	<5	25	<5	110	<5	<5	<5	<5
Cu	9	44	11	53	5	8	37	5
Zn	651	765	705	201	220	15	122	116
Rb	<5	42	4	134	128	234	240	221
Sr	1817	1932	1778	1158	562	379	589	1844
Y	206	207	262	71	87	76	29	92
Zr	n.a.	n.a.	n.a.	n.a.	172	466	406	1516
Nb	991	714	1619	593	837	743	1043	756
Mo	<5	241	<5	9	<5	<5	190	<5
Ba	14531	1828	17035	8690	4766	2638	3385	2509
Pb	139	110	217	30	92	15	140	27
Th	308	229	410	115	115	44	14	30
U	74	43	101	20	33	13	13	30
F	2281	3842	3947	5691	1305	741	897	44920
S	2902	384	3573	1018	872	473	517	458
Cl	164	149	147	148	125	141	105	121

APPENDIX 2, Table 1 continued.

Rock Type	Potassic trachytes, cont'd.							
Sample	WV95-23B	WV95-23C	WV95-27	SK1-B2	SP307-3	SK2-1	SKR-1	SKR-5
SiO_2	59.07	56.88	45.48	50.77	55.55	50.89	50.74	49.06
TiO_2	0.29	0.31	0.22	0.47	0.76	0.44	0.44	0.82
Al_2O_3	16.79	16.29	13.13	14.33	11.32	14.54	14.49	12.83
$Fe_2O_3^{tot.}$	4.54	3.83	5.70	5.42	3.90	12.65	12.61	1.99
MnO	0.06	0.19	0.48	0.08	0.29	0.78	0.78	0.01
MgO	0.08	0.13	1.71	0.23	0.60	0.22	0.22	0.99
CaO	0.51	2.15	9.41	8.81	4.92	1.50	1.49	12.99
Na_2O	1.62	1.77	0.31	0.67	0.47	0.74	0.74	0.42
K_2O	12.85	12.00	11.24	12.03	9.45	12.01	11.98	11.63
P_2O_5	0.46	0.52	0.17	1.03	0.84	1.13	1.13	0.20
SO_3	0.14	0.58	0.04	0.12	0.91	0.06	0.06	0.14
H_2O-	0.24	0.19	0.27	0.46	0.80	0.59	0.37	0.51
LOI	1.44	2.36	10.52	4.11	5.46	3.01	3.51	4.39
Sum	98.09	97.19	98.66	98.53	95.28	98.57	98.57	96.00
Sc	5	6	16	19	10	8	17	23
V	83	70	125	131	311	161	227	990
Cr	13	7	<5	11	40	5	19	<5
Co	<5	<5	<5	<5	10	17	<5	<5
Ni	<5	<5	<5	<5	25	24	6	5
Cu	11	6	5	8	35	15	12	17
Zn	140	152	225	160	455	474	456	487
Rb	245	227	142	201	230	175	59	292
Sr	905	876	546	1606	604	484	306	3236
Y	56	57	79	70	207	107	44	178
Zr	n.a.	330	n.a.	107	n.a.	b.d.	n.a.	5380
Nb	707	672	612	801	1009	649	391	774
Mo	<5	<5	<5	b.d.	<5	34	23	55
Ba	4612	12312	1899	1730	18892	3990	24338	3010
Pb	38	49	57	20	433	65	32	75
Th	68	47	107	19	14	30	105	4
U	16	13	19	22	5	20	5	17
F	1732	2951	1037	40016	1210	1887	564	56562
S	702	1775	371	694	2722	495	3262	650
Cl	110	123	122	184	121	259	241	134

APPENDIX 2, Table 1 continued.

Rock Type	K trachytes, cont'd.		Olivine melilitites					
Sample	SKM5-2	SPK-CRB	SP31-3	SP31-4	SP-43	SP43-1	SP43-2	SP43-4
SiO_2	64.95	73.85	34.88	35.02	32.37	32.95	33.91	32.78
TiO_2	0.53	0.48	3.43	3.43	2.70	2.87	2.80	2.81
Al_2O_3	14.50	8.29	6.78	6.83	7.76	7.28	7.75	7.79
$Fe_2O_3^{tot.}$	3.96	3.02	13.04	12.99	11.54	13.01	12.24	12.37
MnO	0.08	0.04	0.19	0.19	0.22	0.21	0.22	0.21
MgO	0.62	0.11	16.24	16.07	11.05	13.13	12.39	12.07
CaO	0.39	0.29	17.15	16.75	14.38	13.47	14.78	13.24
Na_2O	2.18	0.30	1.03	0.89	3.38	3.24	2.97	3.26
K_2O	9.68	6.98	1.21	1.03	1.98	1.51	1.78	1.85
P_2O_5	0.12	0.22	0.96	0.93	1.18	1.01	1.23	1.10
SO_3	0.01	0.89	0.07	0.13	0.38	0.37	0.33	0.78
H_2O-	0.79	0.46	0.27	0.17	0.69	0.79	0.61	0.14
LOI	1.51	1.63	4.06	4.54	10.34	8.83	7.95	10.34
Sum	99.32	96.56	99.44	99.11	98.07	98.83	99.12	98.89
Sc	6	8	35	33	31	32	31	34
V	214	153	298	299	277	268	308	306
Cr	39	97	626	646	644	667	784	746
Co	8	<5	85	85	54	58	68	68
Ni	28	5	411	403	231	257	297	253
Cu	16	14	88	83	66	63	66	63
Zn	91	319	96	95	105	107	108	100
Rb	263	113	54	49	47	43	45	46
Sr	404	228	1253	1312	1493	1382	1263	1301
Y	24	56	35	29	42	35	29	29
Zr	186	n.a.	306	312	317	268	260	321
Nb	26	551	116	119	150	144	136	141
Mo	46	167	<5	<5	<5	<5	<5	<5
Ba	1542	20041	1256	1492	1266	1282	1165	1270
Pb	69	38	5	8	8	9	9	7
Th	7	111	9	11	11	11	12	10
U	<5	<5	9	10	12	11	10	10
F	682	-647	1068	1065	1649	1519	1622	1497
S	340	3510	425	538	1107	1106	1161	1531
Cl	321	201	138	128	2355	2018	2200	1995

APPENDIX 2, Table 1 continued.

Rock Type	Olivine melilitites, cont'd.							
Sample	SP206-1	SP206-2	SP206-3	SKM1-1	SKM2-1	SKM6-1	SKM5-1	SPK-1
SiO_2	35.97	33.50	32.61	38.53	29.89	34.48	34.37	33.95
TiO_2	3.64	3.59	3.52	2.75	4.27	2.06	2.42	2.29
Al_2O_3	7.13	6.58	6.52	8.33	7.93	7.55	7.62	7.79
$Fe_2O_3^{tot.}$	13.99	13.47	13.17	10.05	12.54	11.03	11.58	11.09
MnO	0.20	0.18	0.18	0.21	0.29	0.18	0.18	0.19
MgO	12.78	12.97	12.31	9.98	10.87	17.68	17.01	17.18
CaO	14.69	13.88	15.03	12.53	15.64	16.88	16.08	18.08
Na_2O	1.95	1.93	1.87	2.78	2.85	1.16	2.61	3.46
K_2O	1.81	1.43	1.27	2.94	2.23	2.15	2.10	1.80
P_2O_5	1.04	1.07	1.01	0.98	0.51	1.25	1.14	1.42
SO_3	0.32	0.33	0.39	0.32	0.22	0.21	0.24	n.a.
H_2O-	0.61	0.04	0.00	0.83	1.21	0.38	0.44	0.42
LOI	5.11	10.31	11.48	8.60	10.32	4.43	3.15	2.06
Sum	99.37	99.41	99.52	98.92	98.85	99.63	99.13	99.73
Sc	28	31	31	24	31	31	28	28
V	299	324	321	274	275	224	240	191
Cr	605	601	635	472	512	915	961	830
Co	83	85	84	48	59	67	67	n.a.
Ni	428	362	353	167	138	453	457	493
Cu	67	68	65	57	35	75	66	n.a.
Zn	107	100	99	95	139	81	83	n.a.
Rb	44	37	29	81	55	47	54	66
Sr	1147	1037	1123	1804	2367	2232	1244	1396
Y	27	32	32	34	40	21	29	26
Zr	317	390	377	342	202	247	205	139
Nb	114	106	107	157	266	134	140	143
Mo	<5	<5	<5	<5	<5	<5	<5	n.a.
Ba	1368	1298	1065	1900	2453	1912	1592	1663
Pb	6	<5	<5	6	3	7	8	n.a.
Th	<5	<5	<5	7	36	11	22	n.a.
U	6	5	5	16	22	18	11	n.a.
F	1306	1237	1257	1646	1524	1030	1041	n.a.
S	803	842	925	1030	801	884	935	n.a.
Cl	130	136	139	751	2704	1087	5746	n.a.

APPENDIX 2, Table 1 continued.

Rock Type	Ol. mel. cont'd.		Ultramafic lamprophyres					
Sample	SPK-2	SPK-3	WV95-19	SP-38	SP38-1	SP38-2	SP38-3	SP367-1
SiO_2	35.20	34.41	33.18	44.73	31.36	30.80	31.02	28.92
TiO_2	2.19	2.33	1.39	1.16	2.75	2.67	2.83	2.64
Al_2O_3	7.59	7.44	6.88	9.70	6.54	6.58	6.52	5.69
$Fe_2O_3^{tot.}$	10.98	11.31	8.09	8.06	10.33	10.31	10.14	11.40
MnO	0.19	0.20	0.21	0.17	0.20	0.19	0.19	0.30
MgO	16.88	17.10	6.56	6.87	9.06	9.52	8.74	14.57
CaO	17.03	17.24	14.75	8.98	15.05	15.13	15.44	14.34
Na_2O	3.28	3.56	0.40	1.85	2.41	2.28	2.13	2.05
K_2O	1.86	1.76	5.29	4.44	1.80	1.84	2.17	2.04
P_2O_5	1.33	1.37	1.40	0.75	1.29	1.25	1.37	1.10
SO_3	n.a.	n.a.	0.03	0.39	0.11	0.15	0.16	0.10
H_2O-	0.37	0.35	0.65	1.00	0.28	0.54	0.63	0.20
LOI	2.35	2.18	19.92	10.60	17.54	17.44	17.17	15.17
Sum	99.25	99.25	98.75	98.81	98.83	98.81	98.60	98.74
Sc	29	32	32	25	32	32	30	32
V	231	201	235	166	296	300	305	260
Cr	841	856	269	490	637	605	580	1195
Co	n.a.	n.a.	28	34	59	63	60	77
Ni	495	502	114	228	164	161	162	366
Cu	n.a.	n.a.	33	39	65	71	71	49
Zn	n.a.	n.a.	79	84	89	89	90	105
Rb	50	43	86	117	79	78	83	64
Sr	1272	1421	2166	1319	2008	2042	2192	2007
Y	24	29	40	28	35	29	27	27
Zr	179	312	90	316	354	338	371	296
Nb	126	155	520	127	179	171	186	152
Mo	n.a.	n.a.	12	13	<5	<5	<5	<5
Ba	2167	2608	469	1453	2237	2708	3265	2695
Pb	n.a.	n.a.	18	13	12	6	11	4
Th	n.a.	n.a.	32	9	7	5	7	24
U	n.a.	n.a.	21	9	13	12	15	16
F	n.a.	n.a.	1276	1740	1326	1255	1544	1993
S	n.a.	n.a.	377	1028	501	614	608	489
Cl	n.a.	n.a.	199	175	274	265	378	195

APPENDIX 2, Table 1 continued.

Rock Type	Ultramafic lamprophyres, cont'd					Fe-rich crusts and breccias		
Sample	SPKC-12	SPKC-14	SD-1G	SD-1M	SKGB-1	SK2-2	SKR-2	SKR-3
SiO_2	31.23	20.86	40.51	40.23	32.07	3.05	2.75	16.88
TiO_2	1.01	2.50	2.44	2.33	3.11	0.05	0.05	0.01
Al_2O_3	7.88	5.32	8.71	8.44	7.38	1.58	1.42	4.35
$Fe_2O_3^{tot.}$	11.20	15.33	11.46	10.72	10.29	73.49	66.27	62.97
MnO	0.78	0.90	0.28	0.29	0.23	0.03	0.03	0.95
MgO	4.79	7.75	7.76	7.67	2.36	0.16	0.14	0.12
CaO	14.54	18.66	13.96	14.48	19.58	0.24	0.22	0.06
Na_2O	0.27	0.21	3.17	3.35	0.37	0.44	0.40	0.40
K_2O	5.99	4.26	1.86	1.82	6.12	0.09	0.08	3.32
P_2O_5	0.81	2.31	0.94	0.93	1.28	1.46	1.32	0.07
SO_3	0.43	0.11	0.27	0.27	0.09	0.63	0.57	0.09
H_2O-	1.04	0.87	0.15	0.40	1.40	1.31	2.38	0.88
LOI	17.96	16.95	6.79	7.32	13.79	10.47	17.40	8.99
Sum	97.99	96.10	98.34	98.29	98.16	93.04	93.02	99.11
Sc	27	34	33	31	32	56	27	11
V	173	320	290	282	404	384	218	121
Cr	300	327	218	192	584	<5	139	37
Co	23	61	44	39	49	64	14	41
Ni	94	117	62	56	161	156	12	10
Cu	28	54	52	42	62	35	34	24
Zn	266	223	118	114	98	1849	233	826
Rb	97	162	63	64	204	10	79	69
Sr	1373	1736	2224	2365	638	167	1216	117
Y	56	80	31	28	69	388	106	182
Zr	114	n.a.	343	357	n.a.	140	197	500
Nb	632	592	132	135	651	78	285	17
Mo	94	<5	<5	<5	<5	43	b.d.	1331
Ba	8463	6472	3361	3444	2372	32895	13585	4665
Pb	36	25	12	12	11	278	53	149
Th	43	125	10	10	20	109	31	1458
U	17	22	15	17	<5	9	12	110
F	1935	11202	1690	1749	18725	3416	1969	4145
S	1382	453	654	638	481	3487	281	861
Cl	190	157	144	143	115	312	119	196

APPENDIX 2, Table 1 continued.

Rock Type	Crusts & breccias, cont.		Crustal xenoliths			
Sample	SK2-3	SKR-4	SP-100	SDCX-3	SDCX-4	SD-SHALE
SiO_2	39.72	55.56	41.53	45.28	41.95	56.00
TiO_2	0.21	1.23	1.99	2.16	3.03	0.58
Al_2O_3	11.18	8.38	4.67	7.26	8.23	14.74
$Fe_2O_3^{tot.}$	25.27	12.39	9.19	14.33	12.97	3.92
MnO	2.67	1.88	0.12	0.27	0.21	0.11
MgO	0.33	0.61	20.91	8.81	11.87	2.23
CaO	1.44	1.80	7.40	16.76	15.46	4.49
Na_2O	1.35	1.04	0.15	2.61	2.04	8.01
K_2O	8.03	7.50	4.21	0.47	1.14	1.81
P_2O_5	0.63	0.79	0.38	0.58	0.06	0.12
SO_3	0.12	0.76	0.15	0.03	0.15	0.01
H_2O-	0.96	1.17	1.47	0.07	0.06	0.44
LOI	5.64	3.70	4.66	0.82	1.90	6.71
Sum	97.56	96.86	97.18	99.54	99.13	99.18
Sc	31	25	16	63	44	15
V	401	418	119	334	405	79
Cr	<5	83	1552	576	460	39
Co	27	15	93	54	45	5
Ni	33	18	1075	35	35	<5
Cu	20	30	20	44	16	<5
Zn	1097	949	58	138	85	58
Rb	116	142	198	<5	11	32
Sr	473	935	607	552	685	471
Y	140	418	13	34	22	32
Zr	834	b.d.	330	244	416	281
Nb	450	1893	119	91	88	19
Mo	121	76	<5	<5	<5	17
Ba	7058	6952	2654	3080	557	1283
Pb	130	393	10	<5	<5	21
Th	41	224	9	b.d.	b.d.	14
U	29	20	<5	<5	<5	<5
F	3978	4494	2619	1128	1324	633
S	646	2976	545	680	650	324
Cl	544	1043	121	207	211	122

APPENDIX 2

Table 2. Trace element data obtained by solution quadrupole ICP-MS techniques

Type	Calciocarbonatites							Ferr. calcio.
Sample	SP-27C	SP-19A	WV95-28	SP-404	SP-27D	WV95-22	WV95-29	SP-331A
Li	17.6	35.2	62.7	51.4	3.59	8.28	44.14	9.05
Sc	n.a.	n.a.	64.7	17.3	n.a.	n.a.	17.43	16.1
V	193.22	214	184	324	15.5	117.4	148	267
Cr	6.84	1.52	12.3	7.78	14.5	6.79	6.52	62.7
Co	b.d.	b.d.	b.d.	b.d.	b.d.	8.86	b.d.	0.340
Ni	b.d.	b.d.	b.d.	b.d.	b.d.	b.d.	b.d.	b.d.
Cu	25.6	14.9	37.4	8.15	10.4	8.53	10.8	90.3
Zn	237	523	161	231	13.7	180	154	830
Rb	110	52.9	76.3	40.9	22.3	36.4	29.7	38.6
Sr	4226	2052	949	1398	310	4029	1170	7415
Y	137	205	308	146	22.9	180	106	391
Zr	906	819	628	642	61.9	165	489	347
Nb	879	1105	813	757	3.62	1202	591	1000
Cs	16.3	1.21	4.16	3.13	1.15	2.31	4.03	0.520
Ba	1661	8974	1434	862	482	1905	679	4695
La	696	1075	992	1162	10.8	1690	1244	2402
Ce	1105	2028	1682	2179	21.8	2596	1774	4634
Pr	111	242	179	273	2.71	259	173	491
Nd	412	878	674	946	11.4	840	556	1582
Sm	56.3	99.5	82.9	106	3.19	93.2	59.5	158
Eu	14.3	24.8	20.1	23.5	0.950	22.7	13.5	35.4
Gd	37.4	55.6	50.8	51.5	3.73	50.3	31.5	81.3
Tb	4.73	7.25	7.14	5.95	0.540	6.79	4.14	11.9
Dy	24.4	37.3	42.0	28.7	2.87	32.4	19.9	62.3
Ho	4.33	6.73	9.14	5.05	0.560	5.70	3.52	11.4
Er	10.6	16.7	30.6	12.5	1.49	14.5	9.03	27.6
Tm	1.27	2.2	5.45	1.93	0.200	1.82	1.22	4.10
Yb	7.27	12.7	37.2	12.8	1.19	11.0	7.99	22.1
Lu	0.960	1.76	5.36	1.86	0.17	1.45	1.23	3.16
Hf	13.4	5.48	6.04	3.69	1.45	1.97	3.83	2.25
Ta	12.7	18.6	8.61	7.28	0.47	5.45	9.02	3.39
Pb	29.7	65.5	25.4	30.7	5.21	67.5	26.1	231
Th	28.6	91.3	123	182	2.24	86.1	83.0	204
U	36.7	63.0	5.89	8.58	1.13	16.4	18.0	29.0

Concentration data are all given in parts per million by weight. All data were obtained in this study except those for SPK-1 and SPK-3, which are from Janney et al. (2002). See text in Chapter 3 for analytical details.

APPENDIX 2, Table 2 continued.

Type	Ferruginous calciocarbonatites, cont'd.							
Sample	SP-26B	SP-27B	WV95-21	WV95-25	SPKC-8	SK1-B1	SP-16A	SPKC-4
Li	49.8	42.7	7.16	8.69	6.08	n.a.	18.3	n.a.
Sc	n.a.	4.42	65.8	38.87	6.74	21.5	24.5	6.18
V	200	171	144	411	269	206	150.1	135
Cr	12.6	11.2	9.7	19.9	13.1	470	38.6	90.8
Co	b.d.	b.d.	b.d.	b.d.	9.53	18.0	0.210	2.37
Ni	4.91	b.d.	b.d.	13.3	b.d.	66.3	b.d.	50.6
Cu	9.38	11.7	13.4	30.0	11.0	42.2	10.8	25.9
Zn	578	484	497	680	448	219	475	670
Rb	65.1	63.0	55.7	58.5	15.5	112	45.6	171
Sr	3030	2762	1244	2418	5228	1808	872	553
Y	192	221	120	553	367	84.4	408	163
Zr	144	127	170	98.9	232	315	82.0	54.7
Nb	1099	1129	193	721	1409	718.2	456	423
Cs	1.81	4.83	0.220	0.420	0.140	2.28	1.29	0.361
Ba	2928	3303	1979	22407	1973	6251	2946	6644
La	4266	4514	3675	2256	1896	2434	2143	288
Ce	6893	6634	5866	3702	3294	3850	3181	588
Pr	691	680	587	400	379	278	323	59.2
Nd	2258	2163	1756	1421	1315	972	1118	218
Sm	172	167	107	173.4	164	89.7	160	38.0
Eu	34.6	34.4	19.5	52.3	41.9	17.3	41.6	10.2
Gd	67.9	70.6	35.7	144	101	37.3	105	34.7
Tb	8.22	8.63	4.52	21.1	13.1	3.58	13.9	5.32
Dy	38.2	40.6	20.0	105	65.9	15.7	69.5	30.1
Ho	6.26	7.07	3.58	17.1	11.6	2.50	12.7	4.78
Er	14.1	16.4	9.05	38.6	27.8	6.72	36.9	10.8
Tm	2.10	2.16	1.6	4.88	3.71	1.06	6.17	1.09
Yb	11.1	12.8	12.8	27.8	21.6	7.80	44.8	5.55
Lu	1.46	1.65	2.28	3.83	2.95	1.31	7.57	0.61
Hf	2.20	1.35	1.96	1.59	2.12	5.20	1.31	1.23
Ta	2.54	1.51	4.14	0.67	8.07	6.36	2.70	1.18
Pb	71.2	70.9	45.3	267	146	23.5	171	149
Th	131	105	204	201	143	204	188	114
U	11.8	14.6	27.4	14.3	89.1	8.77	18.4	2.45

APPENDIX 2, Table 2 continued.

Type	Magnesio- & ferrocarbonatites				Potassic trachytes			
Sample	WV95-24	SP-400	WV95-26	SPKC-9	WV95-23	WV95-23A	WV95-23C	SP307-3
Li	10.7	5.52	4.69	96.8	5.22	17.4	4.28	86.4
Sc	30.0	41.0	60.4	26.7	n.a.	n.a.	n.a.	3.46
V	153	336	306	216	112	71.0	65.7	305
Cr	58.5	2.55	2.48	242	8.9	8.91	10.2	55.5
Co	2.05	b.d.	b.d.	37.3	3.82	b.d.	0.780	11.0
Ni	26.6	b.d.	b.d.	91.0	23.1	b.d.	9.41	27.6
Cu	44.7	17.5	13.1	63.6	44.2	8.67	8.52	47.1
Zn	713	522.8	619	187	34.9	102	71.2	379
Rb	39.8	0.260	0.600	127	223	219	201.1	182
Sr	1882	1639	1688	1109	292	1559	633.3	562
Y	208	189	314	69.4	28.0	81.3	56.5	260
Zr	80.7	79.7	119	137	407	2080	329	467
Nb	874	1136	1538	567	1247	880	799	1360
Cs	0.470	0.140	0.260	7.89	0.630	0.760	0.830	1.72
Ba	1902	16843	20835	10518	4010	3481	15346	23990
La	2875	1322	1711	681	41.4	102	103	164
Ce	4753	2056	2758	1205	16.5	162	73.2	311
Pr	449	187	281	127	7.63	17.9	18.4	28.9
Nd	1330	520	982	445	26.6	58.8	61.7	102.6
Sm	124	72.8	116	57.0	5.69	9.36	8.91	22.8
Eu	26.9	19.5	30.2	12.7	1.97	2.87	2.88	9.23
Gd	67.9	52.4	74.2	28.7	6.42	9.61	8.95	31.6
Tb	9.12	7.88	10.9	3.34	0.97	1.82	1.49	6.03
Dy	42.1	41.1	58.2	14.3	5.13	12.4	8.74	39.1
Ho	6.97	7.34	10.4	2.39	0.97	2.93	1.84	8.15
Er	14.9	18.3	25.6	5.46	2.71	9.47	5.34	23.7
Tm	2.11	2.91	3.67	0.72	0.45	1.69	0.88	3.33
Yb	10.5	18.0	24.0	4.18	2.86	11.2	5.61	20.5
Lu	1.48	2.73	3.61	0.63	0.45	1.75	0.85	2.57
Hf	2.32	0.750	0.79	2.66	5.23	18.5	5.75	7.86
Ta	2.28	6.52	7.38	7.19	26.5	36.6	43.4	10.9
Pb	135	165	269	35.6	95.1	34.1	51.6	461
Th	214	273	285	113	7.55	37.2	39.9	13.8
U	13.6	33.9	44.9	8.02	6.23	16.4	5.42	6.92

APPENDIX 2, Table 2 continued.

Type	Potassic trachytes cont'd.				Olivine melilitites			
Sample	SP-401	SK2-1	SP307-4	SKR-5	SP31-3	SP31-4	SP-43	SP43-1
Li	4.15	n.a.	4.32	n.a.	5.69	3.74	63.5	40.1
Sc	11.0	7.40	n.a.	n.a.	24.6	22.7	25.6	24.4
V	116	151	44.8	1228.6	228	227	244	239
Cr	3.86	9.04	41.0	33.2	566	571	622	694
Co	b.d.	17.3	0.517	b.d.	73.5	72.5	53.5	56.8
Ni	b.d.	117	2.29	b.d.	407	398	253	276
Cu	12.0	16.3	13.5	19.5	195	86.1	109	76.8
Zn	205	462	11.8	453	104	100	127	108
Rb	130	160	178	277	50.9	46.2	47.8	44.3
Sr	572	403	221	2685	1168	1215	1447	1323
Y	94.2	111	44.5	198	29.9	30.8	37.4	36.2
Zr	203	252	803	6315	286	295	318	282
Nb	1174	627	749	756	110	114	152	145
Cs	0.740	1.16	0.690	3.53	0.880	0.655	2.17	2.25
Ba	5705	3811	2945	3928	843	1068	1019	956
La	441	362	202	39.8	102	100	114	116
Ce	770	675	286	75.7	185	182	213	224
Pr	70.8	71.8	33.02	13.5	20.5	20.5	24.0	25.0
Nd	236	240	102	71.9	75.8	76.0	88.9	93.2
Sm	40.3	35.1	10.7	25.1	13.2	13.2	15.2	15.8
Eu	11.1	8.52	2.37	8.26	3.77	3.68	4.09	4.22
Gd	29.1	26.9	6.98	29.6	9.39	9.43	10.5	10.7
Tb	4.07	3.73	1.11	4.92	1.33	1.29	1.36	1.41
Dy	20.7	19.7	6.59	31.9	6.53	6.34	7.13	7.19
Ho	3.41	3.68	1.42	7.08	1.13	1.09	1.14	1.13
Er	7.99	10.4	4.19	20.2	2.63	2.49	2.84	2.84
Tm	1.03	1.53	0.664	2.89	0.32	0.31	0.33	0.32
Yb	6.53	8.69	4.23	16.5	1.78	1.73	1.81	1.77
Lu	0.930	1.22	0.656	2.37	0.25	0.24	0.23	0.23
Hf	37.4	2.84	14.5	80.7	6.49	6.25	6.01	5.42
Ta	27.8	63.4	19.5	1.38	5.44	6.41	5.17	5.47
Pb	116	78.4	11.8	98.0	6.09	6.16	11.6	7.96
Th	88.7	28.1	40.0	23.7	15.5	15.5	15.6	16.3
U	21.8	19.8	10.1	1.76	3.31	3.38	4.9	4.68

APPENDIX 2, Table 2 continued.

Type	Olivine melilitites cont'd.							
Sample	SP43-2	SP206-1	SP206-2	SKM1-1	SKM2-1	SKM6-1	SKM5-1	SPK-1
Li	19.5	40.1	53.3	n.a.	n.a.	n.a.	n.a.	n.a.
Sc	25.3	22.2	20.8	22.02	30.5	26.0	25.8	n.a.
V	257	225	229	231	197	200	210	n.a.
Cr	716	605	557	495	558	935	969	26.2
Co	62.5	72.0	73.7	45.6	52.7	61.6	60.6	139
Ni	311	461	384	128	99.6	449	387	n.a.
Cu	82.7	87.0	170	75.6	49.9	576	79.5	n.a.
Zn	114	119	112	120	160	392	93.3	n.a.
Rb	44.8	44.6	37.8	82.9	59.5	51.5	55.3	69.4
Sr	1206	1107	1013	1713	2448	2264	1174	1477
Y	33.0	28.7	26.8	35.8	43.3	25.4	26.6	26.2
Zr	274	328	382	338	222.8	208	210	139
Nb	137	111	101	154	277	135	142	149
Cs	1.63	0.920	0.913	30.3	15.7	1.28	1.60	1.38
Ba	754	1035	944	1752	2778	1505	1272	1645
La	107	76.8	79.4	146	312	144	171	191
Ce	202	154	158	295	557	259	319	308
Pr	22.7	18.2	19.1	29.7	54.8	23.5	29.3	31.5
Nd	84.4	70.5	73.7	107	195	82.5	101	106
Sm	14.4	12.9	13.4	17.0	29.6	12.8	15.6	15.8
Eu	3.87	3.43	3.69	4.34	7.69	3.15	3.98	4.29
Gd	9.84	8.86	9.27	11.1	19.3	7.58	9.96	10.5
Tb	1.30	1.19	1.27	1.46	2.34	0.969	1.24	1.32
Dy	6.55	5.84	5.92	7.30	10.5	4.91	5.71	6.12
Ho	1.07	0.960	0.98	1.23	1.68	0.797	0.961	0.94
Er	2.58	2.25	2.23	2.89	3.37	1.84	2.09	1.98
Tm	0.290	0.27	0.26	0.348	0.40	0.212	0.269	0.24
Yb	1.60	1.46	1.51	1.87	1.96	1.12	1.41	1.17
Lu	0.20	0.190	0.20	0.254	0.26	0.141	0.185	0.15
Hf	5.53	6.43	7.11	6.48	4.92	4.15	4.26	3.06
Ta	5.16	5.39	5.06	6.11	10.3	3.72	6.13	n.a.
Pb	7.92	4.84	3.91	9.20	8.37	34.5	10.7	15.4
Th	16.1	8.17	8.20	17.7	47.7	20.3	27.9	27.1
U	4.54	2.88	2.87	7.01	6.87	4.64	5.30	5.54

APPENDIX 2, Table 2 continued.

Type	Ol. mel. cont'd.		Ultramafic lamprophyres					
Sample	SPK-2	SPK-3	WV95-19	SP-38	SP38-1	SP38-2	SD-1G	SP367-1
Li	n.a.	n.a.	6.72	43.0	20.5	22.6	29.5	14.5
Sc	25.30	n.a.	27.0	19.9	20.7	23.2	27.4	21.9
V	228	n.a.	207	144	197	214	254	191
Cr	842	28.5	293	479	534	533	215	1017
Co	59.7	312	24.1	37.8	44.8	48.4	38.4	61.6
Ni	304	n.a.	105	232	155	165	54.5	391
Cu	132	n.a.	44.1	49.8	80.7	98.4	68.1	65.7
Zn	86.1	n.a.	79.7	82.1	93.8	102	134	108.0
Rb	48.9	46.0	87.5	115	75.9	81.8	65.7	65.2
Sr	1227	1507	2096	1246	1865	1988	2118	1928
Y	26.8	28.5	45.6	30.1	32.2	33.5	32.2	33.4
Zr	173	312	260	361	331	337	309	271
Nb	139	161	633	120	155	167	121	144
Cs	1.10	0.870	0.860	2.86	4.06	3.77	3.06	29.7
Ba	1452	2573	466	1468	1888	2411	2992	2010
La	171	182	167	244	144	145	203	174
Ce	304	301	327	423	253	256	335	354
Pr	28.1	31.3	31.2	35.01	27.0	27.8	37.0	41.0
Nd	96.6	105	111	108	95.7	98.1	129	154
Sm	14.5	15.4	17.0	12.8	15.4	15.5	16.8	23.2
Eu	3.84	4.13	3.93	2.88	3.93	4.11	3.92	5.62
Gd	9.97	10.1	11.1	7.97	10.1	10.6	9.65	12.7
Tb	1.21	1.29	1.54	1.13	1.31	1.45	1.34	1.60
Dy	5.62	6.14	7.70	5.52	6.66	6.77	6.33	6.89
Ho	0.890	0.99	1.43	1.03	1.15	1.19	1.14	1.16
Er	2.03	2.16	3.83	2.6	2.63	2.79	2.72	2.53
Tm	0.246	0.26	0.660	0.38	0.323	0.36	0.38	0.33
Yb	1.30	1.31	4.44	2.19	1.80	1.89	2.17	1.79
Lu	0.171	0.17	0.790	0.32	0.241	0.26	0.33	0.24
Hf	3.67	6.05	4.52	6.22	6.86	6.92	6.99	5.23
Ta	5.33	n.a.	4.71	2.85	5.71	6.68	5.07	5.87
Pb	19.8	49.3	23.6	14.9	16.3	10.2	17.1	4.80
Th	27.5	29.2	40.0	13.7	15.6	15.3	18.9	34.7
U	5.29	7.04	6.97	4.56	2.75	3.00	2.82	4.07

APPENDIX 2, Table 2 continued.

Type	UM lamprophyres, cont'd.			Fe-rich crusts & mineralised breccias				
Sample	SPKC-12	SPKC-14	SKGB-1	SK2-2	SKR-3	SK2-3	SKR-2	SKR-4
Li	32.8	80.7	n.a.	n.a.	n.a.	n.a.	n.a.	n.a.
Sc	21.8	24.9	32.5	59.8	12.9	33.5	20.9	30.3
V	164	207	300	399	123	339	178	416
Cr	422	263	504	124	39.6	8.46	205	299
Co	17.4	42.0	36.2	19.6	14.0	17.4	2.05	19.2
Ni	85.1	101	143	285	24.3	72.4	71.9	374
Cu	36.6	63.0	79.2	9.38	9.94	8.36	48.8	49.2
Zn	271	220	113	969	782	660	269	923
Rb	99.1	153	203	5.16	45.7	112	83.5	140
Sr	1395	1628	621	167	109	428	1241	905
Y	62.0	76.3	80.3	430	100	148	118	439
Zr	367	202	266	42.1	10.5	707.99	230	561
Nb	614	577	704	82.1	90.7	428	288	1826
Cs	1.92	6.97	9.45	0.544	0.201	0.555	4.05	1.13
Ba	9595	6681	2994	23539	3232	6984	16539	7592
La	536	692	172	1449	452	649	198	1009
Ce	941	1301	309	2850	1453	1370	309	1861
Pr	104	139	34.1	256	216	100.0	36.5	217
Nd	359	495	122	1205	1084	297	136	765
Sm	45.2	59.2	19.8	176	194	34.8	21.0	105
Eu	10.1	12.36	5.11	43.5	35.3	8.90	5.99	31.1
Gd	21.0	25.3	14.8	112	57.4	25.1	18.9	98.3
Tb	2.74	2.80	1.99	13.6	4.48	3.95	2.92	17.0
Dy	12.1	14.0	10.2	68.5	18.9	23.6	16.9	90.3
Ho	2.01	2.37	2.01	14.0	3.27	4.95	3.51	16.9
Er	5.17	6.77	5.82	42.2	7.38	15.7	10.0	39.5
Tm	0.754	1.03	1.04	6.40	1.00	2.45	1.31	4.98
Yb	4.92	7.14	6.85	40.9	5.31	16.1	7.54	26.9
Lu	0.811	1.25	1.13	6.23	0.657	2.19	1.02	3.53
Hf	5.86	2.92	5.51	0.296	0.152	6.90	4.06	7.95
Ta	3.22	5.91	7.22	0.420	0.197	25.4	3.58	3.48
Pb	48.3	31.9	14.1	354	158	158	77.4	516
Th	47.1	121.7	23.8	92.0	1602	36.4	36.3	215
U	7.40	5.53	4.95	3.80	0.141	24.9	6.73	3.26

APPENDIX 2, Table 2 continued.

Type	Crustal xenoliths	
Sample	SP-100	SD-SHALE
Li	177	35.9
Sc	16.8	13.8
V	80.9	71.0
Cr	1562	41.0
Co	99.2	7.83
Ni	1149	16.7
Cu	62.6	23.8
Zn	64.2	61.5
Rb	200	31.6
Sr	611	451
Y	11.4	24.0
Zr	404	150
Nb	128	16.3
Cs	1.93	3.14
Ba	2298	1118
La	94.8	35.5
Ce	170	69.3
Pr	18.2	8.08
Nd	62.1	29.2
Sm	8.31	5.59
Eu	2.05	1.01
Gd	4.76	4.21
Tb	0.583	0.711
Dy	2.61	4.12
Ho	0.409	0.846
Er	0.917	2.41
Tm	0.122	0.343
Yb	0.795	2.25
Lu	0.124	0.329
Hf	9.17	4.11
Ta	6.73	0.640
Pb	9.75	24.3
Th	14.2	16.4
U	2.20	3.43

APPENDIX 2

Table 3. Trace element concentrations for rock standards measured by ICP-MS

Std.	Accepted V5-40-56G	This study V5-40-56G	% RSD (2σ)	Accepted AGV-1	This study AGV-1	% RSD (2σ)	Accepted COQ-1	This study COQ-1	% RSD (2σ)
Li	no data	4.19	4.5	10.7	10.2	2.7	no data	2.80	12.0
Sc	37.6	37.0	6.5	12.6	11.6	2.5	0.91	0.476	6.5
V	250	257	5.0	126	118	3.4	140	129	4.2
Cr	249	235	3.3	9.0	8.53	3.7	no data	n.a.	
Co	44	34.1	2.8	15.3	14.5	3.3	no data	n.a.	
Ni	98	95.2	3.0	16	14.2	10.1	no data	n.a.	
Cu	46	53.5	3.6	58	60.5	13.9	no data	n.a.	
Zn	90	104	6.5	87	92.9	3.7	no data	n.a.	
Rb	2.98	2.97	3.6	68.3	67.1	5.4	13.3	12.6	4.9
Sr	203	197	3.5	655	661	3.8	11781	11696	5.3
Y	37.9	37.6	3.5	21	23.7	3.2	101	91.2	2.1
Zr	175	172	5.4	240	236	3.5	77.0	72.0	2.5
Nb	8.46	8.22	5.1	14.9	14.6	1.9	3900	3778	8.5
Cs	0.035	0.040	11.1	1.3	1.21	2.1	no data	0.216	19.5
Ba	29.9	29.9	5.9	1223	1205	3.2	1110	1091	4.3
La	8.02	7.84	3.0	38.5	38.3	2.1	858	857	4.4
Ce	22.5	21.6	2.1	68.5	68.3	2.4	1744	1737	7.1
Pr	3.42	3.27	3.4	8.45	8.30	2.7	150	145	2.0
Nd	16.7	16.5	3.0	31.6	31.4	2.1	472	461	2.1
Sm	4.98	4.93	4.3	5.82	5.70	3.1	54.1	52.3	3.3
Eu	1.75	1.77	5.8	1.565	1.56	3.3	14.1	14.2	4.0
Gd	6.14	6.29	3.2	4.73	4.66	3.3	29.9	29.5	2.8
Tb	1.06	1.10	4.2	0.664	0.652	3.5	3.81	3.75	1.0
Dy	6.81	6.85	3.3	3.54	3.51	4.5	18.4	18.3	4.0
Ho	1.41	1.41	5.8	0.69	0.685	3.3	3.25	3.14	3.9
Er	3.99	4.06	2.4	1.856	1.83	2.4	8.21	8.06	2.5
Tm	0.6	0.608	3.4	0.28	0.280	5.2	1.1	1.07	7.5
Yb	3.71	3.71	2.4	1.644	1.61	5.1	6.33	6.32	4.5
Lu	0.56	0.584	3.3	0.248	0.249	4.4	0.86	0.868	5.0
Hf	4.08	4.04	4.3	5.0	4.95	2.9	0.28	0.300	4.3
Ta	0.5	0.559	8.2	0.882	0.864	8.7	26.0	27.4	5.3
Pb	0.92	0.948	6.6	37.27	36.9	4.7	4.13	4.39	2.8
Th	0.47	0.480	7.1	6.53	6.35	4.6	11.5	10.9	2.0
U	0.19	0.186	7.2	1.885	1.86	3.0	11.3	10.8	2.2

Sources for standard data are: V5-40-56G (MORB glass in-house standard), Janney et al. (2005) with additional data for V, Cr, Co, Ni, Cu and Zn from Le Roux et al. (2002); AGV-1 (USGS Guano Valley Andesite), Eggins et al. (1997), COQ-1 (USGS Carbonatite Oka Quebec) from recommended values for this standard on the GeoREM website (http://georem.mpch-mainz.gwdg.de/). %RSD is the relative standard deviation (2*standard deviation/mean, expressed as a percentage) for analysis of each of the rock standards, measured with each analysis batch during the course of this study.

APPENDIX 3. PARTITION COEFFICIENT DATA

Table 1. Mineral melt partition coefficients used for melt modeling in Chapter 6

Element	Ol	Opx	Cpx	Gar	Spinel	Phlog	Ilm
Rb	0.001	0.001	0.001	0.001	0.001	2.48	0.0001
Ba	0.001	0.001	0.001	0.001	0.001	3.68	0.00034
Th	0.001	0.001	0.001	0.001	0.001	0.0014	0.00055
Nb	0.001	0.001	0.01	0.001	0.001	0.088	2
K	0.001	0.001	0.01	0.001	0.001	3.67[a]	0.0001
La	0.001	0.001	0.05	0.01	0.001	0.028	0.000029
Ce	0.001	0.001	0.08	0.021	0.001	0.021*	0.000054
Sr	0.001	0.001	0.12	0.001	0.001	0.159	0.0005
Nd	0.001	0.001	0.14	0.087	0.001	0.012	0.00048
Sm	0.001	0.001	0.14	0.13	0.001	0.014*	0.00059
Zr	0.001	0.01	0.2	0.1	0.001	0.017	0.29
Hf	0.001	0.01	0.2	0.1	0.001	0.19	0.38
Eu	0.001*	0.01*	0.15*	0.2*	0.001	0.015*	0.0011
Ti	0.001	0.1	0.17	0.1	0.001	0.98	50[b]
Tb	0.001*	0.019*	0.25*	0.6*	0.001	0.016*	0.0067
Dy	0.001*	0.022*	0.3*	0.9*	0.001	0.017*	0.01
Y	0.001	0.1	0.3	4	0.001	0.018	0.01
Yb	0.001	0.1	0.3	4	0.001	0.018	0.17
Lu	0.001	0.1	0.3	6	0.001	0.001	0.084

Mineral-melt partition coefficient values for olivine, orthopyroxene, clinopyroxene and garnet are from le Roex et al. (2003). Those for phlogopite are from Schmidt et al. (1999) except for the element potassium (marked with superscript a), which is the value from LaTourette et al. (1995). Values for ilmenite are from Zack and Brumm (1998), except for the value for Ti (superscript b), which is an estimated value (used only in the potassic trachyte melt modeling). In all cases, coefficients with asterisks (*) are interpolated values for the rare earth elements obtained by logarithmic interpolation from the nearest REE using data provided in the sources given.